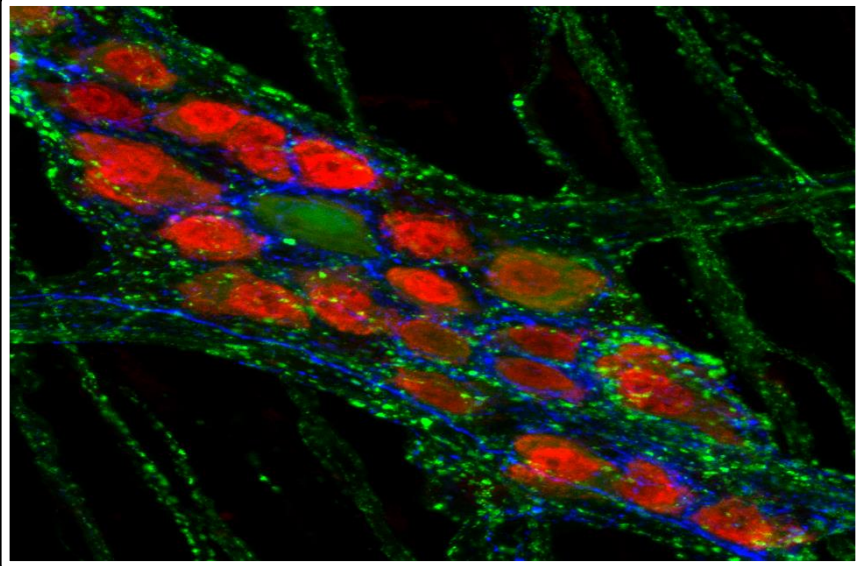


Doctoral thesis in Biomedical Sciences



**IDENTIFICATION OF NEURONAL
CIRCUITS IN THE ENTERIC
NERVOUS SYSTEM**

**Zhi-ling Li
KULEUVEN 2019**

KU Leuven
Biomedical Sciences Group
Faculty of Medicine
Department of Chronic Diseases, Metabolism and
Ageing



IDENTIFICATION OF NEURONAL CIRCUITS IN THE ENTERIC NERVOUS SYSTEM

Zhi-ling Li

Jury:

Promoter: Prof. Pieter Vanden Berghe

Co-promoter: Prof. Werend Boesmans

Dr. Marlene M Hao

Chair: Prof. Kristin Verbeke

Secretary: Prof. Joris de Wit

Jury members:

Prof. Alan E G Lomax

Prof. Dietmar Schmucker

Prof. Jean-Pierre Timmermans

Prof. Joris de Wit

Dissertation presented in
partial fulfilment of the
requirements for the degree
of Doctor in Biomedical
Sciences

March 2019

Table of Contents

List of Abbreviations

| | |
|---|-----------|
| CHAPTER 1 GENERAL INTRODUCTION | 1 |
| 1 THE ENTERIC NERVOUS SYSTEM | 2 |
| 1.1 Organization of the enteric nervous system | 2 |
| 1.2 ENS development | 4 |
| 1.3 Enteric neurons | 4 |
| 1.3.1 Morphological classification of enteric neurons | 4 |
| 1.3.2 Electrophysiological classification of enteric neurons | 5 |
| 1.3.2.1 AH neurons | 8 |
| 1.3.2.2 S neurons | 10 |
| 1.3.2.3 Electrophysiological properties of enteric neurons in human | 12 |
| 1.3.2.4 Neurochemical coding of enteric neurons | 12 |
| 1.4 Glia | 13 |
| 1.5 Other cell types in the gut | 14 |
| 1.6 Control of Gastrointestinal Motility and Circuitry of the ENS | 14 |
| 1.6.1 Intrinsic sensory neurons | 16 |
| 1.6.2 Interneurons | 18 |
| 1.6.3 Secretomotor neurons | 19 |
| 1.6.4 Motor neurons | 20 |
| 2 ADENO-ASSOCIATED VIRUS | 21 |
| 2.1 Genome structure | 21 |
| 2.2 Capsid structure | 22 |
| 2.3 Tissue tropisms | 22 |
| 2.4 Cellular entry to AAV transduction | 23 |
| 3 OPTOGENETIC TOOLS TO DEFINE NEURAL CIRCUIT ACTIVITY | 24 |
| CHAPTER 2 RESEARCH OBJECTIVES | 27 |
| CHAPTER 3 ESTABLISHING A VIRAL VECTOR TRANSDUCTION TECHNIQUE TO TARGET FLUORESCENT REPORTERS TO THE ENS, IN VIVO | 31 |
| 3.1 Introduction | 32 |
| 3.2 Materials & Methods | 33 |

| | | |
|--|---|-----------|
| 3.2.1 | Animals | 33 |
| 3.2.2 | Neuronal process tracing | 33 |
| 3.2.2.1 | Recombinant adeno-associated viral vector (AAV) preparation | 33 |
| 3.2.2.2 | rAAV injection | 34 |
| 3.2.3 | Immunohistochemistry | 34 |
| 3.2.4 | Image analysis | 35 |
| 3.3 | Results | 35 |
| 3.3.1 | Distribution of eGFP-positive cells in the gastrointestinal tract following tail vein injection of rAAVs-CMV-eGFP into adult mice | 36 |
| 3.3.2 | Transduction of myenteric neurons by rAAV8 and rAAV9 | 36 |
| 3.3.3 | Only a minority of cells transduced by rAAV2/8 and rAAV2/9 were non-neuronal | 39 |
| 3.3.4 | N-linked galactose expression in the mouse colon | 40 |
| 3.4 | Discussion | 40 |
| 3.5 | Conclusion | 43 |
| 3.6 | Author Contributions | 43 |
| 3.7 | Acknowledgements | 43 |
| 3.8 | Conflicts of Interest | 44 |
| CHAPTER 4 REGIONAL COMPLEXITY IN ENTERIC NEURON WIRING REFLECTS DIVERSITY OF MOTILITY PATTERNS IN THE MOUSE LARGE INTESTINE | | 45 |
| 4.1 | Introduction | 46 |
| 4.2 | Materials and Methods | 47 |
| 4.2.1 | Animals | 47 |
| 4.2.2 | Calcium imaging | 47 |
| 4.2.3 | Live video imaging of colonic motility | 49 |
| 4.2.4 | Neuronal process tracing | 49 |
| 4.2.4.1 | Recombinant adeno-associated viral vector (AAV) preparation | 49 |
| 4.2.4.2 | rAAV2/9 injection | 50 |
| 4.2.5 | Immunohistochemistry | 50 |
| 4.2.6 | Image analysis | 51 |
| 4.2.7 | Data analysis | 52 |

| | | |
|---|---|-----------|
| 4.3 | Results | 53 |
| 4.3.1 | Motility and underlying neuronal circuitry in the proximal and distal colon | 53 |
| 4.3.2 | Regional differences in myenteric plexus morphology | 55 |
| 4.3.3 | Ca ²⁺ response signatures of individual myenteric neurons | 57 |
| 4.3.4 | The importance of nicotinic cholinergic input scales with distance from the stimulation electrode | 62 |
| 4.3.5 | Distribution mapping of responding neurons | 64 |
| 4.3.6 | Morphology of responding neurons | 67 |
| 4.3.7 | Quantification of cholinergic neurons and synaptic contacts in proximal and distal colon | 69 |
| 4.3.8 | Sparse labeling of neuronal projection patterns using viral vector transduction | 71 |
| 4.4 | Discussion | 73 |
| 4.4.1 | Wiring complexity | 73 |
| 4.4.2 | Circuitry probing using pharmacological inhibition and immunohistochemistry | 75 |
| 4.4.3 | Mapping of the relative location of neurons | 77 |
| 4.4.4 | Projections of myenteric neurons | 78 |
| 4.4.5 | Relation between neuron size, location and response fingerprint | 79 |
| 4.5 | Conclusion | 79 |
| 4.6 | Author Contributions | 80 |
| 4.7 | Acknowledgements | 81 |
| 4.8 | Conflicts of Interest | 81 |
| CHAPTER 5 CHARACTERIZATION OF THE RELATIONSHIP BETWEEN VOLTAGE CHANGES AND [Ca²⁺]_i TRANSIENTS USING SIMULTANEOUS WHOLE-CELL PATCH-CLAMP ELECTROPHYSIOLOGY AND LIVE CALCIUM IMAGING | | 83 |
| 5.1 | Introduction | 84 |
| 5.2 | Materials & Methods | 85 |
| 5.2.1 | Animals | 86 |
| 5.2.2 | Mouse primary enteric nervous system cultures | 86 |

| | | |
|---|---|------------|
| 5.2.3 | Immunohistochemistry | 87 |
| 5.2.4 | Whole-cell patch-clamp electrophysiology | 88 |
| 5.2.5 | Calcium imaging | 89 |
| 5.2.6 | Photostimulation of Channelrhodopsin 2 (ChR2) | 89 |
| 5.2.7 | Fast (kHz) calcium imaging | 90 |
| 5.2.8 | Data presentation and statistical analysis | 90 |
| 5.3 | Results | 90 |
| 5.3.1 | Immunohistochemical characterization of mouse primary myenteric neuron cultures | 90 |
| 5.3.2 | Electrophysiological properties of cultured myenteric neurons | 92 |
| 5.3.3 | Detection of action potentials elicited by illumination of blue light | 93 |
| 5.3.4 | Relation between action potential firing and $[Ca^{2+}]_i$ transients | 94 |
| 5.3.5 | $[Ca^{2+}]_i$ transients properties evoked by repetitive short or long depolarizing current steps | 100 |
| 5.3.6 | Potassium induced depolarization and Ca transients | 101 |
| 5.3.7 | Nicotinic receptor agonist stimulation | 103 |
| 5.4 | Discussion | 105 |
| 5.4.1 | Cell culture | 106 |
| 5.4.2 | Electrical properties of cultured mouse enteric neurons | 106 |
| 5.4.3 | Relationship between AP-firing and calcium transients in mouse enteric neurons | 107 |
| 5.4.4 | Cholinergic transmission | 109 |
| 5.4.5 | Activation of enteric neurons using channelrhodopsin | 110 |
| 5.5 | Conclusion | 110 |
| 5.6 | Author Contributions | 111 |
| 5.7 | Acknowledgements | 111 |
| 5.8 | Conflicts of Interest | 111 |
| CHAPTER 6 GENERAL DISCUSSION AND FUTURE PERSPECTIVES | | 113 |
| 6.1 | General Discussion | 114 |
| 6.1.1 | Application of virus tracing tools in ENS investigation | 115 |
| 6.1.2 | Application of optogenetic tools in ENS investigation | 116 |

| | | |
|---|--|------------|
| 6.1.3 | Application of simultaneous electrophysiological recording with optical imaging in ENS investigation | 118 |
| 6.2 | Future Perspectives | 120 |
| CHAPTER 7 SUMMARY | | 123 |
| 7.1 | English summary | 124 |
| 7.2 | Nederlandse Samenvatting | 126 |
| REFERENCES | | 129 |
| PERSONAL CONTRIBUTION AND CONFLICTS OF INTERESTS | | 148 |
| ACKNOWLEDGEMENTS | | 149 |
| CURRICULUM VITAE | | 152 |
| LIST OF PUBLICATIONS | | 153 |
| PARTICIPATION AT INTERNATIONAL CONFERENCES | | 154 |

List of Abbreviations

| | |
|----------------------------------|--|
| [Ca ²⁺] _i | Intracellular calcium concentration |
| 5-HT | Serotonin |
| ACh | Acetylcholine |
| AChE | Acetylcholine esterase |
| AH | After-hyperpolarizing |
| AoT | Activity over time |
| AP | Action potential |
| ATP | Adenosine triphosphate |
| ChAT | Choline acetyltransferase |
| ChR2 | Channelrhodopsin 2 |
| CIPO | Chronic intestinal pseudo-obstruction |
| CMMC | Colonic migrating motor complex |
| CMV | Cytomegalovirus |
| CNS | Central nervous system |
| DMPP | Dimethylphenylpiperazinium |
| DNA | Deoxyribonucleic acid |
| ECL | Erythrina cristagalli lectin |
| eGFP | Enhanced green fluorescent protein |
| E8.5 | Embryonic day 8.5 |
| EGC | Enteric glia cell |
| ENS | Enteric nervous system |
| ER | Endoplasmic reticulum |
| ES | Electrical stimulation |
| fAHP | Fast after-hyperpolarizing potential |
| fEPSP | Fast excitatory postsynaptic potential |
| GI | Gastrointestinal |
| GECI | Genetically encoded calcium indicator |
| HBSS | Hank's balanced salt solution |
| HCN | Hyperpolarization nucleotide-gated |

| | |
|------------------|--|
| HSCR | Hirschsprung disease |
| HVA | High-voltage activated |
| ICav | TTX-insensitive Ca ²⁺ current |
| ICC | Interstitial cells of Cajal |
| I _h | Hyperpolarization-activated H-current |
| IK _{Ca} | Intermediate conductance calcium-dependent potassium channel |
| IPAN | Intrinsic primary afferent neuron |
| IV | Intravenously injection |
| LMMP | Longitudinal muscle and myenteric plexus |
| mAChR | Muscarinic ACh receptors |
| MP | Myenteric plexus |
| nAChR | Nicotinic acetylcholine receptors |
| NO | Nitric oxide |
| nNOS | Neuronal nitric oxide synthase |
| NPY | Neuropeptide Y |
| rAAV | Recombinant adeno-associated virus |
| S neurons | “Synaptic” class of enteric neurons |
| sAHP | Slow after-hyperpolarizing potential |
| sEPSP | Slow excitatory postsynaptic potential |
| sIPSP | Slow inhibitory postsynaptic potential |
| SMC | Smooth muscle cell |
| SMP | Submucosal plexus |
| SOM | Somatostatin |
| SS | Single strand |
| SP | Substance P |
| TTX | Tetrodotoxin |
| vAChT | Vesicular acetylcholine transporter |
| VDCC | Voltage-dependent calcium channel |
| VGSC | Voltage-gated sodium channel |
| VIP | Vasoactive intestinal peptide |

CHAPTER 1

General introduction

Li Zhiling[#], Fung Candice[#], Vanden Berghe Pieter

Laboratory for Enteric NeuroScience (LENS), Translational Research Center for Gastrointestinal Disorders (TARGID), Department of Chronic Diseases, Metabolism and Ageing, University of Leuven, Leuven, Belgium

*This chapter has been submitted as a book chapter of “**Encyclopedia of Gastroenterology 2nd Edition**” entitled “**Electric activity and neuronal components in the gut wall**”.*

1 THE ENTERIC NERVOUS SYSTEM

The gastrointestinal tract (GI) is our sole route of nutrient absorption and we depend on it to break down food into absorbable nutrients and ultimately eliminate waste. At the same time, the GI tract can also protect itself from toxins, physical damage, irritants, and the multitude of bacteria that reside within its length. Fortunately, coordination of these complex and essential activities is largely controlled by the local nervous system, the enteric nervous system (ENS) ¹. In this thesis, we aim to investigate different circuits in the ENS that are responsible for generating different gut motility patterns. We use novel technology to interrogate enteric neural circuits: viral transduction of enteric neurons using adeno-associated viral vectors (introduced in **section 2** and **Chapter 3**) and optogenetic imaging and manipulation (**section 3** and **Chapter 4 and 5**).

1.1 Organization of the enteric nervous system

The ENS is the largest part of the peripheral nervous system with a total number of 200-600 million enteric neurons in humans, which is approximately equal to the number of neurons in the spinal cord ². The ENS is a complex neuro-glia network embedded within the wall of the gastrointestinal tract where it is organized in two concentric ganglionated layers in mammals: the submucosal (Meissner's) plexus being the innermost layer, located between the muscularis mucosa and circular muscle, and the outer myenteric (Auerbach's) plexus in between the circular and longitudinal muscle (**Figure 1.1.1**). The myenteric plexus is a continuous network from the upper esophagus to the internal anal sphincter, while the submucosal plexus is predominately present in the small and large intestine. In the ENS, there are different types of neurons ². The enteric circuitry formed by these various neurons autonomously controls many aspects of gastrointestinal function, such as gut motility, which results from contraction and relaxation of the intestinal muscle, the control of transmucosal fluid flux, blood flow and secretion. In small animals, neurons of the myenteric plexus are mainly responsible for controlling different motility patterns, while submucosal neurons are involved in regulating secretion and absorption.

However, in humans and larger animals, the submucosal plexus is also involved in GI motility ² and the organization of the submucous plexus is somewhat different in that a third neuronal layer can be defined ³. Some neurons are even located in the mucosa of the gut in human ^{2,4}. Due to its large degree of independence of the central nervous system, the ENS has been nicknamed the “second brain” or “little brain” ⁵.

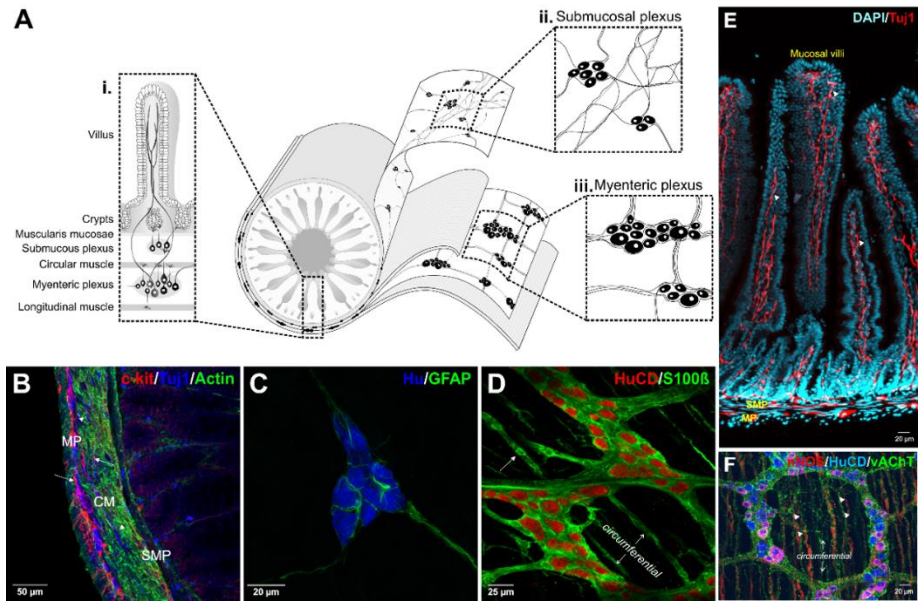


Figure 1.1.1 | Cellular architecture of the intestinal wall.

A, Schematic of the concentric layers of the intestinal wall with circular and longitudinal muscle and myenteric and submucosal nerve layers. Ai-iii. Detailed schematics of the composition of a (i) intestinal villus and crypt; (ii) a submucosal ganglion and (iii) a myenteric ganglion. **B**, Immunohistochemical staining of a radial section of the mouse intestinal wall labeled for an ICC marker (c-Kit, red), muscle (actin, green) and nerves (β III tubulin, blue). Tuj1-immunoreactive nerves form close appositions with ICC (arrows) and α -SMA+ cells (arrowheads) in the MP, CM and SMP. **C**, Typical example of a submucosal ganglion labeled for the neuronal marker Hu (blue) and the glial marker (glial fibrillary acidic protein, GFAP, green). **D**, Typical example of a myenteric ganglion with neurons (HuCD, red) and glial cells (here labeled with S100 β , green). In addition, S100 β + cells are also present within the circular muscle layer (arrows). **E**, Cryosection of the jejunum stained for DAPI (nuclei, cyan) and Tuj1 (red) to identify enteric neurons and their processes (arrowheads) in the MP, SMP and mucosal villi. **F**, Triple immunolabelling of a myenteric plexus preparation

showing nNOS (nitroergic neurons, red), vAChT (a marker of excitatory neurons, green) and HuCD (blue). nNOS+ and vAChT+ varicosities are present throughout the plexus and innervating the circular muscle (arrowheads). CM, circular muscle; ICC, interstitial cells of Cajal; MY, myenteric plexus; SMP, submucosal plexus; α -SMA, α -smooth muscle actin; nNOS, neuronal nitric oxide synthase; vAChT, vesicular acetylcholine transporter. Panel E and F are from Hao et al., Dev Biol. 2016 ⁶.

1.2 ENS development

All the neurons and glia of the ENS arise from neural crest cells, which migrate into the gut during development. The majority of the ENS arises from a pool of vagal neural crest cells emigrating from the neural tube adjacent to somites 1-7 ^{7,8}. During development, they migrate into the developing oesophagus and stomach, and colonize the developing small and large intestines in a rostral-to-caudal wave. In the developing mouse, they enter the stomach at embryonic day (E)10.5, and complete migration by E14.5 ⁹. This is the longest migration of cells during embryonic development, and takes place over 3 weeks during human fetal development ¹⁰. As they migrate, these enteric neural crest-derived cells proliferate and differentiate into the various different subtypes and enteric neurons and glia. They begin to become electrically active, and express neurotransmitter synthetic markers by E11.5 in the mouse ^{11,12}. The ENS is not mature at birth and there is continued postnatal maturation, particularly in neuronal morphology and electrophysiology ¹³. When communication between individual enteric neurons and smooth muscle cells, or between enteric neurons and interstitial cells develops, is not well understood ⁶.

1.3 Enteric neurons

1.3.1 Morphological classification of enteric neurons

The morphological classification scheme stems from the founding work of Dogiel (1899), who was the first to illustrate and define three distinct types of enteric neurons, which we now refer to as Dogiel types I, II, and III ¹⁴ (**Figure 1.1.2**). Type I neurons are uniaxonal and have short lamellar dendrites. Type II neurons have a large

round or oval and smooth cell body, and are multi-axonal with long processes that tend to project circumferentially. While the presence of type III neurons as described by Dogiel has not been definitively verified by modern methods, it is occasionally used to refer to filamentous neurons with long branched processes¹⁵. This nomenclature system has since been expanded to include up to 6 types, to allow classification of the additional neuron subtypes found in pig small intestine¹⁶. While larger neurons can be readily distinguished by the shape of their cell bodies, this is often less clear for smaller neurons. Accordingly, a separate morphological class has been termed “small neurons”, which based on their projections, mainly comprise motor and secretomotor neurons^{14,17,18}. In guinea pig intestine, there is a tight correlation between the AH characteristic and Dogiel type II morphology, while S neurons are uniaxonal Dogiel type I or display filamentous morphologies¹⁹. However, this is not always the case for other species^{20,21,22,23}.

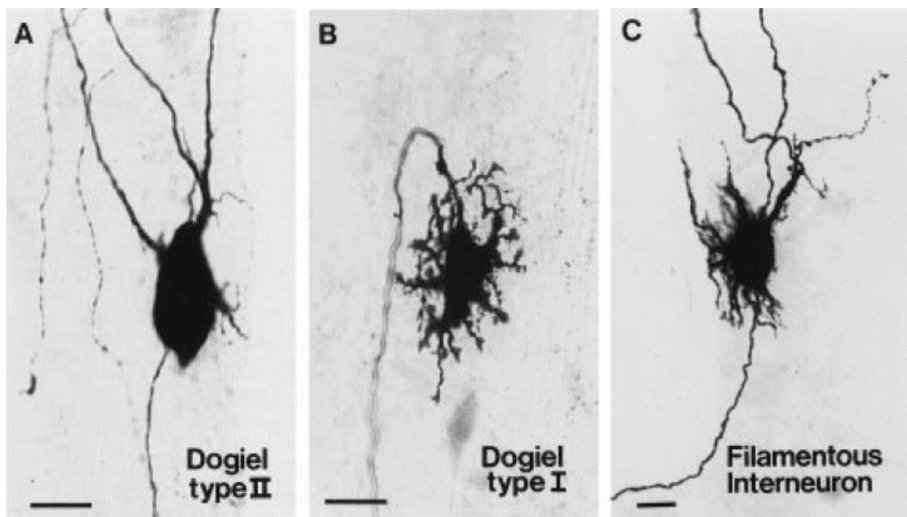


Figure 1.1.2| Examples of the morphology of a Dogiel type I, Dogiel type II and Filamentous neuron. From Clerc et al. 1998²⁴.

1.3.2 Electrophysiological classification of enteric neurons

Back in the 1970s, Nishi and North²⁵ used sharp electrodes to record enteric neuronal activity in the guinea pig ileum. This information provided the basis for the

electrophysiological classification of enteric neurons, which is still in use. Around the same time, Hirst et al., (1974)²⁶ first introduced the terms AH (after-hyperpolarizing) and S (synaptic) based on different properties of two distinctly behaving groups of enteric neurons in the guinea pig duodenum. AH neurons are named after their prominent “slow after-hyperpolarizing potential” (sAHP) following action potential (AP) firing, while S neurons are termed after the “synaptic” potentials (mainly fast excitatory postsynaptic potentials, fEPSPs) they receive (**Figure 1.1.3**). Later, similar intracellular recordings were performed in different regions of the guinea pig gut including stomach corpus²⁷, antrum²⁸, proximal²⁹ and distal colon³⁰. In each of the regions AH and S-neurons were identified. Additional studies have characterized enteric neurons in also other species, such as pig²², rat³¹, human^{23,32,33} and mouse^{20,21}. Again the two electrophysiological classes (AH and S neurons) as defined in the ‘70s have been found consistently across these species.

Membrane potential events

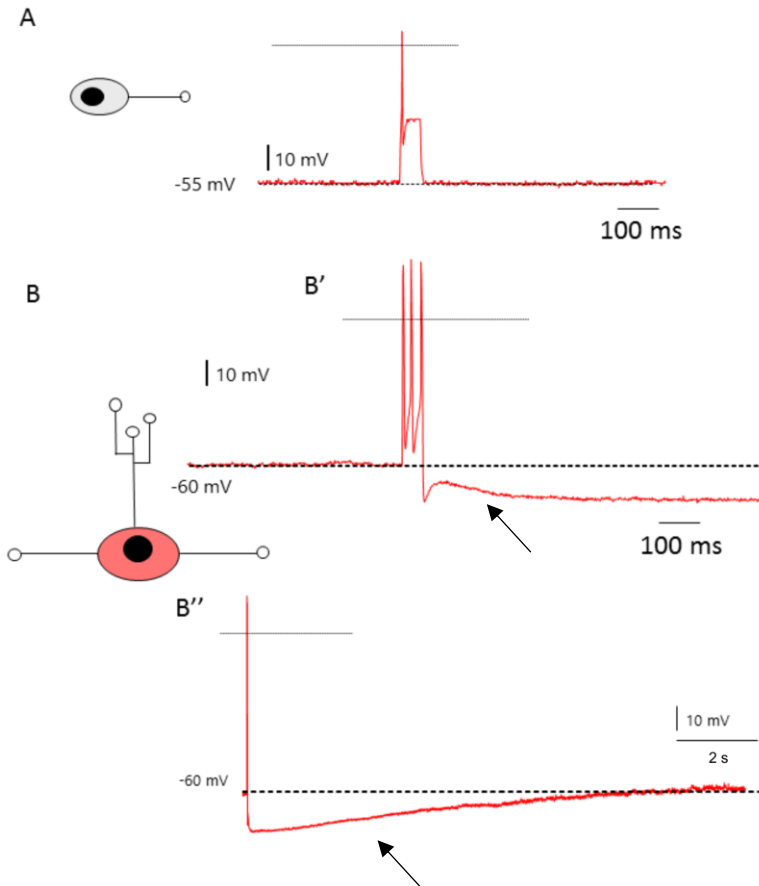


Figure 1.1.3| Schematic representation of two membrane potential events that have been used to classify enteric neurons in S- and AH-type.

A, S-(synaptic) types fire single or multiple action potentials after which the membrane potential immediately returns to baseline. **B**, In AH-type neurons, action potential firing is followed by a prolonged after-hyperpolarization (arrow), which temporarily prevents the neuron from being excited again. **B'** and **B''** show a prolonged after-hyperpolarization (arrow) of multiple firing and single firing neurons, respectively. Recordings performed on guinea pig tissue using sharp electrode.

1.3.2.1 AH neurons

AH neurons typically have a “hump” or “inflection” on the repolarizing phase of their AP, which is followed by a prominent sAHP^{26,34}. This hump results from the Ca²⁺ influx through the plasma membrane via voltage-dependent Ca²⁺ channels (VDCCs) during AP firing²⁴. In AH neurons two inward currents have been found to underlie the AP: a tetrodotoxin (TTX)-sensitive Na⁺ current (*I*_{Na}) and a TTX-insensitive Ca²⁺ current (*I*_{Ca})^{25,35,36}. In the presence of TTX, which blocks most of the Na⁺ current, this Ca²⁺ current is still able to produce small amplitude, broad duration AP. Studies using different Ca²⁺ channel blockers in guinea pig have shown that the TTX-resistant current is near abolished by inhibiting N-type high-voltage activated (HVA) calcium channels with ω -conotoxin-GVIA or ω -conotoxin-MVIIA, indicating that N-type channels are the predominant calcium channels involved in the AH neurons' AP formation³⁶. R-type channels also contribute to the Ca²⁺ current^{36,37}. A TTX-resistant Na⁺ current is also present in guinea pig AH neurons and expression of the TTX-insensitive voltage-dependent Na⁺ channel, Nav1.9, has been identified in guinea pig, rat and mouse^{38,39}. In mouse enteric neurons, it appears that almost all myenteric neurons, and not just AH neurons, exhibit a TTX-resistant Na⁺ current³⁸.

Generally, AH neurons fire only one or at most a couple of APs, as the sAHP hyperpolarizes the cell typically for 2 to about 30 seconds after firing^{25,26,35} (**Figure 1.1.3**). It must be noted that, following an AP, all neurons exhibit a fast after-hyperpolarizing potential (fAHP), however this normally lasts only tens of milliseconds, three orders of magnitude shorter than the sAHP observed in AH myenteric neurons. Though voltage sensor recordings were successfully used to report AP spiking in guinea pig myenteric neurons^{29,40}, slow after-hyperpolarizations were not able to be detected using optical technology due to the relatively small amplitude and slow kinetics of the hyperpolarization.

Simultaneous electrophysiological recordings and Ca²⁺ imaging have shown that a single AP in an AH neuron is capable of inducing a detectable [Ca²⁺]_i transient in guinea pig enteric neurons⁴¹⁻⁴³. Although Ca²⁺ entry through VDCCs is essential, an

amplification step by Ca^{2+} released from intracellular stores, such as the endoplasmic reticulum (ER), is necessary to raise the cytosolic Ca^{2+} concentration sufficiently. This increase in cytosolic Ca^{2+} in turn activates the opening of K^+ channels, which are responsible for the sAHP⁴⁴. The mechanism underlying this prolonged sAHP involves intermediate conductance Ca^{2+} -activated K^+ channels (IK_{Ca}), which are sensitive to the IK_{Ca} antagonists clotrimazole and TRAM-34^{21,45-48}. The IK_{Ca} channel is expressed in AH neurons in several species, including mouse, rat and human^{47,49,50}. Single-channel recordings also suggest that the channel underlying the sAHP is similar to that of the IK_{Ca} based on its conductance properties, sensitivity to Ca^{2+} and voltage dependency²¹. However, it is likely that other Ca^{2+} -activated K^+ channels are also involved, since the large conductance Ca^{2+} -dependent K^+ channel (BK channel) antagonists, charybdotoxin and iberiotoxin, abolish the sAHP⁵¹ while the IK_{Ca} channel inhibitor, TRAM-39 did not⁵². The repolarization of the membrane potential following a sAHP depends on the removal of Ca^{2+} from cytoplasm, in which mitochondria play an active role⁴³.

When I_{AHP} is triggered following the AP, the resultant hyperpolarization is sufficient to reduce subsequent APs⁵³. Especially during the sAHP, which critically determines the excitability of AH neurons, a long refractory period is established, during which they cannot partake in signal transmission. The sAHP acts as a gate in the circuitry and plays an important role in determining the functional output of enteric circuitries in the gut⁵⁴. For instance, pharmacological inhibition of the sAHP in AH neurons directly increased the colonic motility of rats⁵⁵ and the duration of contractions in nutrient-induced segmentation in guinea pigs⁵⁶. This gating mechanism was also shown to be modulated, as for instance during inflammation, where a reduction in sAHP amplitude leads to an increase in the excitability of AH neurons in models of gut inflammation⁵⁷⁻⁵⁹. Also interestingly, it has been reported that intestinal microbiota are involved in regulating the excitability of AH neurons by decreasing IK_{Ca} opening and the sAHP, however, the mechanisms by which luminal microbiota communicate with the host nervous system is not well understood⁶⁰⁻⁶².

Apart from the specific K^+ currents, also the hyperpolarization-activated H-current (I_h) is a distinguishing feature of AH neurons that is not observed in enteric S neurons^{21,36,63}. It is an inward current activated by hyperpolarization (hence H) from the resting potential and is an important modulator of AP firing frequency in many excitable cells⁶⁴. I_h was first studied in cardiac pacemaker cells⁶⁵ and other mammalian neurons, such as cerebellar Purkinje cells, where its presence can modulate the resting potential and the AP firing frequency^{66,67} via cAMP-sensitive or resistant pathways⁶⁴. The I_h current results from the passage of non-specific cations through hyperpolarization-activated cyclic nucleotide-gated (HCN) channels⁶³, which are blocked by extracellular cesium^{21,36,66}. Using immunostaining and intracellular recordings, Xiao et al. demonstrated that HCN2 is the most important channel that mediates this current in AH neurons of guinea pig, mouse and rat⁶⁸. Despite this information, the actual role of I_h in AH neurons is still not completely understood. It has been reported that I_h may be involved in the generation of anodal break APs, which fire to hyperpolarizing current steps⁵⁹, and regulation of neuronal excitability, since induced inflammation increases hyperpolarization-activated AP firing as well as I_h current⁵⁷⁻⁵⁹.

1.3.2.2 S neurons

S neurons were named after the fact that they receive synaptic input (fEPSPs) when the interganglionic connectives are stimulated^{25,26,34}. Cholinergic neurotransmission is the most prominent form of excitatory transmission between enteric neurons⁶⁹⁻⁷¹ and nicotinic acetylcholine receptors (nAChRs) mediate most fEPSPs observed in the ENS^{72,73}. Cholinergic fEPSPs in submucosal and myenteric neurons are abolished by nicotinic antagonists such as hexamethonium, tubocurarine or mecamylamine^{25,26,71,74,75}. Though most of this information is derived from guinea pig myenteric neuron recordings, nAChR-mediated fEPSPs also occur in submucosal and myenteric neurons of the mouse intestine^{20,37,76}. Fast cholinergic transmission involving nicotinic receptors is established early on during gut development⁷⁷.

Other transmitters that mediate fEPSPs include 5-HT and ATP that act on 5-HT₃ and P2_x receptors respectively ^{70,78-81}. Exogenous 5-HT application depolarizes all submucosal neurons and some myenteric neurons ^{54,82,83}, and evokes fEPSPs via 5-HT₃ receptors ^{84,85}. However, comparatively few neurons display 5-HT₃-mediated fEPSPs in response to electrically-evoked endogenous 5-HT release ⁸⁶. Follow-up studies have further shown that the non-cholinergic component of electrically-evoked fEPSPs in myenteric neurons is partly sensitive to purinergic P2_x antagonists. Purinergic signaling via P2_x receptors also contributes to fEPSPs in myenteric neurons of the mouse intestine ^{20,37,87}.

Based on whether or not AP firing is continuous during long intracellular depolarizing current pulses, S neurons can be further categorized into tonically firing or phasically firing (or rapidly-accommodating) neurons ^{24,34}. The first are slowly-accommodating neurons, which discharge APs for a long period of time, while the latter are rapidly accommodating and discharge one or a few APs. It has been suggested that different functional classes of S neurons may relate to this electrophysiological division, where tonically firing neurons include circular muscle motor neurons, longitudinal muscle motor neurons and ascending or descending interneurons ⁸⁸. However, this mode of subdivision of S neurons requires further study.

The APs exhibited by S neurons are abolished by TTX and are independent of Ca²⁺. Previous studies in guinea pig tissue showed that, unlike AH neurons, most single AP from S neurons do not elicit detectable [Ca²⁺]_i changes ^{43,89}. However, in tonically firing S neurons, trains of APs did elicit a slow [Ca²⁺]_i increase of which the amplitude increased with the number of APs ^{43,89}. Whether this also occurs in other species is unclear.

The maximal amplitude of S-neuron APs is generally smaller than that of AH neurons, which seems consistent over a wide range of species and gut regions, including guinea pig small intestine (S neurons: 56 ± 9 mV vs. AH neurons: 72 ± 10 mV) ^{24,36} and colon (S neurons: 53 ± 1.1 mV vs. AH neurons: 77 ± 4.1 mV) ²⁰, as well as mouse colon (S neurons: 48 ± 1.1 mV vs. 78 ± 2.3 mV) ²⁰. However, the half-duration of the AP

varies considerably depending on the species, the recording techniques used and the composition of the intracellular solution. The AP is generally broader in AH compared to S neurons due to the extra Ca^{2+} influx, as measured by conventional intracellular recordings in guinea pig enteric neurons^{20,24,90}. However, this difference was not observed in whole cell patch clamp recordings from guinea pig duodenum³⁶ or in conventional intracellular recordings from mouse colon²⁰. Apart from possible species differences, the composition of the intracellular solution in whole cell patch clamp recording also plays an important role in the detection of AP half-duration differences between two classes of enteric neurons²¹.

1.3.2.3 Electrophysiological properties of enteric neurons in human

Due to limited access to tissue, difficulties with dissection, and poor visibility of enteric ganglia, there are only few studies on the electrophysiological identification of enteric neurons from human tissue²³. More recent studies in healthy³² and pathological³³ human colon, demonstrated that myenteric neurons, similarly as in rodents, can be grouped into S and AH subtypes. To circumvent the difficulties of dissection, voltage sensors can be used, and although the signals have low signal to noise ratios, they do suffice to compare AP firing rates in human submucous neurons as present in biopsies⁹¹.

1.3.2.4 Neurochemical coding of enteric neurons

The “neurochemical coding” of enteric neurons was established by the pioneering work of Costa and Furness that began in the 1980s. Different subtypes of enteric neurons are equipped with distinct sets of molecular constituents such as their primary transmitters, the synthesizing enzymes for these transmitters, cytoskeletal and calcium-binding proteins. Accordingly, the concept of this classification system is that different subsets of enteric neurons can be distinguished by their neurochemistry as revealed using immunohistochemical labelling⁵³. The primary transmitters used by enteric neurons are generally well conserved between gut regions and across species, although the specific neurochemical coding can vary

(**Table 1.1.1**). For instance, calcitonin gene-related peptide (CGRP) is expressed in myenteric Dogiel type II neurons of the mouse, but not the guinea pig⁹², pig⁹³ and human¹⁸. The neurochemical characteristics of enteric neurons together with their morphology can also correlate to their electrophysiological properties. For example, in the guinea pig, calbindin- and substance P-immunolabeling mark type II neurons, which typically display AH-type electrophysiology.

Table 1.1.1 | Proportions of all neurons attributed to different functional classes in myenteric ganglia of the guinea-pig and mouse small intestine

| Neuron type | Guinea-pig small intestine | | | Mouse small intestine | | |
|---|--------------------------------|-----------------------|------------|--------------------------------------|------------------------------------|----------------|
| | Code | Shape | Proportion | Code | Shape | Proportion |
| Intrinsic primary afferent neuron | ACh/NeuNcyt/IB4, 80% calbindin | Type II | 26% | ACh/NF/CGRP/calbindin +/- calretinin | Type II | 26% |
| Inhibitory circular muscle motor neuron | NOS/VIP | Type I | 16% | NOS/VIP +/- NPY | Type I | 23% |
| Inhibitory longitudinal muscle motor neuron | NOS/VIP | Small Type I | 2% | NOS/VIP | Small, no obvious dendrites | 3% |
| Excitatory circular muscle motor neuron | ACh/TK | Medium Type I | 12% | ACh/TK +/- calretinin | Small/medium, no obvious dendrites | 21% |
| Excitatory longitudinal muscle motor neuron | ACh/TK/calretinin | Small Type I | 25% | ACh/calretinin +/- TK | Small, no obvious dendrites | 13% |
| Descending interneurons | ACh/NOS/VIP | Type I | 5% | ACh/NOS | Type I | 3% |
| Descending interneurons | ACh/5-HT | Type I | 2% | ACh/5-HT | Type I | 1% |
| Descending interneurons | ACh/SOM | Type III/ filamentous | 4% | ACh/SOM/calretinin | Filamentous | 4% |
| Ascending interneurons | ACh/TK/calretinin | Type I | 5% | ACh/TK +/- calretinin | Type I | 4% (estimated) |
| Intestinofugal neurons | ACh plus a range of peptides | Type I | <1% | Not identified | Not known | Not known |
| Tyrosine hydroxylase neurons | TH | – | Rare | TH | Type I | <0.5% |

Abbreviations: ACh, acetylcholine; CGRP, calcitonin gene-related peptide; 5-HT, 5-hydroxytryptamine; IB4 isolectin B4; NeuNcyt cytoplasmic NeuN, NF, neurofilament 145 kDa; NOS, nitric oxide synthase; NPY, neuropeptide Y; SOM, somatostatin; TH, tyrosine hydroxylase; TK, tachykinin; VIP, vasoactive intestinal peptide. From Furness et al. 2006^{2,92} and Qu et al. 2008⁸⁹.

1.4 Glia

Enteric glia cells (EGCs) are another major cellular population in the myenteric and submucosal ganglia of the ENS and in extraganglionic spaces. They share many similarities with astrocytes in the CNS, such as morphology, molecular expression and functionality⁹⁴. Hence, they are considered “astrocyte-like glia” of the GI tract⁹⁵.

Although the ENS has been studied for several decades, our knowledge of the physiological properties of EGC still lags behind that of enteric neurons. Only recently, the morphology and classification of the enteric glia was re-examined using genetically-directed sparse labelling⁹⁶. Four distinct subtypes of EGCs located in the different layers of the adult mouse gut wall were defined. It was also demonstrated that purinergic activation elicits differential calcium responses in intraganglionic vs. extraganglionic glia⁹⁶, which further supports the notion that there are distinct populations of EGC also at the functional level. In addition to the traditional roles, EGCs play in nourishing and protecting the enteric neurons, they have more recently been shown to be actively involved in regulating gut motility, synaptic transmission, gut barrier maintenance, as well as in crosstalk between the ENS and innate immune system^{94,97,98}. Taken together, it is clear that EGCs are key mediators in gastrointestinal physiology and pathophysiology. Nonetheless, further studies are necessary to better understand the mechanisms by which glia mediate gut homeostasis.

1.5 Other cell types in the gut

Apart from the enteric neurons and glia cells, there are also other cell types residing the GI tract, such as different layers of interstitial cells of Cajal (ICCs) that contribute to electrical coupling of adjacent muscle regions⁹⁹; or muscularis macrophages, locating in the muscularis externa of the GI tract, which are essential for tissue homeostasis during steady-state conditions as well as during disease¹⁰⁰.

1.6 Control of Gastrointestinal Motility and Circuitry of the ENS

As one of its main functions, the GI tract generates a variety of motility patterns and these can differ depending on the region. Three main motility patterns are observed in the mammalian small intestine: (i) segmentation, which consists of alternating contractions and relaxations in both the oral and anal directions and facilitates local mixing with secretions (e.g. Trypsin) and absorption (e.g. water), (ii) peristalsis, which propagates GI contents unidirectionally (generally anally), and (iii) migrating motor

complexes (MMCs), which mostly originate in the stomach or proximal duodenum and can travel to the distal end of the ileum ¹⁰¹. In animals that feed intermittently, such as humans, segmentation and peristalsis occur following a meal, while MMCs occur in the unfed state. By contrast, in animals that feed continuously, such as sheep, MMCs occur constantly ¹⁰². MMCs consist of four distinct phases, but the most important is phase III, where strong contractions lasting a few minutes sweeps slowly along the GI tract to eliminate undigested food, mucosal secretions, and epithelial debris in the fasted state ¹⁰³.

The large intestine similarly displays both peristaltic and mixing contractile patterns, which enhances exposure of luminal contents to the absorptive mucosa and facilitates its transport along the length of the colon ². However, while colonic migrating motor complexes (CMMCs) have been identified in guinea pig and mouse, it does not exist in human ^{101,104,105}. Although CMMCs are the dominant pattern to propel colonic content in mice, this remains elusive in other species ¹⁰⁵.

There is accumulating evidence suggesting that the coordinated movements of the GI tract mentioned above are governed by a complex interplay between ENS and smooth muscle cells (SMCs), ICC, platelet-derived growth factor receptor (PDGFR) α + cells, and extrinsic neurons ¹⁰⁶⁻¹⁰⁸. Over a century ago, it was observed that peristaltic motility occurs *in vivo* even after the extrinsic nerves to the bowel were severed. It was later shown that segmentation and propulsive movements of the small intestine are neurally-controlled since they are abolished by the Na⁺ channel blocker TTX. More recently, the rhythmic firing in the ENS was shown to underlie the rhythmic electrical depolarization in smooth muscle which generates CMMCs ¹⁰⁹. Therefore, the ENS is likely the primary inducer of complex motility patterns ^{110,111}. To “decide” what to do, intrinsic sensory neurons of the ENS respond to the mechanical or chemical stimulation of the intestinal wall. Signals are then passed to interneurons, which project in both oral (ascending) and anal (descending) directions, and contact excitatory and inhibitory motor neurons, respectively (**Figure 1.1.4**). The enteric motor neurons then activate the contraction and relaxation of the final effectors: the

circular and longitudinal muscle, and this is mediated via ICC and PDGFR α + cells. In following sections, I will discuss the different functional subtypes of myenteric neurons.

Myenteric wiring and synaptic communication

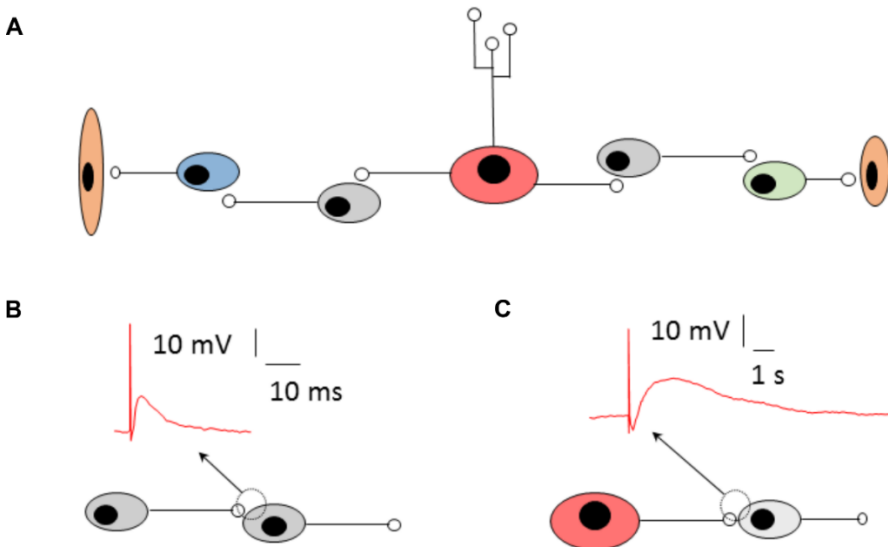


Figure 1.1.4 | Myenteric wiring and synaptic communication.

A, Schematic outlining the most elementary circuit in the ENS: an intrinsic sensory neuron (ISN, red) that is activated by pressure or chemicals from the mucosa, in turn activates interneurons (grey) that synapse onto inhibitory (green) and excitatory (blue) motor neurons, leading to (aboral) inhibition and (oral) excitation of the muscle (brown) respectively. The net result of the contractile and inhibitory events is a peristaltic wave that propagates aborally along the bowel. **B - C**, show a schematic representation of the two main synaptic events observed in the ENS. **B**, is a fast excitatory postsynaptic potential that lasts 10-20 ms, while slow EPSP in **C**. depolarizes the postsynaptic membrane for several seconds. Recordings performed on guinea pig tissue using sharp electrode.

1.6.1 Intrinsic sensory neurons

The largest endocrine system resides in the GI tract, where it is comprised of individually scattered enteroendocrine cells (EECs), such as 5-HT-containing

enterochromaffin (EC) cells, distributed along the entire GI mucosa in the crypts and villi representing 1% of the total gut epithelium cell population ¹¹². EECs provide the first level of integration of the information from the gut lumen and upon stimulation release signaling molecules that can activate intrinsic sensory neurons (ISNs) ¹¹².

ISNs or intrinsic primary afferent neurons (IPANs), are necessary for transducing and encoding the durations, intensities, and patterns of physiologically relevant stimuli including intestinal distention, mechanical distortion of the mucosa, and luminal contents, as well as noxious substances ⁵⁰.

Myenteric ISNs provide slow synaptic inputs to other myenteric ISNs, interneurons and motor neurons ¹¹³, and to submucosal neurons ¹¹⁴. Submucosal ISNs similarly innervate other submucosal ⁷⁵ and myenteric neurons ¹¹⁵. ISNs predominantly have local projections with several long circumferentially-directed processes, although a small population of myenteric AH neurons have long aboral projections ¹¹⁶. Most myenteric AH neurons receive slow excitatory inputs, whereas fast EPSPs occur less frequently, but when observed usually have a lower amplitude (<5 mV) than those recorded in S neurons (=> 20 mV) ^{13,113,117,118}.

Myenteric AH neurons are equipped with mechanosensitive ion channels that open upon distortion of their processes that allow them to respond to mechanical stimuli (e.g. muscle contraction) by Ap firing ^{24,119}. However, the ion channels involved remain unknown. Interestingly, it was also found that the cell soma could respond to stretch, by a hyperpolarization that involves large-conductance voltage-sensitive K⁺ (BK-like) channels ¹¹⁹. The notion that AH/Dogiel type II neurons are the only mechanosensitive neurons is a matter of contention. Some myenteric S-type neurons can also display mechanosensitive properties ¹²⁰⁻¹²². Myenteric ISNs are also chemosensitive, with projections to the mucosa ¹²³, and respond to fatty acids as well as acid and basic solutions ^{124,125}. Furthermore, a subset of these neurons also respond to mechanical distortion of the mucosa ¹²⁵, indicating that ISNs are polymodal.

Submucosal ISNs also have sensory nerve endings in the mucosa that can indirectly detect mechanical distortion of the mucosa via 5-HT released from enteroendocrine cells in the epithelium^{75,126}. In addition, submucosal ISNs project within the submucosal plexus¹²⁷, and to myenteric neurons¹¹⁵. Though the projection length of submucosal ISNs is considerably shorter, like myenteric ISNs, they have projections with dominant aboral polarity within the plexus¹²⁸. Evidence for the presence of submucosal ISNs in the mouse is currently lacking as only S-type submucosal neurons have been reported thus far in the mouse colon^{76,129}.

1.6.2 Interneurons

Interneurons within the myenteric plexus can be defined by the direction of their projections: ascending interneurons project orally and descending interneurons project aborally. These neurons are often further subdivided by their neurochemical coding. In the guinea pig small intestine, there is one class of ascending interneurons that expresses calcitonin and substance P (SP), and three classes of descending interneurons which contain either neuronal nitric oxide synthase (nNOS), somatostatin (SOM), or 5-HT¹³⁰. Neurochemically similar neurons are found in the mouse ileum^{92,131-133}.

Each of the different classes of myenteric interneurons connect with like interneurons to form chains that extend along the length of the intestine⁵³. Ascending interneurons receive inputs from local ISNs and innervate excitatory motor neurons¹³⁴. NOS/VIP- and SOM-immunoreactive descending interneurons project to inhibitory motor neurons^{135,136}. NOS/VIP interneurons also receive inputs from ISNs¹³⁷. 5-HT descending interneurons primarily project to other 5-HT interneurons but not inhibitory motor neurons¹³⁸. 5-HT interneurons are the sole source of neuronal 5-HT in the ENS¹³⁹ and 5-HT₃-mediated fast EPSPs occur in a small population of S neurons^{80,86}; taken together, these data suggest their involvement in descending excitation of neurons. Further, 5-HT interneurons contact and evoke slow EPSPs in myenteric AH neurons^{80,140,141}.

Based on their projections, all three classes of descending interneurons (but not ascending interneurons) may be involved in communication from the myenteric to the submucosal plexus ¹⁴²⁻¹⁴⁴. Intracellular recordings in guinea pig ileum preparations containing both plexuses have demonstrated that there are functional connections from the myenteric to the submucosal plexus ¹⁴⁵. Slow EPSPs were observed in submucosal S-type neurons located within 10 mm anal to the site of focal myenteric stimulation, while fast EPSPs were detected up to 25 mm anally. Retrograde tracing studies have demonstrated the presence of submucosal interneurons which project to the myenteric plexus, although the connections may be sparse as only a small population of uniaxonal submucosal neurons project to myenteric ganglia ¹⁴⁶. Further, focal electrical stimulation of submucosal neurons elicits fast and slow EPSPs in about a quarter of myenteric neurons ¹⁴⁷.

The presence of submucosal interneurons that project within the submucosal plexus remains unclear. There is some supporting anatomical evidence showing that a subset of submucosal neurons provides varicose nerve terminals to other submucosal neurons ¹²⁷. In addition, stimulating cholinergic and some VIP submucosal neurons can elicit fast excitatory inputs in a neuron in an adjacent submucosal ganglion ¹⁴⁸. By contrast, a separate report found that only submucosal ISNs, but not other submucosal neurons, made synaptic contacts within the submucosal plexus ¹⁴⁹. Furthermore, submucosal ISNs can trigger fast EPSPs in S-neurons ⁷⁵, indicating that ISNs are able to directly signal to secretomotor neurons and circumventing the interneuron.

To date, there is only limited electrophysiological evidence for the presence of submucosal interneurons in the mouse. Fast EPSPs that were not tightly stimulus-locked and spontaneous fEPSPs – both of which are suggestive of functional contacts within the plexus – have been reported in the submucosal plexus of mouse colon ^{76,129}.

1.6.3 Secretomotor neurons

Secretomotor neurons in the submucosal plexus regulate intestinal secretion and vasodilation. Like motor neurons in the myenteric plexus, these secretory effector neurons are also uniaxonal and project only short distances (often < 1mm) and display S-type electrophysiology^{148,149}. In the guinea pig small intestine, there are two classes secretomotor/vasodilator neurons (non-cholinergic VIP-immunoreactive and cholinergic calretinin-immunoreactive neurons) that supply both the mucosa and submucosal arterioles, and one class of cholinergic NPY-immunoreactive secretomotor neurons that only innervate the mucosa¹⁴⁹. By contrast, distinctly separate populations of submucosal neurons supply the mucosa and vasculature in the mouse small intestine¹⁵⁰, suggesting that secretomotor and vasodilator neurons require common diverging inputs in order to coordinate local fluid secretion and blood flow.

In the guinea pig, the majority of VIP (but few cholinergic) submucosal neurons exhibit IPSPs evoked by electrical stimulation^{127,151-154}, indicating that VIP submucosal neurons are under a greater degree of regulatory control.

1.6.4 Motor neurons

Excitatory and inhibitory motor neurons that innervate the longitudinal and circular muscle reside in the myenteric plexus. These neurons typically have small cell bodies, are monoaxonal, have short projections (between about 6 – 12 mm orally for excitatory motor neurons and 3 - 25 mm anally for inhibitory motor neurons) and display S-type electrophysiology^{34,155}. The key co-transmitters of excitatory motor neurons are ACh and tachykinins, while the key mediator used by inhibitory motor neurons is nitric oxide (NO), along with the co-transmitters ATP, VIP, and pituitary adenylyl cyclase activating peptide (PACAP)¹³⁵. Activating excitatory motor neurons supplying the circular muscle elicits a depolarization, termed an excitatory junction potential, and muscle contraction; this is largely mediated by ACh and to a smaller extent by tachykinins. While stimulating inhibitory motor neurons innervating the circular muscle evokes a hyperpolarization i.e. an inhibitory junction potential and muscle relaxation. The inhibitory junction potential typically comprises a fast and

slow component, where the fast component involves ATP or NO, while the slow component is mediated by NO, VIP or PACAP¹³⁵. Longitudinal muscle functional innervation is less well understood compared to that of the circular muscle. Both excitatory and inhibitory motor neurons receive inputs from interneurons^{37,135,156}. Dual impalement intracellular recordings of pairs of guinea pig neurons have further shown that both types of motor neurons receive physiological inputs from calbindin-immunoreactive ISNs, indicating that there are also monosynaptic motor reflexes¹¹³.

2 ADENO-ASSOCIATED VIRUS

In order to investigate the projections of individual enteric neurons and with the aim of manipulating their activity, we used adeno-associated viruses (AAVs) to transduce cells in the ENS. The AAVs are small, non-enveloped, single-stranded (ss) DNA, first discovered as a contaminant of adenovirus stocks in the 1960s, which belong to the members of the *Dependovirus* genus of the *Parvoviridae* family¹⁵⁷. They require co-infection with a helper virus gene, such as adenovirus or herpes simplex virus, for their successful productive replication cycle¹⁵⁸. In the past few decades, recombinant AAVs have received a lot of attention as gene delivery vectors both in research as well as in clinical trials, owing to their low immunogenicity and non-pathogenic characteristics compared with other viruses, such as lentivirus or adenovirus¹⁵⁹⁻¹⁶¹.

Gene transfer using viral vectors has been extensively used in CNS studies, however, there have been a limited number of studies applying their use in the ENS¹⁶²⁻¹⁶⁸. Previous studies have used retroviruses, adenoviruses and AAVs to target cells of the gastrointestinal mucosa as well as the ENS derived cells *in vitro*^{169,170}. Recently, AAVs has been shown to be efficient at transducing the ENS *in vivo*^{164,166,171}. AAV9 has especially been shown to be a viable tool for transducing enteric neurons.

2.1 Genome structure

To date, 12 distinct human and nonhuman primate AAV serotypes (AAV1-12), with highly conserved genomes, have been sequenced. Due to both historical (as it was

the first infectious clone) and practical (as it successfully transduces common cell lines) reasons, AAV2, the best characterized serotype will be introduced here as a model. The AAV virion is an icosahedral non-enveloped particle containing a linear, ssDNA genome of approximately 4.7 kilobase (kb). The AAVs genome contains two open reading frames, the *rep* and *cap* regions¹⁵⁸. The *rep* gene encodes four non-structural proteins responsible for DNA replication and packaging. The *cap* gene encodes three structural capsid proteins (VP1, VP2 and VP3) and a newly identified protein, assembly activated protein that is crucial for capsid formation^{172,173}. T-shaped inverted terminal repeats (ITRs) flank both sides of the viral genome and are the only essential cis active sequences in AAV genomes for DNA replication, packaging into capsid and integration¹⁷⁴⁻¹⁷⁶.

2.2 Capsid structure

The AAV2 virion has diameter about 20 nm and consists of 60 copies of the three capsid proteins VP1, VP2 and VP3 in a ratio of 1:1:10. All three capsid proteins share the same C-terminal amino acid sequence, however the VP1 and VP2 have additional N-terminal residues¹⁷⁷. The N-terminus of VP1 (87 kDa) has a conserved phospholipase A2 domain that has been shown to be involved in virus endosomal escape and transduction¹⁷⁸. VP2 (73 kDa) does not really have an effect on virus assembly or transduction. VP3 (61 kDa) constitutes the majority of the capsid's protein and is highly conserved between the AAV serotypes and other parvoviruses¹⁷⁷.

2.3 Tissue tropisms

Vectors derived from naturally occurring AAV variants were shown to have diverse tissue tropisms. Comparisons between the structures of AAV capsids indicate that variation in surface topology between closely related serotypes determines the differences in cell surfaces recognition, intracellular trafficking pathways, and antigenicity¹⁷⁹.

Taking advantage of the natural tissue tropism, specific recombinant AAV (rAAV) vectors can be generated by substituting the entire wild-type coding regions with any gene of interest or DNA sequence within a limited size of up to ~5 kb ¹⁸⁰. AAV2 is an extensively used virus in (biomed) engineering, and its ITR and rep genes can be kept persistent, while various cap genes from different serotypes can be isolated to, dependent on the goal, create any so called “pseudotyped” vectors which only vary by the nature of their capsid proteins ^{181,182}. The usually used term AAV2/X means a pseudotyped vector with an AAV2-based vector genome packaged in a capsid from serotype X ¹⁸¹.

2.4 Cellular entry to AAV transduction

In order to deliver the gene of interest to a target cell for successful transduction, the AAV-based vectors must undergo several complex steps between the cell membrane and the nucleus ¹⁸³. First, the virion must attach to the cell surface via one or more (co-)receptors. The general idea is that binding of AAVs to its primary receptor locks the virion in a transition state that probably augments the affinity for the co-receptors and subsequently triggers AAV endocytosis. A summary of the AAV receptors, co-receptors and preferential tissue tropism is listed in the **table 1.2.1**.

Table 1.2.1 | AAV receptors and preferential tissue tropism

| <i>Virus</i> | <i>Glycan receptor</i> | <i>Co-receptor</i> | <i>Tissue tropism</i> |
|--------------|----------------------------|------------------------------------|---|
| AAV1 | N-linked sialic acid | Unknown | SM, CNS, retina, pancreas |
| AAV2 | HSPG | FGFR1, HGFR, LamR, CD9 tetraspanin | VSMC, SM, CNS, liver, kidney |
| AAV3 | HSPG | FGFR1, HGFR, LamR | Hepatocarcinoma, SM |
| AAV4 | O-linked sialic acid | Unknown | CNS, retina |
| AAV5 | N-linked sialic acid | PDGFR | SM, CNS, lung, retina |
| AAV6 | N-linked sialic acid, HSPG | EGFR | SM, heart, lung |
| AAV7 | Unknown | Unknown | SM, retina, CNS |
| AAV8 | Unknown | LamR | Liver, heart, CNS, pancreas, retina, heart, ENS |
| AAV9 | N-linked galactose | LamR | Liver, heart, lungs, pancreas, kidney, brain, ENS |

Abbreviations: AAV, adeno-associated virus; CNS, central nervous system; EGFR, epidermal growth factor receptor; ENS, enteric nervous system; FGFR1, fibroblast growth factor receptor 1; HGFR, hepatocyte growth factor receptor; HSPG, heparan sulfate proteoglycan; PDGFR, platelet-derived growth factor receptor; SM, skeletal

muscle; VSMC, vascular smooth muscle cell. Adapted from Nonnenmacher and Weber. 2012 ¹⁸³ and Buckinx et al. 2016 ¹⁶⁶.

Following binding to the cell surface receptors, AAV internalization into cell is performed via endocytosis. The next step is to process the capsid into more acidic endocytic compartments for further maturation. During this step, the AAVs' capsid must go through a conformational change in the endocytic system, such as endosome or trans-Golgi network. When the modificatory AAV virions are back to the cytoplama, the next important step is to get access to the nucleus via the nuclear pore complex. After nuclear translocation, ssDNA is released by capsid uncoating and converted into double-stranded DNA to allow transgene expression ¹⁸³.

3 OPTOGENETIC TOOLS TO DEFINE NEURAL CIRCUIT ACTIVITY

Since the introduction of live imaging microscopy and genetically encoded fluorescent probes to monitor cellular activity, optical imaging tools have revolutionized neuroscience by enabling visualization of multiple different forms of neuronal activity at circuit level in integrated systems. The reason why they are so welcomed by neuroscience researchers is mainly due to the “large - scale recording”, which enables thousands of cells to be observed simultaneously, in contrast to current feasible electrical recordings that are mostly confined to single cells, and thus allows sophisticated analysis of cellular interactions and spatiotemporal activity patterns ¹⁸⁴⁻¹⁸⁶. The other advantages include minimized tissue invasion, stable expression of genetically encoded activity indicators and cell-type specific approaching ¹⁸⁶.

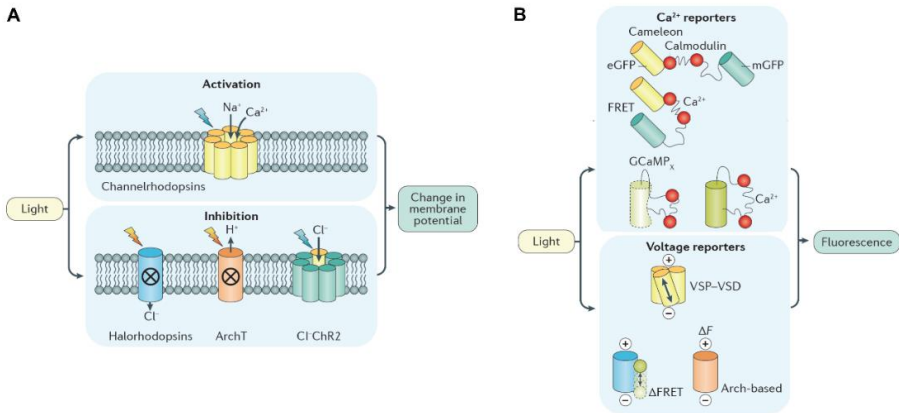


Figure 1.3.1|Schematic overview of available genetically encoded actuators and indicators.

A, The concepts of different actuators for activation and inhibition of cells. The stimulus is indicated on the left-hand side (light). The cellular actions, shown on the right, could be changes in membrane potential. **B**, Schematic overview of two important classes of cellular activity indicator proteins that, upon excitation with specific wavelengths of light (left), emit fluorescence (right) more or less efficiently depending on intracellular Ca²⁺ concentration or membrane potential (voltage). ΔF, change in fluorescence; Cl-ChR2, chloride-conducting channelrhodopsin 2; eGFP, enhanced green fluorescent protein; FRET, Förster resonant energy transfer; GCaMP, green fluorescent protein (GFP), calmodulin and M13; mGFP, membrane-targeted green fluorescent protein; VSD, voltage-sensitive domain; VSP, voltage-sensitive phosphatase. Adapted from Boesmans et al. 2017¹⁸⁵.

More broadly, the optical tools consist of all genetically encoded optical actuators and indicators¹⁸⁷ (**Figure 1.3.1**). Optogenetic actuators allow photostimulation or photoinhibition of genetically defined populations of neurons with millisecond precision at high spatial resolution¹⁸⁸⁻¹⁹¹. The most extensively used actuators are channelrhodopsin 2 from *Chlamydomonas reinhardtii* (ChR2), which can passagage cations (such as Na⁺, Ca²⁺) across the cell membrane thus to depolarize neurons upon blue light illumination, and enhanced halorhodopsin from *Natronomonas pharaonis* (eNpHR), which can pump chloride ion (Cl⁻) thus to hyperpolarize neurons with yellow/orange light illumination^{188,189,192}. While optical indicators enable quantitative readout of neural activity from hundreds of neurons with cellular

resolution^{191,193}. Basically, genetically encoded fluorescent indicators include voltage indicators and ion sensors, especially Ca indicator (GECI). Voltage indicator can monitor membrane potentials owing to its fast kinetics and large fluorescent changes, however, there are still demerits, such as the limited temporal resolution and photostability. Surprisingly, Abdelfattah and his colleagues have recently reported to combine a voltage-sensitive microbial rhodopsin domain with a self-labeling protein tag domain to dramatically improve the brightness and photostability of these chemigenetic indicators for extended *in vivo* voltage imaging¹⁹⁴. Although voltage indicators represent obvious advantages to image the action potential firing, calcium imaging is in many ways the most extensive approach to image the neural activity, allowing studies of neural ensemble dynamics and coding, synaptic function, and dendritic processing in long-term time lapse imaging¹⁹⁵.

The first generations of GECIs were based on large protein conformation shifts to allow FRET signals to be recorded¹⁹⁶. After several generations' optimization, GCaMP family turn to be the most commonly used GECI. GCaMP3 is the first series and has been used in many different neuronal systems, including the ENS¹⁹⁷⁻¹⁹⁹. However, its detection reliability of single AP is still low under physiological conditions¹⁸⁴. Instead, the recent new versions, such as GCaMP6, GCaMP7 and GCaMP8, have intensely improved the sensitivity and kinetics thus to better reflect the action potential events²⁰⁰⁻²⁰².

CHAPTER 2

Research objectives

The coordinated activity of enteric neurons within polysynaptic circuits controls several aspects of gut function including absorption of nutrients, mucosal secretion and gastrointestinal motility ². The minimal neuronal circuit required to orchestrate peristalsis, the textbook example of a gastrointestinal motility pattern, consists of a five-neuron unit with an intrinsic sensory or primary afferent neuron (IPAN) that senses mechanical or chemical stimuli from the intestinal lumen and activates excitatory or inhibitory motor neurons via ascending or descending interneurons. Together this evokes a contraction of the intestinal muscle oral and a relaxation distal to the stimulus ^{203,204} (**Figure 2.1**).

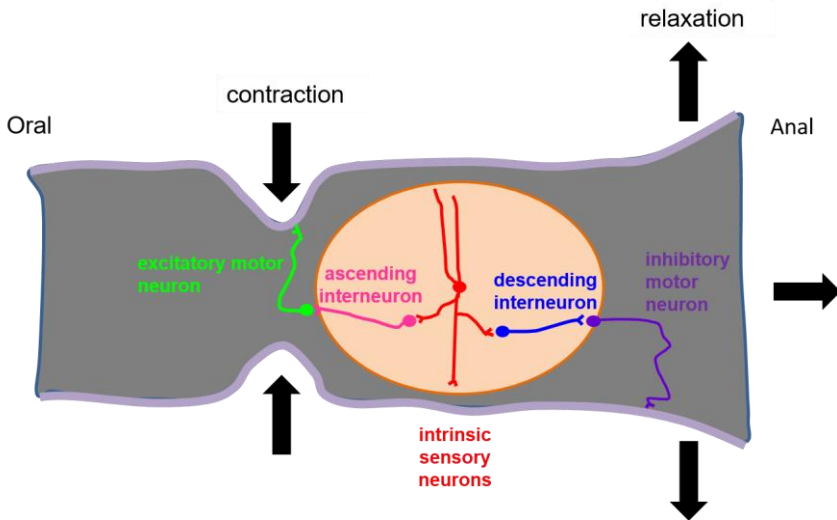


Figure 2.1 | Schematics showing the simplest circuitry to regulate contraction and relaxation of the gut.

Besides peristalsis, other motility patterns are also present, including: relaxation of the stomach wall to accommodate a meal, segmentation for food mixing, storage of waste products and migrating myoelectric complexes for removing residual contents from the bowel, all of which need to be matched with controlled mucosal absorption and secretion ²⁰⁵. The presence of these different modes of gastrointestinal motility substantiates the necessity of different and more complex neural circuits than the simple peristaltic circuit. However, the exact connectivity schemes of the various enteric nerve circuits are unclear. Although enteric neural circuits have been

investigated in many classic electrophysiological studies, it has been difficult to perform extensive in-depth analysis of ENS wiring on large populations of cells. Therefore, we aimed to interrogate enteric nerve circuits by using live calcium imaging in combination with viral vector tracing to examine the activity, phenotypic properties, location and projection orientation of individual enteric neurons in an integrated fashion (**objectives 1 & 2**). Here, we only focus on the role of main excitatory neurotransmitter, acetylcholine, in building enteric circuits. Further, to fully understand how the calcium response signatures in our population-level analysis of neural circuitry in the mouse ENS relate to electrophysiological properties, we aimed to characterize the relationship between action potential firing and $[Ca^{2+}]_i$ transients using simultaneous whole-cell patch-clamp electrophysiology and live calcium imaging (**objective 3**).

Hence, the aims of this doctoral project are:

- I. **To establish a viral vector transduction technique to target fluorescent reporters to the ENS, in vivo.**
- II. **To identify ENS circuits using the colon as a model organ: are there differences in the enteric nerve circuits in the proximal vs. distal colon?**

Compared with the small intestine, which has similar motility patterns (segmentation, peristalsis, and migrating motor complexes) for each region, the proximal colon differs from other parts of the large bowel with rich motility patterns, such as “antiperistaltic” or “colonic migrating motor complexes (CMMC)”, while the distal colon only generates CMMCs.” Therefore, mouse colon, as an intact organ, is a perfect model for this study.

- III. **To characterize the relationship between voltage changes and $[Ca^{2+}]_i$ transients using simultaneous whole-cell patch-clamp electrophysiology and live calcium imaging.**

CHAPTER 3

Establishing a viral vector transduction technique to target fluorescent reporters to the ENS, in vivo

Zhiling Li¹, Werend Boesmans¹, Marlene M Hao¹, Veerle Baekelandt², Chris Van den Haute², Pieter Vanden Berghe¹

¹Laboratory for Enteric NeuroScience (LENS), Translational Research Center for Gastrointestinal Disorders (TARGID), Department of Chronic Diseases, Metabolism and Ageing, University of Leuven, Leuven, Belgium

²Laboratory for Neurobiology and Gene Therapy, Department of Neurosciences, KU Leuven, Leuven, Belgium

The data presented in this chapter have been presented as a poster in the conference: "Development of the Enteric Nervous System: Cells, Signals, Genes and Therapy", Rotterdam, 2015.

3.1 Introduction

Correct functioning of the gastrointestinal tract relies on the coordinated activity of the enteric nervous system (ENS), a polysynaptic circuit of neurons and glial cells embedded in the gastrointestinal wall. In an aganglionic segment, as is the case in Hirschsprung disease ^{206,207}, no motility or coordinated propulsion is possible in the last portion of the intestine, which did not get colonized by the neural crest derived cells or didn't differentiate very well. However also much more subtle defects or dysfunctional wiring ²⁰⁸ within the ENS could result in a range of gastrointestinal problems, such as chronic intestinal pseudo-obstruction, slow-transit constipation ²⁰⁹, irritable bowel syndrome ²¹⁰ and gastroparesis ²¹¹. Furthermore, recent reports have suggested that ENS deficits can also accompany some CNS disorders and dysfunctional gastrointestinal manifestations might occur even before CNS symptoms become evident ^{212,213}. These central disorders range from neurodevelopmental (autism spectrum disorder...) to neurodegenerative (Parkinson disease, Alzheimer disease...) diseases ²¹⁴⁻²¹⁸. Hence, a better understanding of how the connections between enteric neurons are organized, is not only important from a basic neurobiological point of view, but could also help to understand the pathophysiology of both gastrointestinal and neurological diseases.

Although the enteric neural circuits have been investigated in many classical electrophysiological studies, it has been difficult to perform extensive in-depth analysis of ENS wiring. For example, very time-consuming and technically challenging experiments are required in order to stimulate a single cell and investigate its postsynaptic partners. So far, the use of optogenetic tools has increased understanding of ENS structure and function based on their large scale film and cellular specificity ¹⁹³. Except application of a series of transgenic mice, a lot of efforts have been put into investigating alternative strategy to transduce the functional constructs into the ENS. However, the special environment the ENS located in is the most serious challenge the researchers have to face. In order to do this, we aimed to use recombinant adeno-associated viral (rAAVs) vectors, which has been reported

recently to transduce the ENS successfully, to deliver functional constructs into enteric neurons to examine their electrical and synaptic function. AAV9 was the first serotype identified to efficiently cross the blood brain barrier (BBB) leading to extensive transduction in animal models^{163,219,220}. Recently, it has demonstrated that intravenous rAAV9 injection efficiently transduced the ENS in both neonatal and juvenile mice^{164,166}. In addition, direct injection of AAV9 into the descending colon of the rat showed high levels of transduction within the ENS¹⁷¹. Therefore, we tested the efficiency of various rAAVs in transducing enteric neurons, on the one hand to validate the published approach and on the other hand to explore whether tail vein injection of AAVs would cross the placental barrier and transduce embryonic enteric neurons.

3.2 Materials & Methods

3.2.1 Animals

For viral injections, wild type C57Bl6/J mice were used (approx. 2 months). All mice were killed by cervical dislocation. All experiments were approved by the animal ethics committee of the University of Leuven (KU Leuven) guidelines for the use and care of animals.

3.2.2 Neuronal process tracing

3.2.2.1 *Recombinant adeno-associated viral vector (AAV) preparation*

Here we used bio-engineered pseudotyped AAV vectors. They were created by AAV2-based vector genome packaged in a capsid from serotype X, which is called as AAV2/X¹⁸¹. The rAAV2/X vector production and purification were performed by the Leuven Viral Vector Core as previously described²²¹. Adeno-associated viral vector encoding the enhanced green fluorescent protein (eGFP) reporter under the ubiquitous cytomegalovirus (CMV) promoter was packaged in an AAVX-capsid. Briefly, HEK 293T cells were transfected using a 25-kDa linear polyethylenimine solution using the pAdvDeltaF6 adenoviral helper plasmid, pAAV2/X serotypes and AAV-TF CMV-eGFP-

T2A-fluc (AAV transfer plasmid encoding eGFP and firefly luciferase reporters driven by a CMV promoter) in a ratio of 1:1:1. Viral vector particles collected from the concentrated supernatant, were purified using an iodixanol step gradient. The final sample was aliquoted and stored at -80°C. Titers (GC/mL) for AAV stocks were analyzed by real-time PCR.

3.2.2.2 rAAV injection

In this set of experiments, different serotypes of recombinant adeno-associated viral vectors (rAAV2/1, 5, 7, 8 and 9, **Table 3.1**) encoding for the CMV-driven eGFP reporter were delivered to both adult male and pregnant female C57Bl6/J mice via tail vein injection. Mice (N = 3) were placed under an incandescent lamp for 15-20 min and physically restrained. Each serotype supplemented with 5% sucrose in 0.01 M PBS for a total volume of 250 µl were injected into the vein at a slight angle using a 33 gauge needle. Mice were sacrificed 2 weeks after injection and intestinal tissues were fixed, washed and prepared for immunohistochemistry. On embryonic day 12, the same concentration of rAAV2/9 was injected into the female mice. On postnatal day 7, the entire gut from the pups was dissected for later on transduction examination.

Table 3.1 | The details of injected rAAV2/X vectors

| Sex | Vector | Titer (/ml) | Volume (µl) |
|-----------------|---------------|-----------------------|-------------|
| Male | AAV2/1:13-033 | 1.34x10 ¹² | 20 |
| Male | AAV2/5:13-008 | 2.79x10 ¹² | 25 |
| Male | AAV2/7:13-020 | 2.39x10 ¹² | 20 |
| Male | AAV2/8:12-023 | 3.52x10 ¹² | 25 |
| Male | AAV2/9:11-031 | 8.47x10 ¹¹ | 25 |
| Pregnant female | AAV2/9:11-031 | 8.47x10 ¹¹ | 25 |

3.2.3 Immunohistochemistry

To examine the identity of rAAV-transduced cells in the ENS, immunohistochemistry was performed as previously described ²²². Briefly, whole-mount preparations of mouse colon were pinned in a Sylgard plate containing Krebs solution continuously oxygenated with carbogen (95% O₂/5% CO₂). To generate whole mount submucous

plexus preparations, first the mucosa was removed from the other layers by dissection. The entire colon from rAAV2/8 and rAAV2/9 transduced mice was then fixed overnight in 4% paraformaldehyde (PFA, Merck, Overijse, Belgium) in 0.1 M phosphate buffered saline (PBS, pH = 7.2) at 4 °C. Subsequently, the tissue was washed three times with PBS, and submucosal plexus preparations were dissected away from the muscle layers. From this, the longitudinal muscle layer was carefully removed to expose the myenteric plexus for later immunostaining. To identify the rAAV2/8 and rAAV2/9-transduced cells, tissues preparations were permeabilised in 0.5% triton X-100 in PBS containing 4% donkey serum for 2h at room temperature, and incubated in primary antibodies (**Table 3.2**) overnight at 4°C. After primary antibody labeling, all preparations were washed in PBS (3 x 10 min) and incubated in blocking solution containing matched secondary antibodies (**Table 3.2**) for 2h at room temperature. Erythrina cristagalli lectin (ECL, 20 µg/ml in PBS for 30 min) staining was carried out to investigate the transduction specificity of rAAV2/9.

Table 3.2 | Antibodies used for immunohistochemistry

| Antibodies | Host | Dilution | Source |
|------------------|--------|----------|----------------------------|
| GFP | Rat | 1:1000 | Gentaur |
| HuCD | Human | 1:2000 | Gift from Kryzer Thomas J |
| C-kit | Goat | 1:200 | Santa Cruz Biotechnologies |
| S100β | Rabbit | 1:500 | Dako |
| Anti-actin | Mouse | 1:500 | Sigma |
| Anti-rat A488 | Donkey | 1:1000 | Jackson Immuno labs |
| Anti-human A594 | Donkey | 1:1000 | Jackson Immuno labs |
| Anti-goat A594 | Donkey | 1:1000 | Molecular Probes |
| Anti-rabbit A647 | Donkey | 1:1000 | Molecular Probes |

3.2.4 Image analysis

Preparations were imaged on a Zeiss LSM 780 laser scanning confocal microscope (Cell Imaging Core, University of Leuven). At least three pieces of whole mount preparation were performed for each virus serotype.

3.3 Results

3.3.1 Distribution of eGFP-positive cells in the gastrointestinal tract following tail vein injection of rAAVs-CMV-eGFP into adult mice

In order to determine the transduction efficiency of rAAVs into the ENS, several different rAAVs-CMV-eGFP were injected into adult male and pregnant female mice via the tail vein. Two weeks after injection, mice were sacrificed and their intestines were isolated and dissected for later analysis. Using fluorescence microscopy the intestinal wall preparations were screened for eGFP expression in all cell types present (neurons, glia, ICC, muscle, macrophages, ...). Only two of the serotypes, rAAV2/8 and rAAV2/9 showed clear and efficient transduction of cells in the gastrointestinal tract, while after rAAV2/1, rAAV2/5 and rAAV2/7 injection, there was no or extremely little eGFP expression in the GI wall. In order to test whether the tail vein injection approach would be suitable to investigate the developing ENS in the mouse embryo, we also injected rAAV vectors in the tail vein of pregnant female mice. So far, we were not able to detect any eGFP expression in the embryonic ENS, suggesting that the rAAVs do not cross the placental barrier (**Table 3.3**).

Table 3.3| Distribution of eGFP-expressing cells in different regions of the gastrointestinal tract

| Serotypes | Titer (/ml) | Volume (μ l) | Stomach | Duodenum | Jejunum | Ileum | Caecum | Colon |
|-------------|-----------------------|-------------------|---------|----------|---------|-------|--------|-------|
| rAAV2/1 (M) | 1.34x10 ¹² | 20 | - | - | - | - | - | - |
| rAAV2/5 (M) | 2.79x10 ¹² | 25 | - | - | - | - | - | - |
| rAAV2/7 (M) | 2.39x10 ¹² | 20 | - | - | - | + | - | - |
| rAAV2/8 (M) | 3.52x10 ¹² | 25 | + | - | + | + | + | + |
| rAAV2/9 (M) | 8.47x10 ¹¹ | 25 | + | - | + | + | + | + |
| rAAV2/9 (F) | 8.47x10 ¹¹ | 25 | - | - | + | + | - | - |
| rAAV2/9 (P) | 8.47x10 ¹¹ | 25 | - | - | - | - | - | - |

‘-’ means no transduced cells were found; ‘+’ means transduced cells were found. ‘M’ male mice; ‘F’ female mice; ‘P’ mouse pups.

3.3.2 Transduction of myenteric neurons by rAAV8 and rAAV9

To identify the rAAV2/8 and rAAV2/9 transduced cells, whole-mount preparations were stained with the neuronal marker HuCD and the glia marker S100 β . These stainings revealed that eGFP was robustly expressed in myenteric neuronal cell

bodies and processes, as well as in a small number of submucosal neurons. eGFP expression was observed in jejunum, ileum, colon, stomach and caecum but was absent from duodenum (**Table 3.3**). eGFP colocalized almost exclusively with HuCD-positive cells in each of the different regions of the gastrointestinal tract (**Figure 3.1**), indicating that rAAV2/8 and rAAV2/9 target neurons quite selectively.

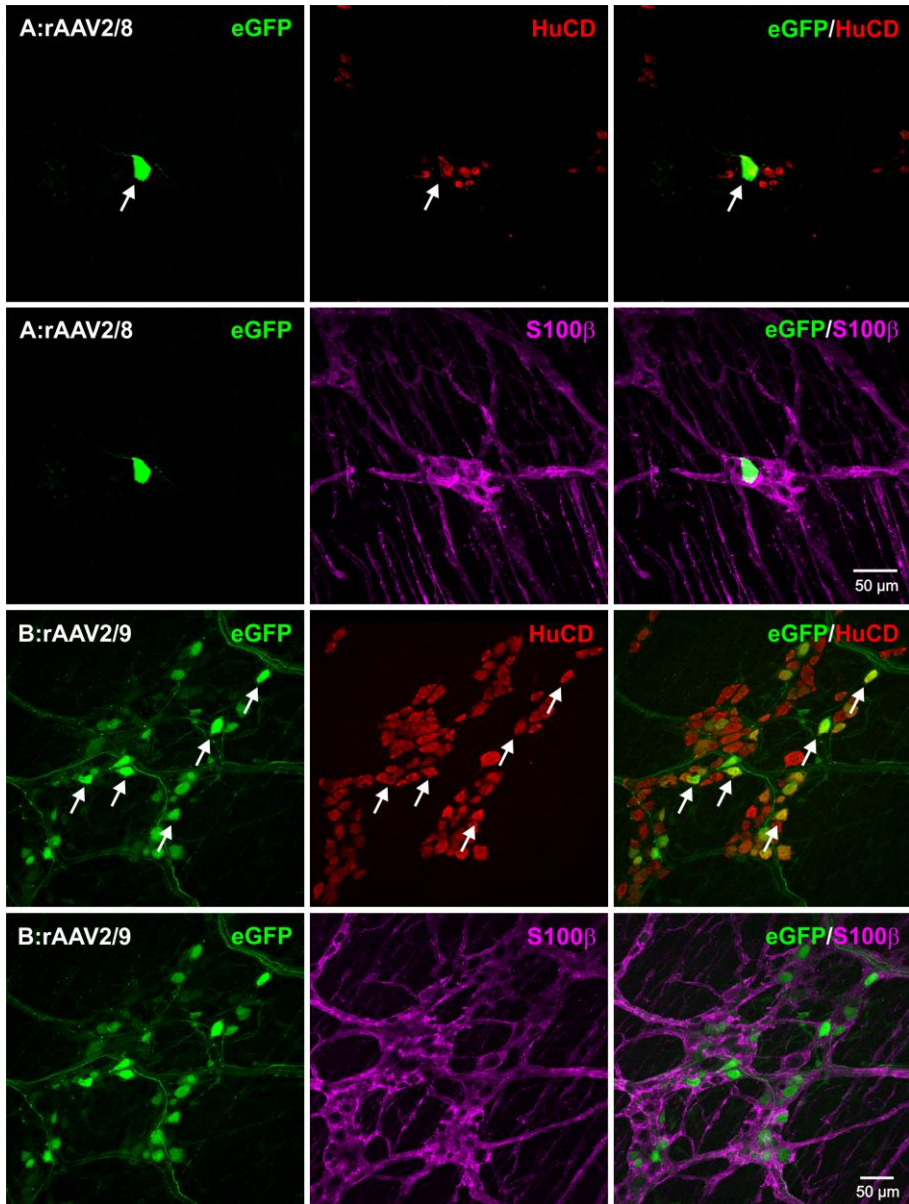


Figure 3.1| Representative images of the ENS in the mouse ileum after transduction with rAAV2/8 (A, top row) and rAAV2/9 (B, bottom row).

To examine the identity of rAAVs-transduced cells, immunohistochemistry with specific markers for enteric neurons (HuCD, red), enteric glial cells (S100 β , blue), and GFP (green) was performed. Arrows point to eGFP expressing neurons.

To identify the processes of individual neurons and track their projection orientation, sparse labeling is warranted. To this end we also injected mice with a lower titer of rAAV2/9 (10 μ l in 250 μ l of a certain titer – actually 4% of the 250 μ l injection solutions). Compared to our standard injections (25 μ l in 250 μ l, 10% of the 250 μ l injection solutions), we now obtained a lower density of eGFP expressing myenteric neurons which allowed us to trace the processes of individual eGFP transduced neurons (**Figure 3.2**).

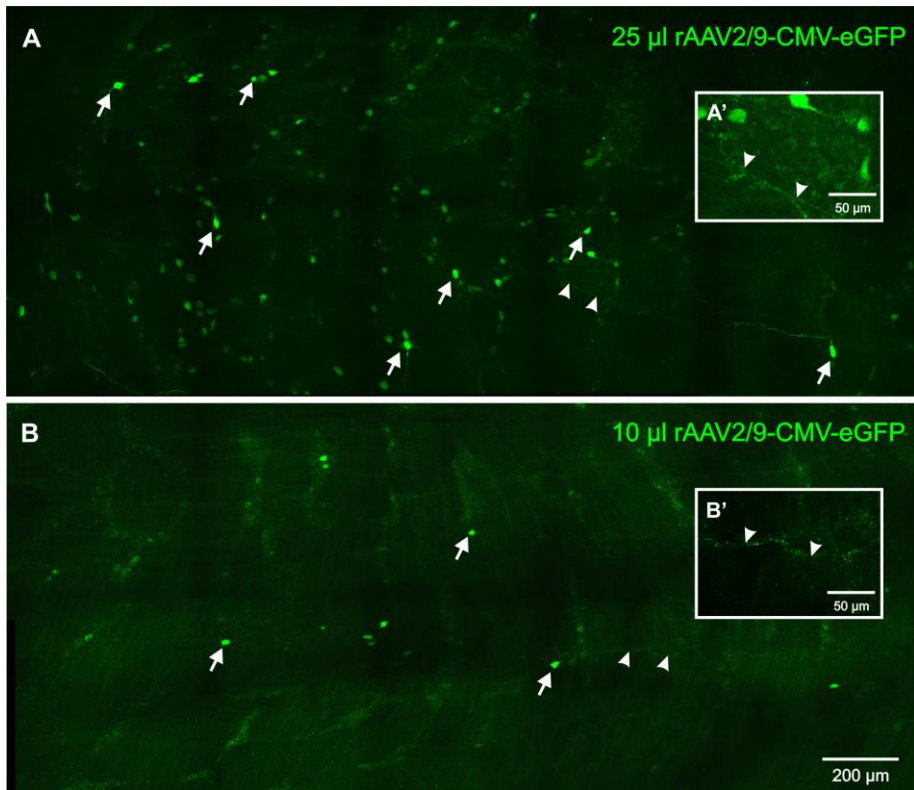


Figure 3.2| Representative images (tile of confocal maximum projections) of the myenteric plexus in the mouse colon after transduction with different concentrations of vector.

Arrows point to eGFP positive cell bodies and positive processes are indicated by arrowheads.

3.3.3 Only a minority of cells transduced by rAAV2/8 and rAAV2/9 were non-neuronal

Apart from enteric neurons we also observed a small number of other eGFP expressing cells within the myenteric plexus preparations. Based on their distinct morphology, these were clearly non-neuronal. To test whether these were enteric glial cells we used an antibody against S100 β and found that none of the identified cells, neither in the myenteric plexus nor in the other layers, expressed S100 β . The non-neuronal eGFP cells were generally not located in the plane of the myenteric plexus and since the morphology of some eGFP-positive cell was reminiscent of interstitial cells of Cajal (ICC), an immunostaining against c-kit, an ICC marker, was performed. Despite comparable morphology, these cells did not label for c-kit (**Figure 3.3**).

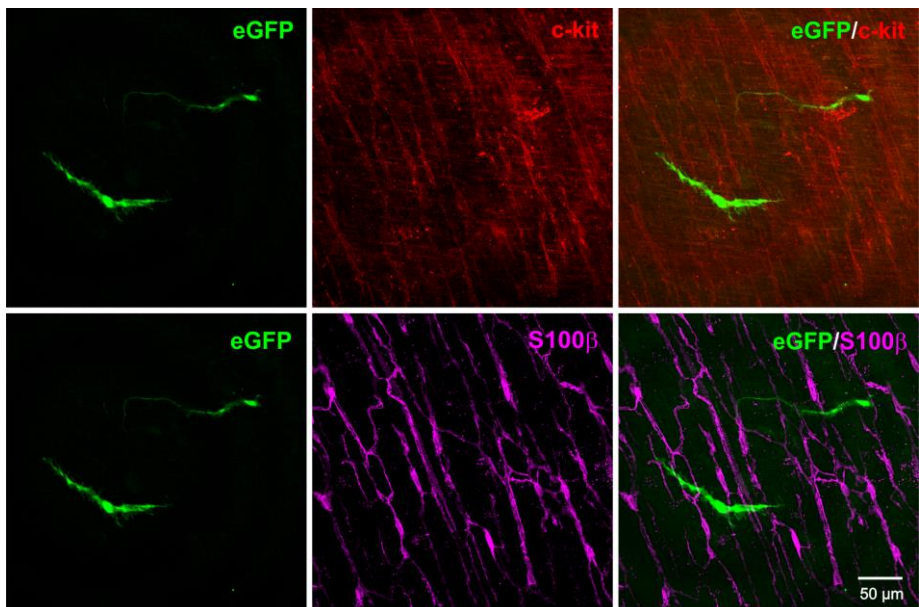


Figure 3.3 | Representative image of rAAV2/8-transduced non-neuronal cells in the ileum.

The eGFP-labeled cells did not express S100 β (blue) or c-kit (red) and therefore could not be identified as glia or ICC.

Given the neuronal focus of our study and the success of rAAV2/8 and rAAV2/9 to transduce neurons we decided to halt any further attempts to identify the rare GFP positive non-neuronal cells.

3.3.4 N-linked galactose expression in the mouse colon

It has been elucidated that the cell surface glycan terminal N-linked galactose is the primary receptor for rAAV2/9²²³⁻²²⁵. To investigate why this serotype targets enteric neurons so specifically, we tested whether N-linked galactose is present within the ENS. Therefore we performed a staining with fluorescently labeled ECL (Erythrina Cristagalli Lectin), a specific carbohydrate-binding protein that localizes to N-linked galactose²²⁶. Contrary to our expectation, the fluorescent ECL staining did not label any neurons but was only detected on smooth muscle cells (**Figure 3.4**).

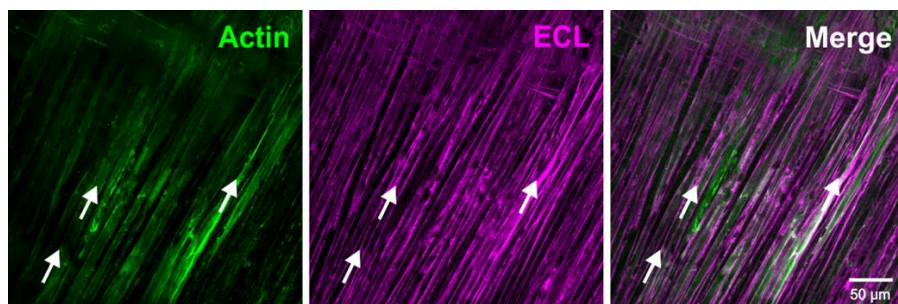


Figure 3.4 | Representative image showing that ECL staining (magenta) was not found in the ENS but primarily located in smooth muscle cells (actin, green).

3.4 Discussion

About 2 decades ago, rAAVs emerged as promising tools to transduce cells without the risk to elicit a massive immune response. Nowadays, rAAVs have been widely accepted as efficient gene delivery systems in biomedical research and important

candidates for gene delivery in therapeutic applications. To date plenty of studies demonstrate that rAAVs can be used as tools to deliver target genes in a range of different CNS regions^{162,227,228}. However, there are still only few studies about rAAV transduction into the gastrointestinal tract and the ENS¹⁶²⁻¹⁶⁸. Better understanding of the mechanisms and specificity of rAAVs transduction in the ENS will benefit possible future gene therapies directed to cure ENS related gastrointestinal and central degenerative diseases. Here we set up a study to investigate rAAV transduction efficiency following intravenous injection of rAAV2/9 and other serotypes rAAV2/1, 2/5, 2/7 and 2/8. Our data extend the existing reports on viral vector-mediated gene delivery in the ENS and show that both rAAV2/8 and rAAV2/9 can efficiently transduce enteric neurons. Lowering the dose of rAAV2/9 can be used to sparsely label neurons, which allows to identify the processes of individual neurons and track their axons to the target cells.

Comparing the transduction efficacy across various serotypes of rAAVs in the adult mice, we demonstrate that rAAV2/8 and rAAV2/9 most efficiently transduce enteric neurons in the gastrointestinal tract, which is consistent with previous studies^{164,166}. The level of transgene expression achieved by rAAVs was suggested to be determined by both the viral capsid and the expression cassette^{164,171}. Despite the fact that a general promoter (CMV) was used to drive eGFP expression, the resulting transduction in our experiments was remarkably specific for enteric neurons. Although the mechanism underlying this neuronal tropism remains unknown, the interaction of AAV8 and 9's capsid molecules with a specific receptor seems to play a dominant role. Interaction between the rAAVs capsid and the unique cell surface receptors/co-receptors defines the specific tissue tropism^{229,230}. For AAV9 it was shown that on the one hand it is capable of crossing the epithelial barrier and that it efficiently transduces those tissues that express high levels of N-terminal β -galactose glycans²²³⁻²²⁵. However, the latter contrasts with our finding showing ECL positive labeling on smooth muscle cells only. The reason for this discrepancy could be due to the *in vitro* environment used in the earlier studies^{223,225}, while, *in vivo*, other ENS molecules may be responsible for AAV9's neuronal tropism. Although

confirmed as an excellent practical tool, more studies are needed to figure out how the muscular location of this cell surface glycan links to the specificity of rAAV9 for enteric neurons.

To date, the unique receptor for AAV8 remains elusive, however, both AAV8 and AAV9 share the same co-receptor, laminin, which could partially contribute to the transduction into the ENS²³¹. In contrast to rAAV2/8 and rAAV2/9, rAAV2/7, 2/1 and 2/5 failed to transduce cells, indicating that N-linked sialic acid, known as a primary receptor for AAV1 and 5^{182,232}, may not be present in the intestinal wall.

It should be noted that, except for the neuronal transduction, some non-neuronal cells neither identified as glia nor interstitial cells were transduced by rAAV2/8 and rAAV2/9. This finding is in contrast with a previous study showing that AAV8 also transduced enteric glia¹⁶⁴. The choice of species and even (mouse) strain, the age of the animals, route of administration and promoter may all contribute to the difference in efficacy of transduction^{164,166,171,233}. One obvious difference between our and previous studies^{164,171,233}, was the use of a CMV promoter rather than the hybrid chicken β -actin/CMV promoter.

To test whether tail vein injection of AAV9 would be useful to investigate ENS development during embryogenesis, we also injected viral vectors in the tail vein of pregnant females. In comparison with a previous study showing that AAV9 efficiently facilitates neuronal transduction of both the central and peripheral nervous system through the intrahepatic continuation of the umbilical vein in fetal macaques²²⁸, the scarcity of embryonic neuronal transduction observed in the mouse pups suggests that the placental barrier restricts the access of circulating rAAV2/9. Crossing the placental barrier is a slow process which is determined by placenta structure and function^{234,235}. While a rate limit could be the primary element, other factors such as species difference or the titer of vector may contribute to the lack of embryonic expression. Interestingly, although we injected the same titer of rAAV2/9 vector into both male and pregnant female mice, less expression (2 weeks post injection) was observed in the ENS of pregnant mice compared to the male cohort.

Given that AAV9 is the first serotype described to cross the BBB, it has become the prime candidate for gene therapy in the context of therapy for neurological diseases, such as spinal muscular atrophy or amyotrophic lateral sclerosis ²¹⁹. Furthermore, it has been reported that combinations of direct CNS injection together with systemic injection of AAVs could possibly provide a simultaneous treatment for some central degenerative disorders with GI complications, for instance Parkinson's disease ^{164,236,237}.

3.5 Conclusion

Our results corroborate recent reports on viral vector-mediated gene delivery in the ENS. Employing specific neuronal or glial promoters may allow for AAV9 gene delivery to further improve specificity in transducing specific ENS subpopulations. Future studies will be needed to optimize transgene delivery approaches to induce expression in the ENS, not only for research purposes but also in view of possible future medical applications.

3.6 Author Contributions

Z.L.L. collected the data, performed the analysis and drafted the manuscript. W.B., M.M.H., and P.V.B. determined the experimental design, contributed to the conception of the project and revised the manuscript. C.V.H., and V.B. provided materials (viral vectors).

3.7 Acknowledgements

We thank Joris Van Asselberghs (Laboratory for Neurobiology and Gene Therapy) for the help with the tail vein injections and the members of LENS for critical comments and useful discussions. The study was supported by the FWO (G.0921.15) and Hercules foundation (AKUL/11/37 and AKUL/13/37). Z.L.L. is supported by the China Scholarship Council (CSC) (201408370078). M.M.H. (2013-2016) and W.B. (2010-2016) received support as postdoctoral fellows of the Fund for Scientific Research

Flanders (FWO). We also would like to thank Micky Moons for the excellent technical assistance during experiments.

3.8 Conflicts of Interest

The authors declare no conflicts of interest.

CHAPTER 4

Regional complexity in enteric neuron wiring reflects diversity of motility patterns in the mouse large intestine

Zhiling Li¹, Marlene M Hao², Chris Van den Haute^{3,4}, Veerle Baekelandt³, Werend Boesmans^{1,5*}, Pieter Vanden Berghe^{1*}

* shared senior author & correspondence

¹*Laboratory for Enteric NeuroScience (LENS), Translational Research Center for Gastrointestinal Disorders (TARGID), Department of Chronic Diseases, Metabolism and Ageing, University of Leuven, Leuven, Belgium*

²*Department of Anatomy and Neuroscience, University of Melbourne, Melbourne, Australia*

³*Laboratory for Neurobiology and Gene Therapy, Department of Neurosciences, KU Leuven, Leuven, Belgium*

⁴*Leuven Viral Vector Core, University of Leuven, Leuven, Belgium*

⁵*Department of Pathology, GROW-School for Oncology and Developmental Biology, Maastricht University Medical Center, Maastricht, The Netherlands*

E-life (2019)

4.1 Introduction

The gastrointestinal (GI) tract is of key importance in the control of whole body homeostasis. On the one hand, it serves to take up energy and essential nutrients from ingested foods, on the other hand, it has to protect the host from pathogens and dietary antigens, while still maintaining a fine symbiotic balance with the luminal microbiome. In order to do so the GI tract exhibits different motility patterns, which include peristaltic, accommodating, mixing and segmenting activity that varies not only according to the region along the gut but also to the dietary status ²³⁸. The accurate control of GI motility relies on the activity of different types of neurons present in the enteric nervous system (ENS), a ganglionated neural network located in the wall of the gut ²³⁹. Through largely unresolved circuits, enteric neurons relay information from the gut lumen via interneurons to motor neurons that steer the action of intestinal smooth muscle cells resulting in coordinated contractions and relaxations of smooth muscle syncytia.

In contrast to the central nervous system where spatial distribution and function of neurons are often linked, the architecture of the ENS is seemingly chaotic. Recently, Lasrado et al. were able to show that functional ENS units in the small intestine are spatially organized in overlapping clonal clusters ²⁴⁰. However, whether the different motility patterns are hard-wired in the ENS and whether these arise from specific or overlapping and possibly multifunctional circuit elements remains elusive. The large intestine executes a variety of different motor patterns including segmental activity, tonic inhibition, antiperistaltic and peristaltic waves ²⁰⁵. It has been demonstrated that especially the proximal colon differs from other parts of the large bowel in that it can generate antiperistaltic waves that mix contents to maximally reabsorb water and electrolytes from the lumen, whilst the distal colon is mainly responsible for propelling the fecal pellet along the large intestine via colonic migrating motor complexes (CMMC) ²⁴¹. Although the peristaltic reflex has been studied extensively and the underlying mechanisms are largely resolved ²⁴²⁻²⁴⁶ little is known about the relationship between peristalsis and other (emptying) motor patterns. Furthermore,

the neurogenic control elements for storage, mixing and the transition between the different motor patterns are still far from being understood. Taking advantage of the clearly different motor capabilities of two these regions, we investigated, whether diverse enteric circuits exist that may reflect the neuronal control of these tasks. To do so, we used live Ca^{2+} imaging and focal electrical stimulation to evaluate the connectivity of large numbers of enteric neurons while simultaneously mapping their physical location within the myenteric plexus. We combined this set of experiments with immunofluorescence labeling and viral vector tracing to analyze neuronal identity, morphology, projection orientation and synaptic complexity within the network.

We found that neuronal connectivity is different in two adjacent regions of the large intestine. The neuronal wiring in the proximal colon is clearly more complex than in the distal colon, where a larger fraction of neurons completely depends on cholinergic input. The straightforward wiring of the distal colon reflects its limited portfolio of motility patterns and proves that complexity of functional output scales with complexity of the enteric neural network.

4.2 Materials and Methods

4.2.1 Animals

For calcium imaging, adult *Wnt1::Cre;R26R-LsL-GCaMP3* mice (short: *Wnt1|GCaMP3*) were used, where the genetically-encoded Ca^{2+} indicator, GCaMP3, is expressed in all neural crest-derived cells, including enteric neurons and glia^{247,248}. *Wnt1|GCaMP3* mice were bred by mating *Wnt1::Cre* mice²⁴⁹ with *R26R-LsL-GCaMP3* mice (also known as Ai38, purchased from The Jackson Laboratory, Bar Harbor, ME, USA, stock # 014538)²⁴⁸. For viral injections, wild type C57Bl6/J mice were used. All mice were killed by cervical dislocation. All experiments were approved by the animal ethics committee of the KU Leuven guidelines for the use and care of animals.

4.2.2 Calcium imaging

The entire colon was removed from adult male Wnt1|GCaMP3 mice (approx. 3 months) and dissected in Krebs solution (containing in mM: 120.9 NaCl, 5.9 KCl, 1.2 MgCl₂, 2.5 CaCl₂, 1.2 NaH₂PO₄, 14.4 NaHCO₃, and 11.5 glucose, bubbled with 95% O₂/5% CO₂), cut along the mesenteric border and pinned flat, mucosa side up, in a dish lined with silicone elastomer (Sylgard 184; Dow Corning). The mucosa and submucous plexus were removed from the underlying smooth muscle and myenteric plexus layers. Strips of longitudinal muscle were carefully peeled off and the resultant circular muscle - myenteric plexus (CMMP) preparations were stretched over a small inox ring and immobilized by a matched rubber O-ring and placed in an organ bath^{43,77}. In this study, the proximal colon was defined as 2 cm below the caecum with V-shaped ribbon mucosa and the distal colon 4 cm from the caecum with flat mucosa.

GCaMP3 was excited at 470 nm, and its fluorescence emission was collected at 525/50 nm using a 5x objective on an upright Zeiss microscope (Axio Examiner.Z1; Carl Zeiss), equipped with a monochromator (Poly V) and cooled CCD camera (Imago QE), both from TILL Photonics. Images, 80 ms exposure each, were captured at a frame rate of 2 Hz. The tissue was constantly superfused with Krebs solution (in mM: 120.9 NaCl, 5.9 KCl, 1.2 MgCl₂, 2.5 CaCl₂, 1.2 NaH₂PO₄, 14.4 NaHCO₃, 11.5 glucose) at room temperature via a gravity-fed electronic valve system. Nifedipine (1 μM) was routinely added to the solution to prevent spontaneous muscle contraction. For both regions, electrical stimulation (ES; 300 μsec, 30 V, 20 Hz, 2 s) was delivered using a Grass S88 stimulator with SIU5 stimulus isolation unit via a focal mono-polar stimulating electrode (50 μm diameter tungsten wire insulated except at the tip) placed on an interganglionic fiber tract. To inhibit nicotinic receptors, the tissue was superfused with hexamethonium (200 μM). Preparations were stimulated 3 times, 10 min apart: first in control Krebs, a second time in the presence of hexamethonium, following a 10 min drug wash-in period, and finally again in control Krebs (washout). Time controls for electrical stimulation were performed twice, 10 min apart, in control Krebs. Changes in GCaMP3 fluorescence, which reflects the intracellular Ca²⁺ concentration ([Ca²⁺]_i), were collected using TILLVISION software (TILL Photonics) and analysis was performed as described previously²⁴⁷ in IGOR PRO (Wavemetrics) using

custom written macros. Regions of interest (ROIs) were drawn in the activity over time images and fluorescence intensity for each cell was calculated and normalized to its baseline starting value. Although the GCaMP3 fluorescence at rest was not identical between proximal and distal neurons, the difference was small enough (~ 1 %) to assume equal GCaMP3 expression levels. The 5x approach basically operates as filter that makes the subtle glial responses invisible in favor of detecting the larger round neuronal cell bodies. We cannot fully exclude that in some of the experiments a glial cell was included, but upon carefully visual inspection of the data files (limited of course by the resolution at 5x, NA 0.4) we did not find evidence of glial infiltration in the dataset. The center of the ROI served to determine the location of the responding neuron relative to the stimulation electrode. To compute their size, we used the long and short axis of the ROI to calculate the surface of an ellipsoid shape with the same dimensions.

4.2.3 Live video imaging of colonic motility

Ex vivo video imaging and analysis of colonic motility was performed as described previously^{208,250}. Entire colons with adhering caecum were carefully isolated and loosely pinned in an organ bath chamber, continuously superfused (flow rate: 3 ml per min) with Krebs solution bubbled with carbogen (95% O₂/5% CO₂) and kept between 35 °C and 37 °C. Intestines were allowed to equilibrate, which led to the expulsion of varying amounts of luminal content. After 30 minutes, movies of colonic motility were captured (4 Hz frame rate, 15 min duration) with an ORCA-Flash 4.0 camera using HCLImage Live software (Hamamatsu Photonics, Germany). Images were read into IGOR PRO and spatiotemporal maps were created and analyzed using custom-written algorithms.

4.2.4 Neuronal process tracing

4.2.4.1 *Recombinant adeno-associated viral vector (AAV) preparation*

The rAAV2/9 vector production and purification were performed by the Leuven Viral Vector Core as previously described²⁵¹. Adeno-associated viral vector encoding the

enhanced green fluorescent protein (eGFP) reporter under the ubiquitous cytomegalovirus (CMV) promoter was packaged in an AAV9-capsid. Briefly, HEK 293T cells were transfected using a 25-kDa linear polyethylenimine solution using the pAdvDeltaF6 adenoviral helper plasmid, pAAV2/9 serotype and AAV-TF CMV-eGFP-T2A-fLuc (AAV transfer plasmid encoding eGFP and firefly luciferase reporters driven by a CMV promoter) in a ratio of 1:1:1. Viral vector particles collected from the concentrated supernatant, were purified using an iodixanol step gradient. The final sample was aliquoted and stored at - 80°C. Titers (GC/mL) for AAV stocks were analyzed by real-time PCR.

4.2.4.2 *rAAV2/9 injection*

Intravenous tail vein injections of rAAV2/9-CMV-eGFP were delivered into wild type C56Bl6/J adult mice. Mice (N = 3) were placed under an incandescent lamp for 15-20 min and physically restrained. In a set of preliminary experiments, we compared several concentrations for AAV2/9-CMV-eGFP, and found that a 10 - 25 µl tail vein injection could sparsely transduce neurons in the mouse myenteric plexus. For the data presented in this paper, 10 µl viral particle solution (titer: 8.47×10^{11} GC/ml) supplemented with 5% sucrose in 0.01 M PBS for a total volume of 250 µl were injected into the vein at a slight angle using a 33 gauge needle. Mice were sacrificed 2 weeks after injection and intestinal tissues were fixed, washed and prepared for immunohistochemistry.

4.2.5 Immunohistochemistry

Immunohistochemistry was performed as previously described²²². Briefly, whole-mount preparations of mouse colon were pinned in a Sylgard plate containing Krebs solution continuously oxygenated with carbogen (95% O₂/5% CO₂). The mucosa and submucosal layers were dissected away and the tissue was fixed in 4% paraformaldehyde (PFA, Merck, Overijse, Belgium) in 0.1 M phosphate buffered saline (PBS, pH = 7.3-7.4) for 40 min. After washing in PBS, the longitudinal muscle layer was carefully removed to expose the myenteric plexus for later immunostaining.

To visualize cholinergic neurons, the tissues were permeabilised in 1% triton X-100 in PBS for 4 - 6 h at room temperature, and incubated in primary antibodies (goat anti-ChAT: 1:500, Table 1) diluted in blocking solution (PBS with 3% bovine serum albumin with 0.1% Triton X-100) for 48 h at 4 °C. To visualize AAV2/9-CMV-eGFP transduced neurons, a rat anti-GFP (Table 1) antibody was used. To visualize the cholinergic neuronal varicosities, tissues preparations were permeabilised in 0.5% triton X-100 in PBS containing 2% donkey serum plus 2% goat serum for 2 h at room temperature, and incubated in primary antibodies (guinea pig anti-vAChT: 1:500, **Table 4.1**) overnight at 4 °C. After primary antibody labeling, all preparations were washed in PBS (3 x 10 min) and incubated in blocking solution containing matched secondary antibodies (**Table 4.1**) for 2 h at room temperature.

Table 4.1 | Antibodies used for immunohistochemistry

| Antibodies | Host | Dilution | Source/Catalog number/RRID number |
|----------------------|------------|----------|--|
| ChAT | Goat | 1:500 | Fisher scientific; AB144P; AB_2079751 |
| GFP | Rat | 1:1000 | Gentaur; 04404-84; AB_10013361 |
| HuCD | Human | 1:2000 | Gift from Kryzer Thomas J |
| nNOS | Sheep | 1:5000 | Gift from Miles Emson |
| Tuj1 | Rabbit | 1:2000 | Covance; PRB-435P-100; AB_291637 |
| vAChT | Guinea pig | 1:500 | Synaptic Systems; 139105; AB_10893979 |
| Anti-goat A488 | Donkey | 1:1000 | Molecular Probes; A-32814 |
| Anti-rat A488 | Donkey | 1:1000 | Molecular Probes; A-21208; AB_141709 |
| Anti-rabbit A488 | Donkey | 1:1000 | Molecular Probes; A-21206; AB_141708 |
| Anti-human A594 | Donkey | 1:1000 | Jackson Immuno Labs; 709-585-149; AB_2340572 |
| Anti-sheep A647 | Donkey | 1:500 | Molecular Probes; A-21448 |
| Anti-human AMCA | Goat | 1:250 | Jackson Immuno Labs; 109-155-003; AB_2337696 |
| Anti-guinea pig A594 | Goat | 1:500 | Molecular Probes; A-11076; AB_141930 |

Abbreviations: ChAT, choline acetyltransferase; GFP, green fluorescent peptide; nNOS, neuronal nitric oxide synthase; Tuj1: neuronal class III β -tubulin; vAChT, vesicular acetylcholine transporter.

4.2.6 Image analysis

Choline acetyltransferase/nitric oxide synthase (ChAT/nNOS) and HuC/D preparations were imaged on a Zeiss LSM 780 laser scanning confocal microscope (25 x, H₂O immersion lens, NA = 0.8). Cells were counted manually using ImageJ (NIH,

Bethesda, MD) and the ChAT/nNOS identity of a neuron was scored using a single plane where the nucleus and cytoplasm were clearly visualized. A minimum of three fields of view in each region were analyzed for each animal and data were obtained from a minimum of three mice from three different litters. The preparations, used for visualization of cholinergic varicosities, were imaged on a Zeiss LSM 880 laser scanning confocal microscope (40 x, oil immersion lens, NA = 1.3). Image stacks (approx. 70 images) were deconvolved using Huygens professional (SVI, Hilversum, The Netherlands). The background fluorescence was automatically estimated and corrected for using Huygens's default parameters. Subsequently, the deconvolved image stacks were imported in IMARIS 9.02 (Bitplane, Zurich, Switzerland) to assess the surface to surface contact area between the Hu+ neuronal bodies and vesicular acetylcholine transporter immunoreactive (vAChT+) varicosities. First, we created a surface area based on the Hu channel that was used to make a 3D mask channel for vAChT later. Then a new surface for vAChT mask channel was established. Lastly, the surface to surface contact area algorithm available in IMARIS Xtensions was applied to calculate overlap between the vAChT and HuC/D surface areas. Neuronal class III β -tubulin (Tuj1) preparations were imaged on a Zeiss LSM 780 laser scanning confocal microscope (63x, H₂O immersion lens, NA = 0.8). After image stacks were deconvolved using Huygens professional (SVI, Hilversum, The Netherlands), fibers were counted manually using ImageJ (NIH, Bethesda, MD). To facilitate the detection of eGFP, an antibody against GFP was used. The labeled axons were traced (for at least 200 μ m) to determine their individual projection orientation. In those neurons where the axon could be fully traced we also measure the length of individual GFP-immunoreactive fibers using Image J.

4.2.7 Data analysis

All data are presented as mean \pm SEM. "n" refers to the number of cells, "N" refers to the number of animals. Actual p values (up to 3 decimal digits) were listed, unless they were smaller than 0.001 or they were not specified by Graphpad (as is the case for Bonferroni *post hoc* following an ANOVA test). Student's t-tests were used to

compare results unless mentioned otherwise. At least three animals were used for each experimental condition. All Ca^{2+} transient analysis, spatial mapping algorithms used to correlate size, position and response characteristics were custom-written in IGOR (Wavemetrics, Oregon, US) and are available upon request. Statistical analyses were performed with Microsoft Excel or GraphPad. Differences were considered to be significant if $p < 0.05$.

4.3 Results

4.3.1 Motility and underlying neuronal circuitry in the proximal and distal colon

The proximal and distal large intestine have a different function and display a distinct set of motility patterns. For example, while CMMCs are consistently initiated in the proximal part of the colon, propagating CMMCs not always travel into the distal colon^{208,252}. Video recordings and spatiotemporal map analysis of colonic motility *in vitro* clearly show that CMMCs start at a regular frequency ($0.38 \pm 0.03 \text{ min}^{-1}$, $N = 4$) in the proximal colon (**Figure 4.1A**). In the distal large intestine these peristaltic contractions are observed less frequently ($0.22 \pm 0.07 \text{ min}^{-1}$, $N = 4$, $p = 0.0804$) and they are dependent on the presence of luminal content, which is supplied by propagating contractions travelling from more proximal regions. To compare the neuronal circuit complexity underlying the differential motor behavior between the proximal and distal large intestine, we used GCaMP3 (Wnt1|GCaMP3) based Ca^{2+} imaging combined with focal electrical stimulation and tested the response signature and location of all neurons that were functionally connected (directly and synaptically) with a specific stimulus stimulation spot. Myenteric ENS preparations from both regions were imaged with a low magnification (5 x) lens to maximize the number of ganglia within one field of view, while still being able to resolve individual GCaMP3 expressing neurons. With this imaging configuration (**Figure 4.1B**), we were able to record from a large population of neurons in $\sim 25.0 \pm 2.0$ (from 8 myenteric plexus preparations, $N = 5$ animals) and $\sim 34.0 \pm 2.0$ ganglia (from 7 myenteric plexus preparations, $N = 5$ animals) simultaneously in a 1.3 mm x 1.7 mm field of view from the proximal and distal colon, respectively.

Electrical stimulation (300 μ sec, 20 Hz, 2 s) was delivered with a focal electrode onto an interganglionic fiber tract. We used a volley of 40 pulses, considered to be a maximal stimulus²⁵³, to assure that all neurons functionally (both synaptically or directly) connected to the stimulation site were activated. This induced a sharp increase in $[Ca^{2+}]_i$ in myenteric neurons scattered around the electrode in both the proximal and distal large intestine (**Figure 4.1C and D**). Both the number (#) of responding (R) neurons (#R) (**Figure 1E**) and the maximal Ca^{2+} transient amplitude ($\Delta F_i/F_0$, **Figure 4.1F**) were significantly higher in the proximal compared to the distal colon ($\#R_{Dis}/\#R_{Prox} = 33\%$).

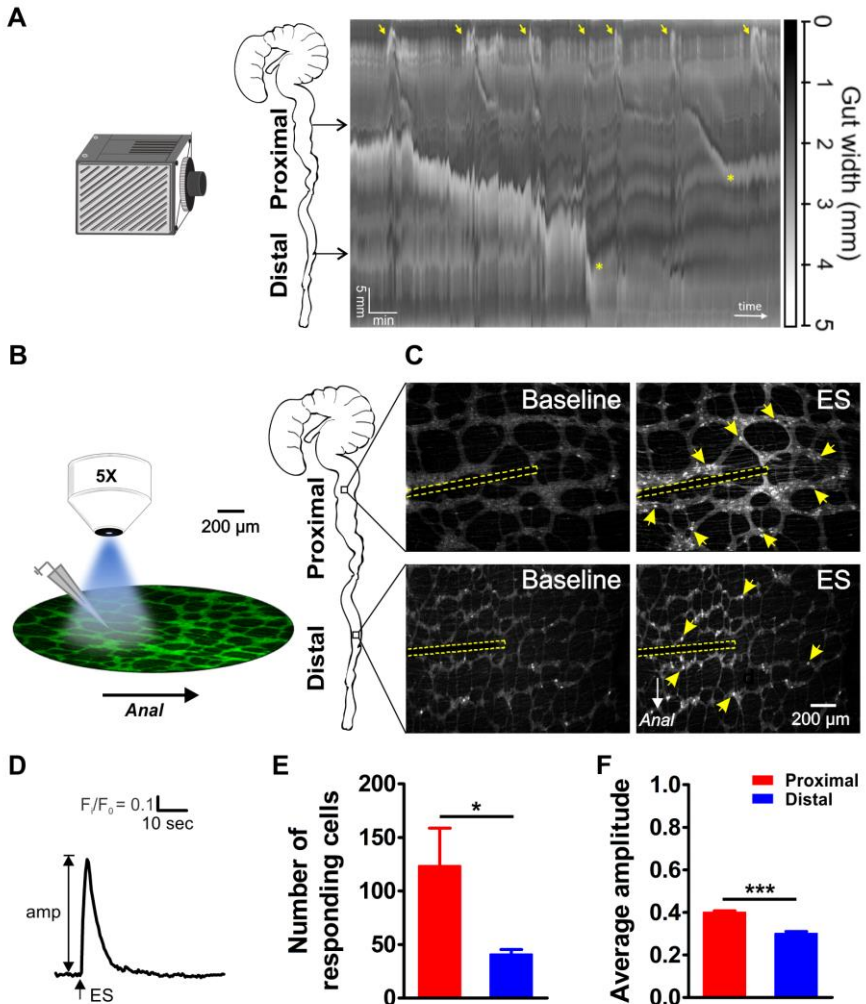


Figure 4.1 | Video imaging of colonic motility in vitro and in situ calcium imaging of myenteric neuron activity in the proximal and distal colon.

A, Video recordings of the isolated mouse colon (with caecum attached) were analyzed using spatiotemporal mapping of the intestinal diameter (representative example of 4 experiments). Maximum constriction (black), maximum dilation (white), and intermediate levels of constriction (grayscale) of the whole colon (vertical axis: 6 cm in total) are represented over time (horizontal axis, 15 minutes total duration). Colonic migrating motor complexes (CMMCs) are initiated in the proximal colon (yellow arrows). Propagating CMMCs proceed into the distal large intestine when associated with luminal content supplied by more proximal regions (yellow asterisks). **B**, Schematic overview of the experimental setup (left) and regions of the mouse large intestine that were compared (right). Colonic myenteric plexus preparations obtained from *Wnt1::Cre;R26R-GCaMP3* (*Wnt1|GCamp3*) mice were visualized under an upright fluorescence microscope using a 5X objective lens. Neuronal Ca^{2+} transients were elicited by trains of electrical pulses (300 μ sec, 20 Hz, 2 s) transmitted via a focal electrode positioned on interganglionic fiber tracts in the center of the field of view. **C**, Representative single frames taken from GCaMP3 fluorescence recordings of neurons within myenteric ganglia of proximal (top row) and distal (bottom row) colon before (baseline) and during electrical stimulation (ES, the position of the focal electrode is depicted by the yellow dotted line). A random subset of responsive neurons is marked with yellow arrows. **D**, Representative trace of an ES-evoked Ca^{2+} transient of an individual myenteric neuron. The amplitude of each Ca^{2+} transient was calculated as the difference between baseline (F/F_0) and maximal F_i/F_0 GCaMP3 fluorescence. **E**, Comparison of the average number of neurons responding per field of view (2.2 mm²) (123.5 ± 35.3 vs 41.0 ± 4.4 , * $p = 0.049$). **F**, Comparison of the average Ca^{2+} transient amplitude (0.40 ± 0.01 vs 0.30 ± 0.01 , *** $p < 0.001$). A total of 988 neurons in the proximal (from 8 myenteric plexus preparations, $N = 5$ animals) and 287 neurons in the distal (from 7 myenteric plexus preparations, $N = 5$ animals) colon displayed Ca^{2+} transients upon electrical stimulation was used for calculating E and F.

4.3.2 Regional differences in myenteric plexus morphology

To investigate why more myenteric neurons in the proximal colon responded to the stimulus, we first assessed whether this difference could simply be explained differences in the density of neurons. Using immunohistochemistry for the pan-neuronal marker Hu, we found a higher density of neurons (number of neurons: #N) in the proximal colon compared to the distal (**Figure 4.2A-B**), resulting in a ratio of

$\#N_{Dis}/\#N_{Prox} = 85\%$. Next, we also quantified the number of neuronal fibers present in one interganglionic fiber tract by staining for neuronal class III β -tubulin (Tuj1) and found that interganglionic fiber tracts in the proximal colon contained more neuronal processes than those in the distal colon (**Figure 4.2C-D**). Therefore, given that the focal electrode covers the entire width of the interganglionic fiber tract in both regions, a greater number of neuronal fibers is activated in the proximal colon with each electrical stimulus. However, even taken together, the higher density of myenteric neurons and the difference in activated fiber (F) number ($\#F_{Dis}/\#F_{Prox} = 50\%$) cannot fully explain the higher number of responding neurons in the proximal colon ($\#N_{Dis}/\#N_{Prox} (85\%) * \#F_{Dis}/\#F_{Prox} (50\%) = 42.5\%$, which is greater than the observed responder (#R) ratio $\#R_{Dis}/\#R_{Prox} = 33\%$). In a simplistic model where all targeted processes belong to monoaxonal neurons that connect with only one postsynaptic neuron, interganglionic fiber tract stimulation would activate 2 neurons per fiber: one synaptically and one antidromically. In the distal colon, this oversimplified assumption does not deviate too much from the numbers of responding neurons observed (18 fibers stimulated * 2 = 36 responding neurons), while in the proximal colon this assumption definitely does not appear to hold true and suggests that there is far more complex wiring, including an increased number of synaptic targets for each neuron.

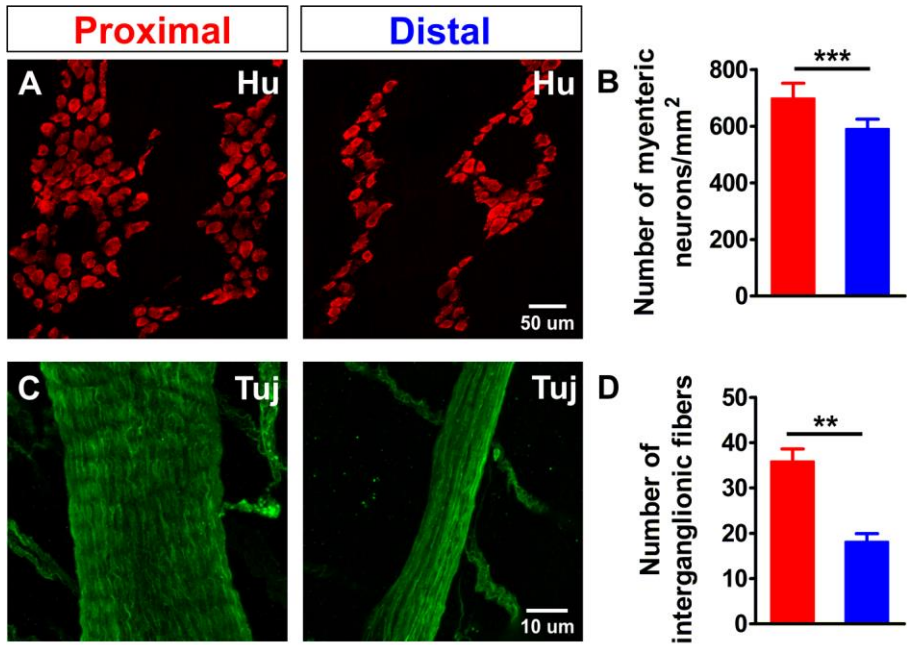


Figure 4.2| Density comparison of myenteric neurons and interganglionic processes in the proximal and distal colon.

A, Confocal maximum projection of whole-mount preparations of the myenteric plexus from the proximal and distal colon immunostained for the pan-neuronal marker Hu (red). **B**, Quantification of the number of myenteric neurons per square millimeter (698.3 ± 52.9 vs 591.3 ± 33.2 per mm^2 , $***p < 0.001$; $N = 3$) in the proximal (red) and distal (blue) colon, asterisks indicate statistical difference. The ratio between number of neurons ($\#N$) distal and proximal ($\#N_{\text{Dis}}/\#N_{\text{Prox}}$) is 85%. **C**, Confocal maximum projection of whole-mount preparations of the myenteric plexus from the proximal and distal colon immunostained for neuronal class III β -tubulin (Tuj1, green). **D**, Quantification of the number of processes per interganglionic fiber bundle (35.9 ± 2.7 vs 18.2 ± 1.8 , $**p = 0.005$; $N = 3$), the ratio between the number of fibers in the distal vs. proximal ($\#F_{\text{Dis}}/\#F_{\text{Prox}}$) is 50%.

4.3.3 Ca²⁺ response signatures of individual myenteric neurons

To assess the role of individual neurons and their synaptic inputs in the enteric circuitry, we constructed “activity over time” (AoT)²⁴⁷ images in which responding cells, color coded by amplitude, can be identified (**Figure 4.3A**). For each neuron we determined a response signature, which we defined as the ratio of their Ca²⁺

response amplitude in two consecutive rounds of electrical stimulation. As seen in the AoT images, neurons display a variety of response signatures, with some having increased while others show decreased amplitudes during the second stimulus (over 95% of the neurons responded twice). Based on their response signature, we classified the neurons into one of five types (**Figure 4.3B**). Type I (black) “blocked” neurons only responded to the first stimulus ($> (-\Delta 90\%)$ change in peak Ca^{2+} signal); type II (blue), “reduced” neurons, in which the Ca^{2+} response to the second stimulus was reduced compared to the first stimulus (between $(-\Delta 10\%)$ and $(-\Delta 90\%)$ change in peak Ca^{2+} signal); type III (green), “unchanged”, where both stimuli elicited a similar Ca^{2+} transient ($\pm \Delta 10\%$ change in peak Ca^{2+} signal); type IV (red), neurons with an “increased” response ($> (+\Delta 10\%)$ change in peak Ca^{2+} signal); and type V (purple), “new” cells that did not respond to the initial stimulus but appeared during the second electrical stimulation (“+” means increase; “-” means reduce, **Figure 4.3B**). The frequency histograms (**Figure 4.3C**) illustrate the consistency of Ca^{2+} responses over consecutive experiments as over 85% of the neurons displayed equal Ca^{2+} transients or were only slightly (> 0.8) reduced or increased (< 1.2).

We used this classification scheme to investigate the contribution of cholinergic synaptic activation in the myenteric circuitry of the large intestine. Cholinergic transmission, involving the activation of nicotinic receptors (nAChRs) is established early on in development⁷⁷ and remains a crucial component of excitatory synaptic transmission in the ENS throughout life^{70,80}. We used hexamethonium, an effective blocker of the nicotinic acetylcholine receptor, to inhibit nicotinic cholinergic neurotransmission and refine the wiring identity of individual neurons. As in our control experiments, each preparation was stimulated twice, once in control Krebs and a second time after 10 min incubation in hexamethonium (200 μM ; **Figure 4.3D**). Logically, in the presence of hexamethonium, the frequency histograms shifted to the left (**Figure 4.3E**) as more neurons were present in the blue bins both in the proximal (56.6% vs 29.6% in control) and distal (44.8% vs 32.8% in control) colon. In line with the reduction in amplitude, also the proportion of blocked neurons (black bin) was higher in the hexamethonium versus the control condition. This proportion of Type I

“blocked” neurons was significantly higher in the distal as compared to the proximal colon (**Figure 4.3E**), indicating that in the distal colon a larger fraction of neurons completely depends on cholinergic input from the stimulation site. Even though most fast excitatory neurotransmission is blocked by hexamethonium, a considerable number of neurons remain responsive and some even displayed enhanced responses to interganglionic fiber tract stimulation (**Figure 4.3D**).

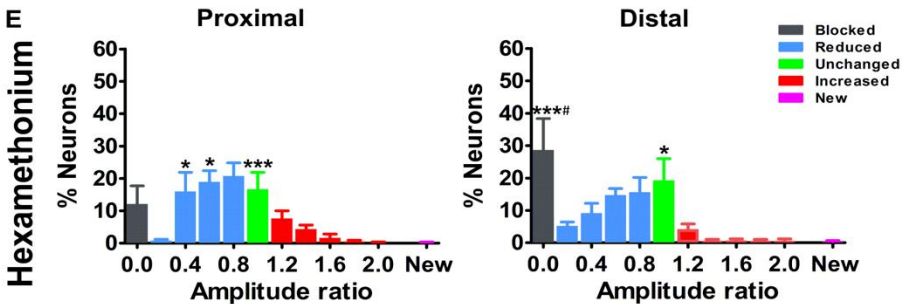
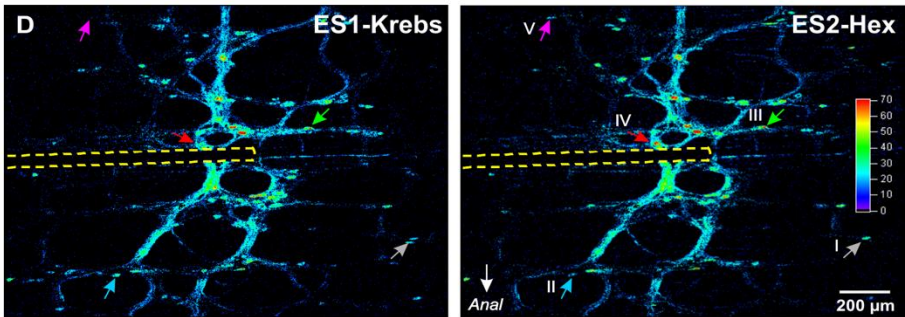
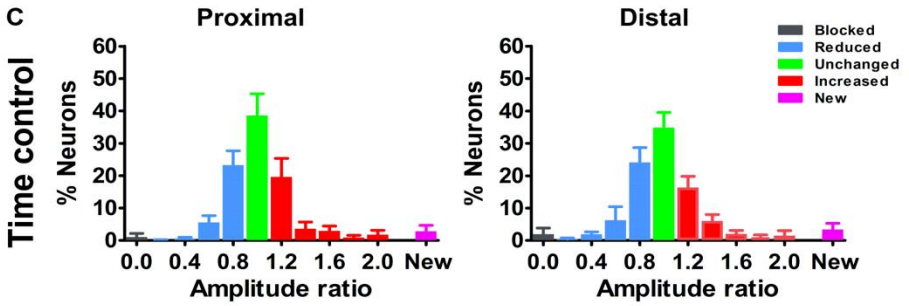
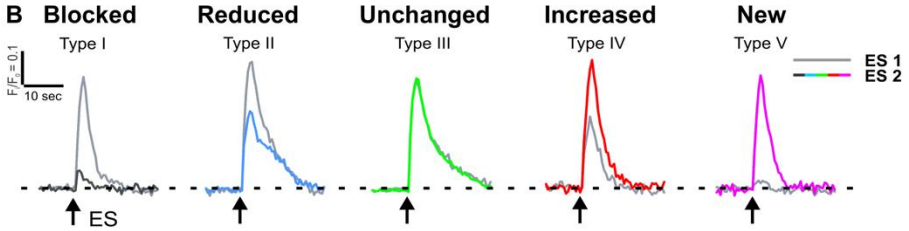
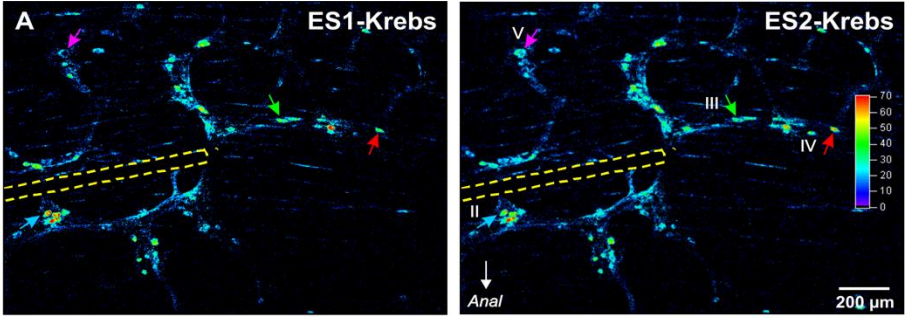


Figure 4.3] Ca²⁺ response signatures of enteric neurons during two consecutive rounds of electrical stimulation in control conditions and in Hexamethonium.

A, Activity over Time (AoT) images in which the Ca²⁺ transient amplitude for active cells only is color-coded (absolute values in arbitrary units, see color scale). Left and right respectively show an example of the responses (arrows point at individual examples) to a first electrical stimulation (ES1) and a second consecutive electrical stimulation (ES2) in control conditions (Krebs). The location of the focal electrode is indicated by the yellow dashed line. Colored-coded arrows mark responder subtypes as explained in B. **B**, The amplitude ($\Delta F/F_0$) of the second (color trace) response was compared to the first (gray trace) and expressed as a ratio $(\Delta F/F_0)_{ES2} / (\Delta F/F_0)_{ES1}$ for each individual neuron. Based on this response signature, responsive neurons were classified into five different classes: blocked (Type I), reduced (Type II), unchanged (Type III), increased (Type IV) and new (Type V) cells (see color-coded arrows in A, A'). Note that in this field of view no Type I neuron was present, as these are very rare in control (saline) conditions. **C**, Histograms showing the percentage of neurons (mean \pm SEM) belonging to the different (color coded) classes as found in the myenteric plexus of the proximal (left) and distal (right) colon. Results are expressed as the amplitude ratio binned by 0.2. Note that the distributions approximate a standard normal distribution both in the proximal and distal colon do not differ substantially between the proximal and distal colon, indicating a robust response behaviour. A total of 717 neurons in the proximal (N = 4) and 252 neurons in the distal (N = 4) colon displayed Ca²⁺ transients upon electrical stimulation. **D**, Activity over Time (AoT) images in which the maximal Ca²⁺ amplitude (color-coded) of responsive neurons is shown during a first electrical stimulation (ES1) in control Krebs (left) and a second consecutive stimulation (ES2) in the presence of hexamethonium (Hex, 200 μ M, right). The location of the focal electrode is indicated by a yellow dashed line. Neurons belonging to each of the five different types of responders classes (blocked (Type I), reduced (Type II), unchanged (Type III), increased (Type IV) and new (Type V)) are indicated by color-coded arrows. **E**, Histograms showing the percentage of neurons (mean \pm SEM) belonging to the different (color coded) classes in the presence of Hex as found in the myenteric plexus of the proximal (left) and distal (right) colon. These frequency histograms show a shift to the left (more neurons in the blue and black bars) as compared to the control situation. About \sim 10% of proximal neurons and \sim 30% of distal neurons were completely blocked by Hex (Prox: 12.2% vs 1.1%, $p > 0.05$; Dis: 28.7% vs 1.9%, $***p < 0.001$, two-way ANOVA with Bonferroni *post hoc* test). Comparing the Hex effect between both regions, it is clear that the proportion of blocked neurons in the distal is significantly higher than in the proximal colon (Dis: $28.7 \pm 9.7\%$ vs Prox: $12.2 \pm 5.6\%$, $^{\#}p < 0.05$, two-way ANOVA with Bonferroni *post hoc* test). A total of 653 neurons in the proximal (from 6 myenteric plexus preparations, N = 4) and 288 neurons in the distal (from 7 myenteric plexus

preparations, N = 5) colon displayed Ca²⁺ transients upon electrical stimulation and was used in the analysis. The * symbols denote the comparison between control and Hex, while # reflects the comparison distal vs proximal.

4.3.4 The importance of nicotinic cholinergic input scales with distance from the stimulation electrode

As many of the blocked neurons were located aborally to the electrode, we hypothesized that the subtle circuitry differences observed in the vicinity of the stimulated interganglionic fiber tract might be more explicit when monitoring the neurons even more distal to the stimulation site. We therefore extended the experiments by imaging one field of view below the original field (*see schematic figure 4.4A*).

Indeed, for both the proximal and distal colon, the effect of hexamethonium on inhibition of neural activity was more explicit further away from the stimulation site (**Figure 4.4B-C**). The average Ca²⁺ transient amplitude of the neurons in this field of view was lower than for neurons closer to the electrode (data not shown). The proportion of fully blocked neurons (type I) was significantly higher compared to the original field of view (**Figure 4.3E & 4.4C**). In addition, the fraction of blocked neurons in the distant field (> 650 μm) was significantly larger in the distal colon compared to the proximal colon (**Figure 4.4C**), which indicates that, in the distal large intestine, more neurons fully depend on cholinergic input in the field distant from the electrode. This further highlights ENS wiring differences between the proximal and distal large intestine.

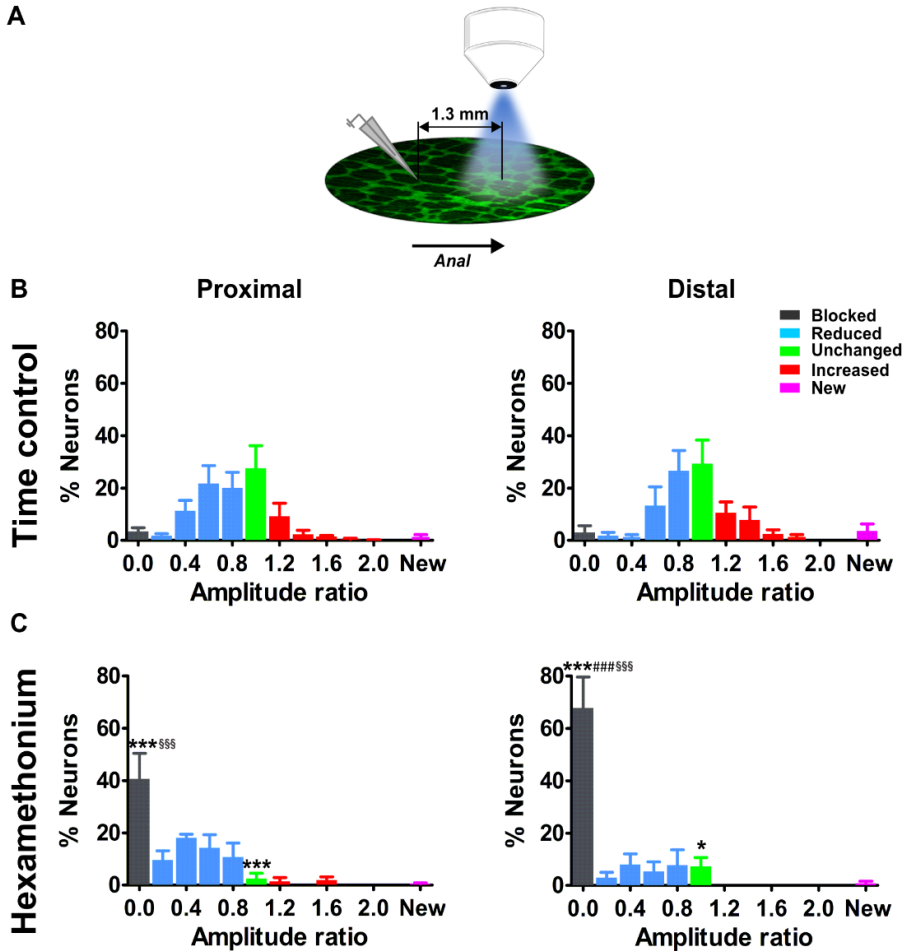


Figure 4.4| Effects of blocking cholinergic nicotinic neurotransmission on electrically evoked Ca^{2+} transients of myenteric neurons distal to the stimulation site.

A, Schematic representation of the stimulation site and imaging field. For the current set of experiments, the electrode was placed one field of view (= 1.3 mm) orally to the field of view. **B - C**, Histograms showing the percentage of neurons (mean \pm SEM) belonging to the different (color coded) classes as found in the myenteric plexus of the proximal (left) and distal (right) colon at a distance away from the stimulation electrode. **B**, shows the control condition (2 stimuli in control Krebs) and **C**, the situation when the second stimulus was given in the presence of hexamethonium (Hex, 200 μM). Note that the histograms in **B** are still normally distributed but with a larger spread compared to the neurons closer to the electrode (Fig. 3). The frequency histograms in **C** show a robust shift to the left (more neurons in the blue and black

bars) as compared to the control situation. About ~ 40% of proximal neurons and ~ 70% of distal neurons were completely blocked by Hex (Prox: 40.7% vs 3.5%, *** $p < 0.001$; Dis: 67.8% vs 3.1%, *** $p < 0.001$, two-way ANOVA with Bonferroni *post hoc* test). Comparing the Hex effect between both regions, many more neurons were completely blocked in the distal compared with the proximal colon (Dis: 67.8 ± 11.7% vs Prox: 40.7 ± 9.7%, ### $p < 0.001$, two-way ANOVA with Bonferroni *post hoc* test). In addition, comparing the Hex effect between both fields of view, the proportion of blocked neurons was significantly higher in the field further away than close to the electrode (see in Figure 3E) (Prox: 40.7 ± 9.7% vs 12.2 ± 5.6%, §§§ $p < 0.001$; Dis: 67.8 ± 11.7% vs 28.7 ± 9.7%, §§§ $p < 0.001$, two-way ANOVA with Bonferroni *post hoc* test). A total of 284 neurons in the proximal (from 4 myenteric plexus preparations, N = 2) and 101 neurons in the distal (from 4 myenteric plexus preparations, N = 3) colon displayed a Ca²⁺ transient upon electrical stimulation and were used in the analysis. The * symbols denote the comparison between control and Hex, the # symbols reflect the comparison distal vs proximal and the § symbols the comparison between the fields of view (close and further away from the electrode).

4.3.5 Distribution mapping of responding neurons

Given that the proportion of hexamethonium blocked neurons (type I) is much larger in the distal colon (certainly at greater distances), we investigated whether there was a specific spatial distribution pattern along the length axis of the large intestine. To do this, we plotted the relative positions of all responding neurons on a spatial distribution map and color-coded them for their response signature (type I-V). When stimulated twice in control Krebs only, the different types of neurons were scattered throughout the network without any apparent pattern with respect to location or amplitude (**Figure 4.5A,B**).

In contrast, the spatial plots of the hexamethonium experiments revealed specific locations for the different responder types. Two distinct phenomena were uncovered. First, we found that apart from an increased proportion of type I blocked cells in the distal colon compared to proximal (as shown also in **Figure 4.3E & 4.4C**), the spatial distribution of these type I blocked neurons differs significantly between the two regions. In the distal colon, the type I blocked cells are uniformly spread along the longitudinal axis of the myenteric plexus (**Figure 4.5C,D**), while for the proximal colon

almost 90% of the type I blocked neurons are located aboral to the stimulation site (**Figure 4.5C,D**).

Mapping the location of responding neurons also revealed that the majority (over 70% and 60% in distal and proximal colon respectively) of neurons whose amplitude was not reduced by hexamethonium (type III and IV), were located close to the electrode (in a 500 μm oral - aboral band) (**Figure 4.5D**), while a random distribution was observed in time control experiments.

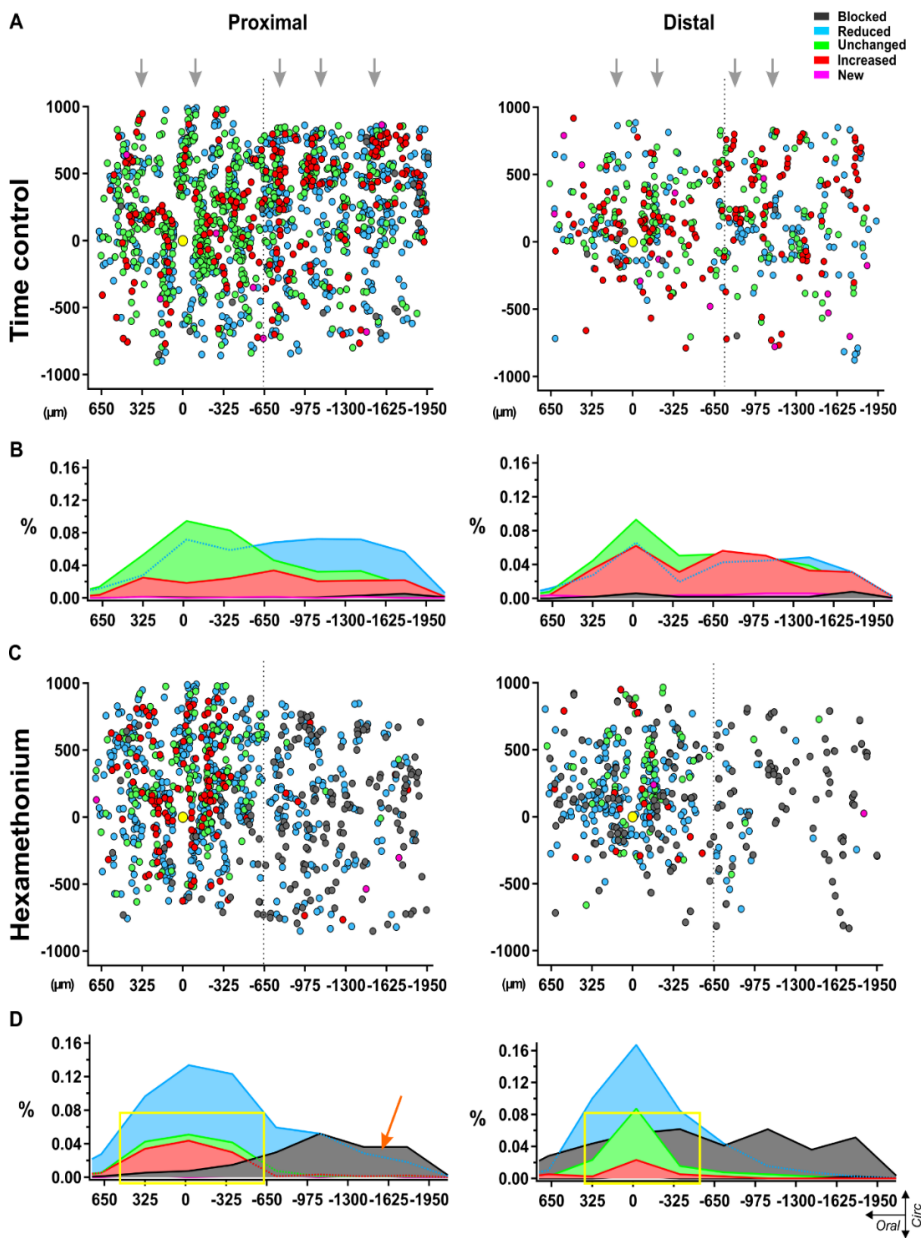


Figure 4.5] Spatial distribution of myenteric neurons responding to electrical stimulation of a single interganglionic fiber tract.

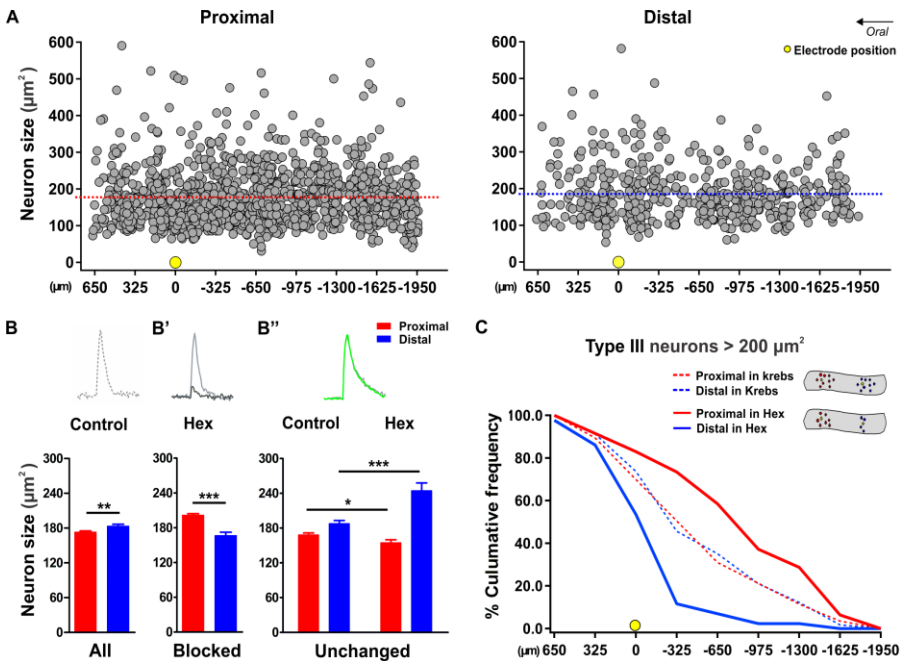
Dotplots of the location of each individual neuron pooled from all recordings in control Krebs (top, A-B) and hexamethonium (200 μ M, bottom, C-D) conditions in proximal (left) and distal (right) colon. Individual neurons are shown as circles color coded according to their response signature (= ratio of responses to two consecutive

responses). The location of the focal stimulation electrode is indicated with the yellow circle. **A**, All responsive neurons in control conditions were scattered without any apparent pattern, except that the ganglionic network was reflected in the distribution, indicating morphologic consistency over different preparations (grey arrows). **B**, Summarizing histograms show uniform distribution of the neurons, slightly reduced (Type II: light blue) or slightly enhanced (Type IV: red), while neurons that were unchanged (Type III: green) were more centered around the electrode. Only few blocked (Type I: dark grey) and new (Type V: pink) neurons were detected in control conditions. **C**, Spatial distribution of the responding cells in hexamethonium (200 μ M) in proximal and distal colon. **D**, Summarizing histograms show a preferential aboral location of fully blocked (Type I: dark grey) neurons in the proximal colon (orange arrow) while in the distal colon, fully blocked neurons are more spread over the entire length. Neurons showing the same (Type III) or an increased response (Type IV) cluster around the electrode in the proximal and even more so in the distal as indicated by the yellow box.

4.3.6 Morphology of responding neurons

Next, we took advantage of the distinctive expression pattern of the genetically-encoded Ca^{2+} indicator in enteric neurons to determine the size of their cell bodies (see methods). We found that the larger and smaller neurons were randomly scattered along the longitudinal axis of both the proximal and distal colon (see scatterplots in **Supplementary figure 4.1A**). Furthermore, although the size of responsive neurons varied substantially, the size of the responders in the proximal colon was on average smaller than in the distal (Prox: 173.2 ± 2.0 (SD: 74.9) vs Dis: 183.4 ± 3.1 (SD: 71.5) μm^2 , $p = 0.008$) (**Supplementary figure 4.1B**). However, when specific responder subpopulations were compared, apparent size differences were detected. First, the type I (blocked) neurons were significantly smaller in the distal than the proximal colon (Dis: 166.4 ± 5.9 vs Prox: 201.7 ± 2.6 , $p < 0.001$, **Supplementary figure 4.1B'**). Second, we found that in the distal colon the size of the type III (unchanged amplitude) neurons was significantly larger in the hexamethonium condition than in control (244.5 ± 13.3 vs 187.8 ± 5.4 μm^2 , $p < 0.001$, **Supplementary figure 4.1B''** blue bars). While in the proximal colon these type III neurons were even a little smaller in hexamethonium compared to the control situation (154.8 ± 5.2 vs 168.4 ± 3.2 μm^2 , $p = 0.040$, **Supplementary figure 4.1B''** red

bars). When we mapped the location of the larger ($> 200 \mu\text{m}^2$) type III (unaffected amplitude) neurons along the longitudinal axis of the proximal and distal colon, we found that in control conditions these neurons were spread out fairly uniformly in both gut regions (**Supplementary figure 4.1C** dotted lines). However, in hexamethonium, these large neurons were clearly centered around the stimulation site in the distal colon, but not in the proximal (**Supplementary figure 4.1C** solid lines). This indicates that groups of neurons exist with larger cell bodies and who do not depend on cholinergic transmission, these neurons operate in synchrony and are located in a defined band around the stimulus site.



Suppl. Figure 4.1 | Size versus location of responding neurons.

A, Scatterplots in which size (y-axis) of the responding neurons is plot against their oral to distal location (x-axis) along the length axis of the proximal (left) and distal (right) colon. Smaller and larger neurons are randomly distributed without any apparent preferential location. The average size of the responding neurons is shown by the red square. **B**, Histogram summarizing the size distribution of all responsive neurons in the proximal (red) and distal (blue) colon in control (Prox: 173.2 ± 2.0 (SD: 74.9) vs Dis: 183.4 ± 3.1 (SD: 71.5) μm^2 , $**p = 0.008$). **B'**, Bar graphs showing the size of the Type I (fully blocked) neurons in hexamethonium (Hex), which are larger in the

proximal than in the distal colon (Prox: 201.7 ± 2.6 vs Dis: $166.4 \pm 5.9 \mu\text{m}^2$, $***p < 0.001$). **B''**, Bar graphs showing the size of the neurons that displayed a Ca^{2+} transient with the same amplitude (Type III) both in control and in hexamethonium (Hex, 200 μM). The size of those neurons is smaller in proximal than in the distal, an effect that is amplified by the presence of Hex. **C**, Cumulative frequency histogram summarizing the location of the larger neurons (defined as $> 200 \mu\text{m}^2$) with the same amplitude (Type III) in the proximal (red) and distal (blue) colon relative to the electrode position (as indicated by the yellow circle). The shallow sigmoid curves indicate that in control conditions (dashed lines), this specific subset of neurons (large and same amplitude) are uniformly distributed. In the presence of Hex, the large neurons that maintain their response, cluster around the electrode in the distal while in the proximal colon they are further away. The inset shows a schematic of how the larger neurons with the same amplitude distribute around the stimulation electrode in the proximal and distal large intestine.

4.3.7 Quantification of cholinergic neurons and synaptic contacts in proximal and distal colon

To test whether the differences in wiring are reflected in the chemical coding of both regions, we quantified the proportion of excitatory colonic myenteric neurons using immunohistochemistry against the pan-neuronal marker Hu and the excitatory cholinergic neuron marker ChAT (**Figure 4.6A**). Though the total number of neurons was different (see also **Figure 4.2**), the proportion of cholinergic neurons did not differ between the proximal and distal colon (Prox: $52.9 \pm 3.9\%$ vs Dis: $50.3 \pm 4.4\%$, $p = 0.689$, **Figure 4.6B**). Interestingly, the proportion of nitrergic neurons was found to be slightly higher in the myenteric plexus of the distal as compared to the proximal colon (Dis: $39.2 \pm 1.3\%$ vs Prox: $33.1 \pm 1.3\%$, $p = 0.029$, **Figure 4.6C**).

Since Ca^{2+} imaging revealed that cholinergic transmission plays a more important role in the distal versus the proximal part of the large intestine, we investigated whether this could be reflected in the density of cholinergic synaptic contacts per neuron. We quantified the percentage of overlap between the cholinergic synaptic release sites (as labeled by vAChT, **Figure 4.6D**) and HuC/D surfaces and found a significantly larger fraction of surface contact area between Hu+ myenteric neuronal bodies and vAChT+

cholinergic varicosities in the distal colon (Dis: $7.4 \pm 0.8\%$ vs $4.3 \pm 0.4\%$, $p = 0.002$, **Figure 4.6E**).

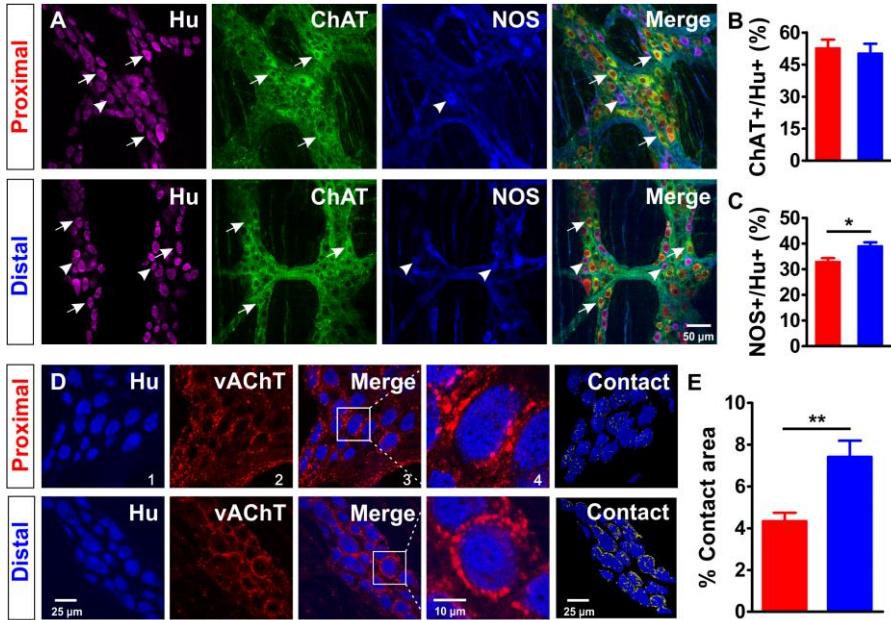


Figure 4.6] Extensive cholinergic innervation of myenteric neurons in the distal colon.

A-C, Cholinergic and nitergic neurons in the myenteric plexus of the proximal (red) and distal (blue) colon. **A**, Single confocal plane of a whole-mount myenteric plexus preparation of the proximal and distal colon immunostained for Hu (magenta), choline acetyltransferase (ChAT, green) and nitric oxide synthase (nNOS, blue). Arrows and arrowheads mark some typical ChAT and NOS neurons respectively. **B-C**, Quantification of the ChAT (**B**) and NOS (**C**) populations in the proximal (red) and distal (blue) colon, asterisks indicate statistical difference (Dis: $39.2 \pm 1.3\%$ vs Prox: $33.1 \pm 1.3\%$, $*p = 0.029$; $N = 3$). **D-E**, Vesicular acetylcholine transporter (vAChT+) stainings indicate a larger contact area between cholinergic synaptic contacts and Hu+ myenteric neurons in the distal colon. **D**, Single confocal plane of the myenteric plexus immunostained for Hu (blue) and vAChT (red) and its merge image (labeled with 1-3). A typical neuron (white square) is shown at higher magnification (labeled with 4). A 3D reconstruction showing the contact area (yellow) between Hu+ myenteric neuronal bodies and vAChT varicosities (labeled with contact). **E**, Quantification of the proportion of the surface contact area between the Hu+ myenteric neuronal bodies and vAChT+ cholinergic varicosities in the proximal (red)

and distal (blue) colon, asterisks indicate statistical difference (Dis: $7.4 \pm 0.8\%$ vs Prox: $4.3 \pm 0.4\%$, $**p = 0.002$; $N = 4$).

4.3.8 Sparse labeling of neuronal projection patterns using viral vector transduction

Since the Ca^{2+} imaging data indicate that there are substantial differences in the projection patterns of neurons in the distal and proximal colon, we used viral vector transduction to sparsely label enteric neurons and track individual neuronal projections (**Figure 4.7A**). At two weeks post-injection, a limited number of myenteric plexus neurons along the entire colon expressed eGFP in cell bodies and fibers, which allowed us to trace their projection orientation. All traced neurons were monoaxonal and are likely motor and interneurons (**Figure 4.7B**) or a subset thereof, while intrinsic sensory neurons most probably escaped our labeling strategy.

We divided all eGFP-labeled neurons (57 in the proximal and 61 in the distal colon) into three groups based on their oral, aboral or circumferential projection (**Figure 4.7C**) as determined from the first parts of their axon. We found that significantly more neurons project aborally in the distal colon compared to the proximal colon ($27.3 \pm 7.9\%$ vs $11.0 \pm 3.4\%$, $p = 0.004$, χ^2 test, **Figure 4.7D**). Assuming that viral transduction labels proximal and distal neurons equally, our measurements indicate that aborally projecting neurons in the distal colon are longer, while in the proximal colon the orally projecting neurons are longer. It is important to note that the projection termini could not be conclusively identified and therefore only length and not functional projection should be considered. The bimodal distribution of the neuronal projection lengths suggests that there are indeed shorter and longer projections, which can be roughly split at 3.1 mm (valley in bimodal Gaussian fit). Remarkably, this cutoff does not differ much from the subdivision based on Dil labelling made by Spencer et al ²⁵⁴. who suggested that the neurons with projections over 4 mm were interneurons. Our data showed that there was a significant difference for longer range projecting neurons in the distal versus the proximal colon,

suggesting that there is a higher proportion of descending interneurons in the myenteric plexus of the distal compared to the proximal colon (**Figure 4.7E**).

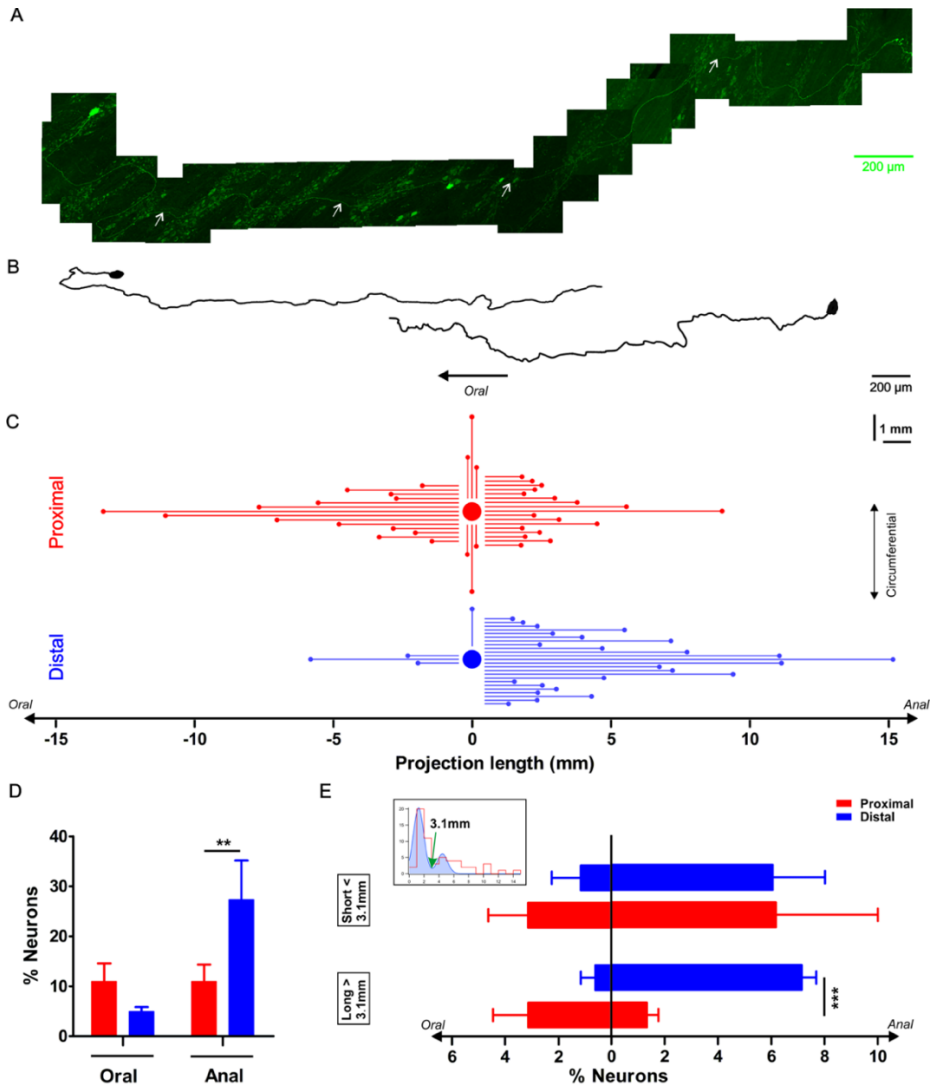


Figure 4.7 | Characterization of the axonal projection length and orientation of myenteric neurons in the proximal and distal colon.

A, Composite image of a eGFP+ enteric neuron and its axon located in the colonic myenteric plexus of a mouse that was sparsely transduced with rAAV9-CMV-eGFP two weeks prior to tissue collection. The fiber's (marked with white arrows) total length is 4.35 mm. **B**, Two examples of reconstructed projection (one oral and one

aboral) orientations of eGFP transduced myenteric neurons. **C**, Graphic summarizing the axonal length and projection orientation of all tracked myenteric neurons. For about half of the eGFP expressing neurons (Prox: 37/57 and Dis: 28/61), it was possible to trace the axon to its final target. Of those, 14 projected orally (mean length of 4.6 ± 1.0 mm), 17 aborally (mean length: 2.6 ± 0.4 mm) and 6 circumferentially (length of 1.7 ± 0.4 mm in the proximal, while in the distal 3 projected orally (mean length: 2.9 ± 1.2 mm), 24 anally (mean length: 4.7 ± 0.7 mm) and only 1 projected circumferentially (1.4 mm). **D**, Percentage of neurons projecting orally or aborally in the proximal and distal colon, asterisks indicate statistical difference (Dis: $27.3 \pm 7.9\%$ vs Prox: $11.0 \pm 3.4\%$, $p = 0.004$, χ^2 test). **E**, The inset shows the bimodal distribution of projection lengths (all pooled) and a bimodal Gaussian fit (blue) with a clear trough at 3.1 mm (green arrow). Using this value as a cutoff, the neurons were sorted in long and short projecting ones. Percentage of orally or aborally projecting neurons in the proximal and distal colon, asterisks indicate statistical difference (Dis: $7.1 \pm 0.5\%$ vs Prox: $1.3 \pm 0.4\%$, $***p < 0.001$; Prox: N = 4; Dis: N = 3).

4.4 Discussion

Different regions of the gut each exhibit specific motility patterns regulated by the ENS. Intestinal peristalsis is by far the best studied motor event, but little is known about how ENS circuits are differentially organized to generate regionally distinct motility patterns. In this study, we examined whether there are fundamental differences in neuronal wiring in the ENS that might reflect the capacity to initiate and control a richer portfolio of motility patterns. To do so, we designed a Ca^{2+} imaging approach that allowed us to map the location and connectivity of individual neurons. Our experiments reveal that the enteric nerve circuits differ between regions of the intestinal tract and that more complex wiring is present in those regions that display more diverse motility patterns.

4.4.1 Wiring complexity

The peristaltic reflex (law of the intestine) as described by Bayliss and Starling²⁰³, experimentally confirmed by Trendelenburg²⁵⁵ and later refined in compartmentalized organ bath experiments^{242,245,256-260} has been investigated in

many different studies. Despite currently available information on electrophysiological, morphological and neurochemical characteristics of enteric neurons^{130,261-263}, understanding of enteric circuits and actual connectivity in the ENS remains limited. This is largely because tools to probe circuits are limited, as electrophysiological recordings fail to record from many neurons simultaneously and chemical coding based on a selected number (one to three) of markers can only be applied to fixed tissues.

We used low magnification GCaMP-based Ca²⁺ imaging, to include a large number of neurons in the recording field at the minor expense of losing some detail provided by higher magnification and numerical aperture lenses^{77,247,253,264}. Despite the fact that the temporal resolution of Ca²⁺ recordings does not resolve individual synaptic events, the signal quality was sufficient to monitor Ca²⁺ transients reliably in consecutive rounds of stimulation, which allowed us to combine functional imaging and response characterization with spatial mapping at the cellular level. Responding neurons were located in all directions surrounding the electrode, without any apparent spatial pattern. In the proximal colon, more neurons respond to electrical stimulation of interganglionic fiber tracts, which can partially be attributed to a higher density of neurons and neuronal fibers in this gut region. However, although the mere presence of extra neurons may already reflect a more diverse set of motor patterns, it does not necessarily imply differences in neuronal wiring. To address this issue, we assumed a simple model in which one neuron only connects to one postsynaptic neuron. Simple arithmetic suggests that the distal colon matches this assumption quite well (18 (fibers) times 2 = 36, which closely approximates the observed 40 responsive neurons per field of view). However, the observed number of responding neurons in the proximal colon exceeds this prediction, suggesting that wiring is more complex in the proximal colon, with neurons connecting to multiple postsynaptic neurons (**Figure 4.8**).

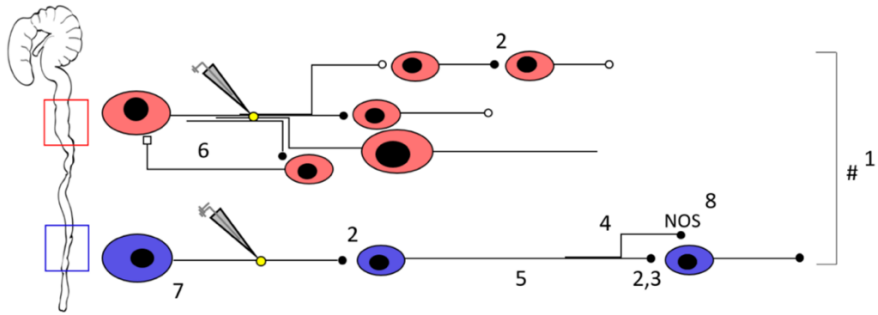


Figure 4.8 | Schematic representation of the neuronal circuitry differences in the proximal versus the distal colon as determined by Ca^{2+} imaging, focal electrical stimulation (represented by electrode and yellow circle), spatial analysis, viral vector tracing and immunohistochemistry.

Using a 5x lens, we observed that fewer neurons (1) respond to focal electrical stimulation in the distal colon, which cannot be simply explained by the fewer number of neurons present and the fewer neuronal fibers that were stimulated. This suggests that the proximal circuitry is more complex and has more branching projections. Nicotinic transmission (represented by the black full circles, 2) plays a more important role in the distal colon (as evidenced by the effect of hexamethonium, Hex, 200 μM , and supported by (3) VAcHT immunohistochemistry), a phenomenon that scales with distance from the stimulation electrode (4). AAV9 viral vector tracing indicated that there are more long distally projecting neurons in the distal colon (5). In addition, we identified an inhibitory circuit component that is dependent on cholinergic transmission (6) in the proximal colon. Neuronal size measurements reveal that Hex-independent neurons with large cell bodies are localized in the vicinity of stimulation site in the distal colon (7). Immunohistochemical stainings showed a higher proportion of nitric oxide synthase (NOS) neurons in the distal colon (8), these are likely to be inhibitory motor neurons and therefore endpoints of the circuitry. Taken together, the neuronal circuitry in the proximal colon is clearly more complex in its wiring compared to the distal colon. This difference in complexity may well reflect the richness of the palette of motor patterns that the specific gut regions can exert. See also Suppl. Movie 1 for an animated buildup of the schematic.

4.4.2 Circuitry probing using pharmacological inhibition and immunohistochemistry

To control for possible potentiating or inhibiting effects of our electrical stimulation protocol, we compared the Ca^{2+} transients generated by two consecutive stimuli and used amplitude ratio as a fingerprint for every individual neuron's behavior in the network. Based on the limited signal to noise ratio in the low magnification recordings, we chose a rather strong stimulus to ensure that all neurons functionally connected to the stimulation site could be resolved. Because our stimulation paradigm, normally used to elicit slow excitatory postsynaptic potentials in the ENS, also releases other transmitters (e.g. substance P, 5-HT, ...), future experiments, using other specific receptor blockers, alternative electrical stimuli, or stimulation at physiological temperatures, will be necessary to refine circuitry maps.

The responses to two consecutive stimuli were robust and the distribution of response signatures (from blocked to enhanced) did not differ between the proximal and distal colon when tested in control solution. However, in hexamethonium many more neurons were completely blocked in the distal colon than in the proximal colon, indicating that transmission in the more distal region has a heavier dependence on cholinergic excitatory synaptic potentials. The majority of type I (blocked) neurons in the presence of hexamethonium was located aboral to the site of the electrode. By extending the recording field further in the aboral direction, our data show that a greater proportion of neurons in the distal colon had responses that were abolished by hexamethonium and that this effect scales with distance from the stimulus site. This finding reiterates that neuronal wiring in the distal colon is more simple than in the proximal colon, consisting of a greater number of serial monosynaptic nicotinic cholinergic neurotransmission units.

We also used immunohistochemistry to identify the cholinergic constituents (ChAT neurons and vAChT terminals) that could correlate with the functional differences observed in both regions. The proportions of cholinergic neurons were similar to those previously reported for the mouse colon^{132,265,266}, but in contrast to the submucous plexus¹²⁹, we did not detect differences in the proportion of cholinergic neurons between the proximal and distal colon. Next, we explored whether the

organization of cholinergic synaptic contacts reflected the importance of cholinergic transmission in the distal compared to the proximal colon. The overwhelming abundance of vAChT positive terminals did not allow quantifying synaptic contact numbers, but the fraction of surface overlap between the vAChT and neuronal soma surfaces was significantly higher in the distal colon. This corroborates our findings derived from the functional Ca^{2+} recordings that, in the distal colon, circuitry relies more importantly on cholinergic transmission.

4.4.3 Mapping of the relative location of neurons

Further analysis of the spatial distribution of responding neurons allowed us to draw four important conclusions. First, whilst there is little orally-projecting cholinergic transmission, in the proximal colon, about 90% of the neurons blocked by hexamethonium are found aboral to the stimulation site. This indicates that in the proximal colon, a greater proportion of neurons projecting aborally primarily relies on cholinergic transmission. Many other excitatory neurotransmitters are found in the ENS and likely also contribute to the communication with the postsynaptic neurons oral to the electrode.

Second, in the distal colon, neurons whose activity is abolished (type I) in the presence of hexamethonium are more randomly scattered around the electrode, indicating that cholinergic transmission is employed more generally in this region. Third, in the proximal colon, a relatively large fraction of neurons concentrated around the stimulation site showed enhanced responses in the presence of hexamethonium. This finding indicates that, at least locally, there are also nicotinic receptor dependent inhibitory pathways that act to reduce Ca^{2+} responses in control conditions, possibly by utilizing nitric oxide as observed in guinea-pig large intestine²⁵⁶. Considering that Ca^{2+} transients are responsible for K^+ ion efflux and match the slow afterhyperpolarisation (AH) in AH-type neurons^{42,43,267}, it remains to be determined whether increased Ca^{2+} transient amplitude is a reflection of increased neuronal firing or a sign of enhanced inhibition. Last, the fact the cholinergic blocker leaves a large fraction of neurons close to the stimulation site unaffected, indicates

little or no contribution of cholinergic transmission in circumferential direction, and is very likely due to antidromic activation of intrinsic sensory neurons. For those cells whose response was only partially reduced by hexamethonium, we conclude that apart from cholinergic input they also receive input mediated by other excitatory neurotransmitters, which is consistent with previous reports^{70,268,269}. The remaining hexamethonium-resistant responses could result from direct antidromic non-synaptic neuronal activation^{77,270} or rely entirely on other transmitters. Together, this information confirms that specific spatial patterning is present in both colonic regions and suggests that the apparent 'salt and pepper' distribution of neuronal subtypes in myenteric ganglia is due to spatial overlap of functional units. In keeping with Lasrado et al. (2017)²⁴⁰ who showed that clonal clusters form the basis for the spatial and functional organization of the ENS in the mouse small intestine, it remains to be determined whether similar genetic lineage rules dictate ENS patterning in more distal intestinal regions.

4.4.4 Projections of myenteric neurons

To address the projection orientation and length of individual neurons we used the AAV2/9 viral vector system¹⁶⁴. Though viral vector transduction based protein expression is influenced by the choice of promoter, mouse strain and the mode and age of administration^{164,166,233}, our approach preferentially labels uniaxonal myenteric neurons. Labelled neurons located in the proximal colon were found to be shorter and have a greater proportion of orally-projecting fibers compared to the distal colon, suggesting the need for the myenteric circuitry to act more locally. In contrast, in the distal colon, more neurons projected aborally and for greater lengths, which corroborates the importance of expanding the recordings in the aboral direction. Although our sparse labeling strategy did not allow full characterization of neuronal projection termini, it is likely that the long distance neurons are descending interneurons²⁵⁴. Apart from the fact that intrinsic sensory neurons escaped the viral labeling, we cannot exclude that a specific population of interneurons or motor neurons is preferentially labeled. However, given that more long distance aborally

projection neurons are present in the distal colon, it is more likely that these were targeted in the calcium imaging experiments, which agrees with the observation that hexamethonium dependent effects are more important in the distal as one moves further away from the stimulation site.

4.4.5 Relation between neuron size, location and response fingerprint

Apart from response signature and location, the GCaMP3 recordings also inform us about neuronal soma size. One characteristic of enteric neurons that seems preserved over different species and regions is that some cells have large and smooth cell bodies²³⁹. These neurons, often express Ca²⁺-binding proteins (calbindin or calretinin) and are associated with *sensory or primary afferent* function²⁶³. We show that, although larger neurons appear randomly scattered in the network, the subgroup that is unaffected by hexamethonium in the distal colon has a defined location in a band close to the stimulation site. This suggests that in the distal colon a narrow band of circumferentially projecting neurons act together, and as suggested^{80,271} form a self-reinforcing network. Again, this situation is simpler than in the proximal colon, where also neurons with large cell bodies whose activity is not affected by hexamethonium are spread over a larger distance. Assuming that these are the *sensory primary afferent* neurons, this finding fits the canonical model underlying peristalsis in which these cells (or a pool thereof) are responsible for reflex initiation. These findings also fit with the fact that peristalsis is the dominant motor pattern in the distal colon. Finally, we show that inhibition of cholinergic neurotransmission mainly abolishes the responses of small diameter neurons, which are likely to be motor neurons, and hence, do not participate in relaying nerve activity in the network as they are an exit point of the circuitry. This is also confirmed by the identification of a higher fraction of (generally small) nitrergic neurons in the distal colon, which are most probably inhibitory motor neurons responsible for descending relaxation.

4.5 Conclusion

Although knowledge about neurochemical and neurophysiological properties of enteric neurons^{92,132,272} and how they communicate in neural circuitries to organize intestinal motility^{135,273} has been expanding steadily, it remains elusive how enteric neurons are organized in circuits, how they are physically built into a network and whether regional motility differences are reflected in the complexity of the underlying ENS.

In this study, we investigated whether the capacity of an intestinal region to generate a large palette of motor functions, would be reflected in the complexity of the underlying enteric nerve circuit. Using low magnification Ca²⁺ response fingerprinting we show that the neuronal wiring in the regions with more diverse tasks (proximal colon) is more complex than in the distal colon, where there is one predominant motility pattern, peristalsis. The greater complexity of the proximal colon ENS, suggests a higher computational capacity, which might be necessary to regulate a set of functions specific for this region. Our study shows that motility control is hard-wired in the ENS and circuitry complexity matches the task portfolio of the specific region. Our data does not provide evidence in support nor argue against the possibility that different motility “programs” are run in the different sections of the intestine as suggested by Wood (2016)⁵⁵, , rather we show that regional differences in hardwiring exist in gut regions with different functions. The prominent ascending (cholinergic) inhibitory component observed in the proximal colon fits with its capacity to also and uniquely generate mixing patterns in addition to propulsive peristalsis that is present throughout the large intestine. Better understanding of ENS circuits and further refinement of connectivity schemes will be necessary to fully comprehend gut function but may also help to understand GI motor disorders like pseudo-obstruction where at first glance numbers of neurons are not affected^{274,275} but subtle wiring defects are the cause of impaired motility²⁰⁸.

4.6 Author Contributions

Z.L.L. collected the data, performed the main analysis and drafted the manuscript. W.B., M.M.H., and P.V.B. determined the experimental design, contributed to the

conception of the project and revised the manuscript. P.V.B. wrote the analysis routines in Igor pro. C.V.H., and V.B. provided materials (viral vectors) and helped with the preliminary viral vector tracing experiments. All authors approved the manuscript.

4.7 Acknowledgements

We would like to thank Joel C. Bornstein from University of Melbourne, Australia for insightful comments on the manuscript. We thank the members of LENS for their assistance during experiments and for their constructive comments on the project and manuscript. M.M.H., and W.B. were supported by a postdoctoral fellowship of the Fund for Scientific Research Flanders (FWO). Z.L.L. is supported by the China Scholarship Council (CSC) (201408370078). The study was supported by the FWO (G.0921.15 SBO/S006617N), the IWT (SBO/130065), the KU Leuven (C32/15/031) and Hercules foundation (AKUL/11/37 and AKUL/13/37).

4.8 Conflicts of Interest

The authors declare that there are no conflicts of interest.

CHAPTER 5

Characterization of the relationship between voltage changes and $[Ca^{2+}]_i$ transients using simultaneous whole-cell patch-clamp electrophysiology and live calcium imaging

Li Zhiling¹, Boesmans Werend^{2,3}, Kazwiny Youcef¹, Hao M Marlene⁴, Vanden Berghe Pieter¹

¹Laboratory for Enteric NeuroScience (LENS), Translational Research Center for Gastrointestinal Disorders (TARGID), Department of Chronic Diseases, Metabolism and Ageing, University of Leuven, Leuven, Belgium

²Department of Physiology - biochemistry - immunology, University of Hasselt, Hasselt

³Department of Pathology, GROW-School for Oncology and Developmental Biology, Maastricht University Medical Center, Maastricht, The Netherlands

⁴Department of Anatomy and Neuroscience, University of Melbourne, Melbourne, Australia

To be submitted, 2019

5.1 Introduction

Transmission of neuronal information in a network occurs via action potentials (AP) that travel along the neuronal axon to induce neurotransmitter vesicle release at the synaptic terminal, which depolarizes the next neuron in line. Although APs are carried by Na^+ ions, they are often accompanied by an influx of Ca^{2+} ions into the cytosol, which in turn may trigger release from intracellular Ca^{2+} stores and lead to an overall increase in intracellular Ca^{2+} concentration ($[\text{Ca}^{2+}]_i$). The $[\text{Ca}^{2+}]_i$ is maintained by a tight balance between Ca^{2+} influx and efflux as well as by exchange of Ca^{2+} with internal stores. Calcium ions through the plasma membrane happens either directly via activated ionotropic receptors or via voltage-dependent calcium channels (VDCC) activated as a consequence of membrane depolarization²⁷⁶. VDCCs are present in the cell membrane of virtually all excitable cell types and are involved in regulating cellular excitability and intracellular Ca^{2+} signaling. The activity of VDCCs is essential to couple electrical signals to an increase of the cytosolic Ca^{2+} concentration²⁷⁷.

Intracellular Ca^{2+} signals are involved in the control of a large variety of neuronal functions, such as neurotransmitter exocytosis²⁷⁸, synaptic plasticity²⁷⁹, neuronal growth and degeneration²⁸⁰. Furthermore, it has been demonstrated that Ca^{2+} ion fluctuations could guide developmental processes, such as axon pathfinding, synaptogenesis, and the development of functioning neural circuits^{281,282}.

Calcium imaging has been used for many studies in investigating neuronal activity in the enteric nervous system (ENS)⁹⁸. In the ENS, there are many different functional subtypes of enteric neurons, but they are generally classified in two electrophysiologically distinct groups: AH (after-hyperpolarizing) and S (synaptic) (see also **section 1.3.2**). Back in the 1970s, Hirst et al. (1974) introduced the terms AH and S, based on his recordings with sharp intracellular electrodes in the guinea pig small intestine. AH neurons typically have an “inflection” on the repolarizing phase of their AP, which is followed by a prominent slow after-hyperpolarizing potential (sAHP)^{26,34}. A key property of these neurons is that their action potential is carried in part by Ca^{2+} ion influx, which underlies the observed inflection point^{24,36,37}.

S neurons are named after the fast excitatory “synaptic” potentials (fEPSPs) they receive^{26,34}. Although this AH/S classification is derived from guinea pig it has also been used, albeit not exactly and with adaptations, to subdivide enteric neurons in other species^{20,22,23,31-33,87,283}.

Although electrophysiological approaches have been classically used to investigate neural circuitry, there are a number of drawbacks, the most important one being the inability to target large groups of neurons¹⁹¹. Because of the tight link between electrical activity and transient intracellular Ca^{2+} changes, calcium imaging techniques have been used as a valuable alternative, especially as Ca^{2+} imaging allows simultaneous visualization and quantitative evaluation of activity in hundreds of neurons with cellular resolution¹⁹³.

Live calcium imaging is therefore a valuable tool that allows population-level analysis of enteric neural activity. Previously, three studies have been conducted in guinea pig myenteric neurons, showing single APs in AH neurons elicit a corresponding $[\text{Ca}^{2+}]_i$ transient, however, multiple APs are required in S neurons to trigger a detectable $[\text{Ca}^{2+}]_i$ transient^{41,89,284}. Although these studies have provided important information regarding the calcium handling properties of enteric neurons, recordings were understandably performed on small numbers of cells and used classical chemical dyes. With the increased use of transgenic mice for ENS studies and genetically-encoded calcium indicators (such as GCaMPs), in the current study, we aimed to further characterize the relationship between voltage changes and $[\text{Ca}^{2+}]_i$ transients using simultaneous whole-cell patch-clamp electrophysiology and GCaMP6f live calcium imaging on primary cultures of mouse myenteric neurons. Furthermore, we set out to test whether the $[\text{Ca}^{2+}]_i$ signaling characteristics, independently or in combination with the electrical properties, could serve to refine mouse enteric neuron classification, and whether specific Ca^{2+} signaling properties can be used to distinguish between electrophysiological subtypes.

5.2 Materials & Methods

5.2.1 Animals

For simultaneous patch clamp recording and calcium imaging, adult *Wnt1::Cre;R26R-RCL-GCaMP6f* mice (short: *Wnt1|GCaMP6f*) were used. In these mice, the genetically-encoded Ca^{2+} indicator, GCaMP6f, is expressed in all neural crest-derived cells, including all enteric neurons and glia. *Wnt1|GCaMP6f* mice were bred by mating *Wnt1::Cre* mice ²⁴⁹ with *R26R-RCL-GCaMP6f* mice (also known as Ai95, purchased from The Jackson Laboratory, Bar Harbor, ME, USA, stock # 028865) ²⁰². For some experiments, primary cultures of wild type C57Bl6/J mice were used. For photostimulation experiments, adult *Wnt1::Cre;R26R-LsL-ChR2-eYFP* mice (*Wnt1|ChR2-eYFP*) were used, where the genetically-encoded actuator, ChR2, is expressed in all neural crest-derived cells. *Wnt1|ChR2-YFP* mice were bred by mating *Wnt1::Cre* mice ²⁴⁹ with *R26R-LsL-ChR2(H134R)-eYFP* mice (strain Ai32, purchased from The Jackson Laboratory, Bar Harbor, ME, USA, stock # 012569) ²⁸⁵. All mice were sacrificed by cervical dislocation. All experimental procedures were approved by the animal ethics committee of the KU Leuven.

5.2.2 Mouse primary enteric nervous system cultures

The preparation of mouse primary enteric neuron cultures was adapted from previous studies ^{286,287}. First, the ileum of adult *Wnt1|GCaMP6f*, *Wnt1|ChR2-eYFP* or C57Bl6 mice (15-20cm proximal to caecum) was removed and flushed using cold oxygenated Krebs solution (containing in mM: 120.9 NaCl, 5.9 KCl, 1.2 MgCl_2 , 2.5 CaCl_2 , 1.2 NaH_2PO_4 , 14.4 NaHCO_3 , and 11.5 glucose, bubbled with 95% O_2 /5% CO_2). Then the mucosa, submucosa and circular muscle were peeled off, leaving the longitudinal muscle with adherent myenteric plexus (LMMP) intact. Strips of LMMP were collected and rinsed three times in Krebs solution before dissociation in collagenase II (2 mg/ml, Worthington) and 3 mg bovine serum albumin (0.3 mg/ml, Serva) in sterile Krebs for 1 h at 37 °C in a water bath with shaker. The suspension was centrifuged (8 min, 360 g, 4 °C) and the pellet was resuspended in 4ml sterile Hank's balanced salt solution (HBSS) containing 0.05 % trypsin (Gibco). Subsequently the cell suspension was further digested at 37 °C in a shaking water bath for 7 min.

The trypsin was neutralized with cold DMEM/F-12 medium (containing 10 % fetal bovine serum (FBS) and 1% penicillin/streptomycin; Gibco). After centrifugation (8 min, 360 g, 4 °C), the pellet was resuspended in 3 ml neuronal medium (Neurobasal A medium containing 1x B-27, 1 % FBS, 2 mM L-glutamine, 10 ng/ml Glial Derived Neurotrophic Factor (GDNF) and 1% penicillin/streptomycin; Gibco). The cells were then filtered through a 40 µm cell strainer (Falcon) and centrifuged (8 min, 360 g, 4 °C). After resuspending the pellet in 2.4 ml neuronal medium, the cells were gently triturated using a 1 ml plastic pipette tip until the medium became cloudy. Then 200 µl of the triturated cell solution was added to each well of a 12-well plate containing a glass coverslip coated with poly-D-lysine hydro bromide (0.5 mg/ml in borate buffer) and laminin (20 µg/ml in PBS) (Sigma-Aldrich). The cells were cultured for 4 - 5 days before whole-cell patch clamp and calcium imaging recordings were performed.

5.2.3 Immunohistochemistry

Coverslips were fixed on day 4 and 5 of culture in 4% paraformaldehyde dissolved in 0.1 M phosphate buffer saline (PBS, pH = 7.2) for 1 h. After washing three times in PBS, the cells were permeabilised in 0.5% Triton X-100 (Sigma) in PBS containing 4% donkey serum for 2h at room temperature, then incubated overnight at 4°C in primary antibodies (**Table 5.1**) diluted in blocking solution. After washing in PBS (3x 10 min) the cells were incubated in secondary antibodies (**Table 5.1**) for 2h at room temperature. DAPI (1:5000) was used to stain all nuclei.

During patch-clamp recordings, neurons were filled with biocytin (0.2%, Sigma), which was present in the internal solution. After electrophysiological recordings, cells were fixed in 4% paraformaldehyde in 0.1 M PBS for 1 h and washed three times, after the application of primary antibodies as described above. Fluorescent-conjugated streptavidine was applied in the secondary antibody mix.

Immuno-labeled primary myenteric cell cultures were imaged on an Olympus fluorescence microscope (BX41, XM10 camera). Afterwards the neurons were counted manually aided by the cellcounter plugin in ImageJ (NIH, Bethesda, MD).

Cells were counted from a minimum of three fields of view per coverslip. Data were obtained from a minimum of three mice from three different litters.

Table 5.1 | Antibodies used for immunohistochemistry

| Antibodies | Host | Dilution | Source |
|---|--------|----------|--------------------------|
| Calbindin | Rabbit | 1:1600 | Swant |
| Calretinin | Rabbit | 1:2000 | Chemicon International |
| HuCD | Human | 1:2000 | Gift from Vanda Lennon |
| nNOS | Sheep | 5000 | Gift from Piers Emson |
| Anti-rabbit A488 | Donkey | 1:500 | Molecular Probes |
| Anti-human A594 | Donkey | 1:1000 | Jackson Immuno labs |
| Anti-rabbit Cy3 | Goat | 1:500 | Jackson Immuno labs |
| Anti-sheep A647 | Donkey | 1:500 | Molecular Probes |
| Fluorescent-conjugated streptavidine A594 | | 1:250 | Thermo Fisher Scientific |

Abbreviations: nNOS: neuronal nitric oxide synthase.

5.2.4 Whole-cell patch-clamp electrophysiology

Cells were visualized on an upright Zeiss Examiner microscope (Axio Examiner.Z1; Carl Zeiss), equipped with a monochromator (Poly V) and cooled CCD camera (Imago QE), both from TILL Photonics. In this set of experiments, patch clamp recordings and Ca imaging were performed simultaneously, in which both bright-field and fluorescence images were recorded. Cells were superfused with HEPES-buffered saline (in mM: 140 NaCl, 5 KCl, 10 HEPES, 2 CaCl₂, 2 MgCl₂, and 10 D-glucose, adjusted to pH = 7.4 using NaOH). Patch pipettes were pulled from borosilicate glass capillaries (Harvard Apparatus) using a P-87 puller (Sutter Instruments). Pipette were filled with a potassium methanesulfonate internal solution (in mM: 115 KMeSO₃, 9 NaCl, 10 HEPES, 0.1 CaCl₂, 1 MgCl₂, 0.2 BAPTA.K₄, 2 Mg-ATP and 0.25 Na-GTP)¹² and had a resistance of ~ 6 MΩ. Pipette capacitance was compensated before whole-cell recording. All recordings were performed at room temperature using a HEKA amplifier and Patchmaster software (both from HEKA Devices, Germany). Liquid junction potentials were calculated using JPCalcW (Molecular Devices) and corrected offline. Data were acquired at 10 kHz and filtered at 2 kHz. All data were analyzed using Patchmaster and Igor software. Once the whole-cell configuration was established, APs were stimulated in current clamp mode. Membrane potential was

adjusted to approx. -70mV (as the resting membrane potential of the neurons) and cells were depolarized by either 10 or 500 ms current pulses in 10 pA increments until APs were elicited. The amplitude of APs was measured between the baseline membrane potential and the peak of the AP, and the duration was measured at half-amplitude. The first 10 ms current step that triggered an AP was picked as the single pulse stimulus for combined patch-clamp and Ca imaging recordings. High K⁺ solution was made by substituting the Na⁺ component of extracellular solution (in mM: 78 NaCl, 75 KCl, 10 HEPES, 2 CaCl₂, 1 MgCl₂, and 10 D-glucose, adjusted to pH = 7.4 using NaOH). The agonists dimethylphenylpiperazinium (DMPP; 10 μM; Fluka) and high K⁺ were diluted in control HEPES-buffered extracellular solution and applied via the inflow. For incubation in tetrodotoxin (TTX; 1 μM; Sigma), TTX was diluted in extracellular solution and perfused over cells prior to recording. For experiments involving TTX, cells were stimulated 3 times: first in control extracellular solution, a second time in the presence of TTX (1 μM, following a 5 min drug wash-in period), and finally again in control extracellular solution after 5 min washout.

5.2.5 Calcium imaging

GCaMP6f was excited at 470 nm, and its fluorescence emission was collected at 525/50 nm using a 20x (NA 1) water dipping objective on an upright Zeiss microscope (Axio Examiner.Z1; Carl Zeiss). Images were captured at a frame rate of 4 Hz. The changes in GCaMP6f fluorescence, reflecting the intracellular Ca²⁺ concentration ([Ca²⁺]_i) changes, were collected using TILLVISION software (TILL Photonics) and analysis was performed as described previously²⁴⁷ in IGOR PRO (Wavemetrics) using custom written macros. Regions of interest (ROIs) were drawn, fluorescence intensity for each cell was calculated and normalized to its baseline starting value and presented as F/F₀. Compound calcium transients caused by volleys of depolarizing current steps were analyzed using Matlab (code written by Y. Kazwiny).

5.2.6 Photostimulation of Channelrhodopsin 2 (ChR2)

Blue (470 nm) light (Polychrome V, Till Photonics) was used to deliver photostimuli (10 ms) to the patched neurons and test the efficiency to evoke APs in myenteric neurons. Light-induced voltage changes were recorded while holding neurons in current clamp at -70 mV. The amplitude of APs was measured between the baseline membrane potential and the peak of the AP.

5.2.7 Fast (kHz) calcium imaging

kHz frame rate calcium imaging was performed using a previously described method. Briefly, in addition to the cooled CCD camera (PCO; Kelheim, Germany) used to record at 4 Hz, a CMOS camera (Focuscope SV200-I, Photron; Tokyo, Japan) was used to record images at a rate of 1000 frames/sec. The cameras were attached, respectively, to the top and side port of an upright Zeiss microscope (Axio Examiner.Z1; Carl Zeiss). Switching between the two cameras was done by inserting a 100% mirror slider. During the recording, the image intensifier was adjusted to ~ 550 with high signal-to-noise ratio. This is based on our previous study²⁷⁰ in which average counts over 50 dark frames with an exposure time of about 1 ms per image intensifier voltage (in steps of 50) only show a sharp increase above 750 of image intensifier voltage. The read noise, at least up to 750, is also not influenced by the imaging intensifier. All analysis was also performed in Igor, as described previously²⁷⁰.

5.2.8 Data presentation and statistical analysis

All data are presented as mean \pm SEM. “n” refers to the number of cells, “N” refers to the number of animals. Statistical analyses were performed with Microsoft Excel or GraphPad. Differences were considered to be significant if $p < 0.05$. All data were analysed using the Students’ *t*-test, unless otherwise stated.

5.3 Results

5.3.1 Immunohistochemical characterization of mouse primary myenteric neuron cultures

To test if different subpopulations of enteric neurons were present in equal proportions in our cultures compared to intact tissue preparations, we quantified the proportions of calbindin, calretinin and nNOS immunoreactive neurons (**Figure 5.1**). Calbindin is a marker of intrinsic sensory neurons, calretinin is generally expressed by excitatory neurons and nNOS by inhibitory neurons, although there is overlapping expression of these 3 proteins ⁹².

The proportions of calbindin, calretinin and nNOS-immunoreactive neurons out of the total population of HuC/D+ enteric neurons were calculated to be around 30 %, 50 % and 40% respectively. There were no significant differences between these proportions on 4 or 5 of culture (day 4: calb: 31.9 ± 1.7 %, calret: 49.0 ± 1.8 % and NOS: 39.6 ± 2.1 %, N = 4; day 5: calb: 31.2 ± 4.2 %, calret: 49.8 ± 3.4 % and NOS: 35.1 ± 3.8 %, N = 3; $p > 0.05$; **Figure 5.1C**). A small proportion of neurons were immunoreactive for both NOS and calbindin (5.7 ± 1.0 %) and NOS and calretinin (2.2 ± 0.8 %) on day 4 of culture. Simultaneous expression of Calb and Calret could not be tested because both antibodies were raised in rabbit. Our observed proportions are similar to what has been reported for adult myenteric neurons in situ ⁹².

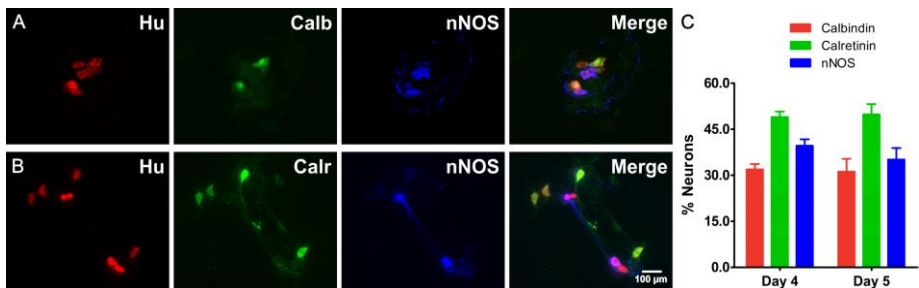


Figure 5.1| Visualization and quantification of myenteric neuron subtypes via immunohistochemistry.

A, Representative images of primary mouse myenteric neuron cultures with immunohistochemistry against the pan-neuronal marker Hu (red), calbindin (green), and NOS (blue). **B**, Cell cultures stained against Hu (red), calretinin (green), and NOS (blue). **C**, The proportion of neurons coding for each of the markers was determined on day 4 and 5. The percentages of neurons are expressed as mean \pm SEM. Calb: calbindin, nNOS: neuronal nitric oxide synthase, Calr: calretinin.

5.3.2 Electrophysiological properties of cultured myenteric neurons

In total, simultaneous whole-cell patch-clamp and calcium imaging recordings were made from 41 neurons. Immediately after the whole-cell configuration was established, an average resting potential (V_{rest}) of -58.3 ± 1.3 mV ($n = 41$) was recorded. The average input resistance (R_{in}), which was measured by holding the neuron for 10 ms at a hyperpolarizing voltage of -80 mV, was 505.6 ± 43.9 M Ω ($n = 41$). The average capacitance of the cell membrane was 13.2 ± 1.0 pF ($n = 41$). The average series resistance was 17.2 ± 1.8 M Ω ($n = 41$).

We used a stepwise current injection (10 ms) protocol to test the excitability of patched neurons, the average threshold current that was necessary to elicit an AP was 77.1 ± 5.8 pA. The AP amplitude and half-width (calculated as duration at half-amplitude) were 89.5 ± 1.4 mV and 2.4 ± 0.04 ms, respectively. Longer (500 ms) current injections were used to test the capacity for tonic firing, but in most cases, only a single action potential was elicited ($n = 27/41$).

Although AH neurons are generally identified by the presence of a prominent sAHP, this has been difficult to identify in mouse enteric neurons, particularly using whole-cell patch-clamp^{12,283}. Therefore, to identify AH neurons, we investigated the presence of an “inflection” on the repolarizing phase of the action potential, as previously described³⁴. Briefly, the first time derivative (dV/dt) was calculated, and the inflection identified by the presence of a second component during repolarization (**Figure 5.2A,A'**). Seventeen cells were found to have such an inflection point and could be classified as AH neurons. Only 2 of these cells displayed a clear AP induced slow after-hyperpolarization. The remaining cells were classified as S neurons (**Figure 5.2B,B'**).

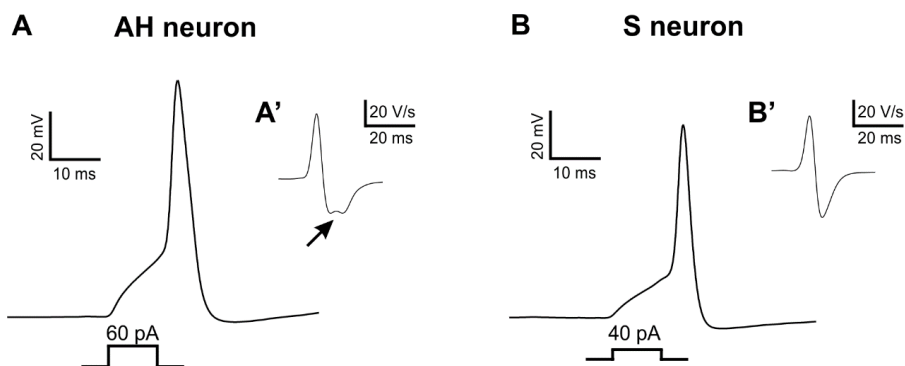


Figure 5.2| Action potential characteristics of AH and S neurons.

A - B, APs from an AH neuron (A) and an S neuron (B). Differentiated traces (A' and B') of the AP show the inflection on the falling phase in AH neurons (arrow in A'), while in S neurons the repolarization is monophasic (B'). Resting membrane potential was -70mV. Current pulse injections are indicated by lower traces in (A) and (B).

Interestingly, when neurons were split according to their AH/S classification, significant differences with respect to capacitance, input resistance and amplitude of the action potential were found between the two groups (**Table 5.2**). This is consistent with previous studies performed in the guinea pig ileum using sharp electrode recordings that identified AH neurons to be generally larger in size, have larger amplitude APs and lower input resistance, although there are some discrepancies between different studies^{26,34,288}.

Table 5.2| Passive and active membrane properties of AH and S neurons.

| Electrophysiological type | RMP (mV) | R_{in} (M Ω) | C_m (pF) | AP amplitude (mV) | AP width at half-amplitude (msec) | AP threshold (pA) | Presence of slow after-hyperpolarizing potential (number of neurons) |
|---------------------------|-----------------|------------------------|-------------------|--------------------|-----------------------------------|-------------------|--|
| AH (n = 17) | -58.0 \pm 2.3 | 387.5 \pm 33.4*** | 17.4 \pm 0.9*** | 92.97 \pm 1.92** | 2.3 \pm 0.04 | 99.4 \pm 8.9*** | 2 |
| S (n = 24) | -58.5 \pm 1.6 | 667.9 \pm 55.5 | 9.6 \pm 0.8 | 86.10 \pm 1.62 | 2.4 \pm 0.05 | 61.3 \pm 6.0 | 0 |

**Significantly different from S neurons, $p < 0.01$;

***Significantly different from S neurons, $p < 0.001$.

5.3.3 Detection of action potentials elicited by illumination of blue light

In addition to direct depolarization via the patch pipette, we also used optogenetic stimulation to stimulate APs in ChR2 expressing neurons. To compare illumination evoked membrane potential changes with APs evoked by depolarizing current pulses,

we delivered a 10 ms blue pulse (470nm) to excite enteric neurons. We found that the appearance of APs triggered by blue light activation in ChR2+ enteric neurons was different from those elicited by depolarizing current pulses. The AP amplitude and half-width of AP was 95.8 mV and 2.08 ms (**Figure 5.3B**), in comparison with 101.7 mV and 2.04 ms (**Figure 5.3A**). Out of 4 ChR2-expressing neurons examined, 2 were identified to be AH by the presence of the inflection on repolarization. In these two AH neurons, light-evoked APs also had a prominent after-depolarizing potential (**Figure 5.3B**), which was not observed in electrically-evoked APs. We have not been able to obtain successful optogenetic recording so far in S neurons.

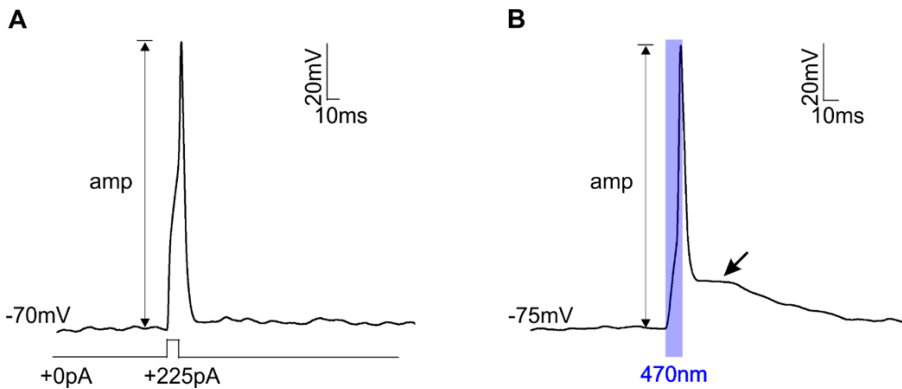


Figure 5.3] Comparison of action potentials elicited by current injection or blue light illumination

A, Representative trace of an AP in an AH neuron triggered by a 10ms +225pA current pulse. **B**, AP from the same neuron triggered by 10ms blue light illumination. Light-evoked APs had a prominent after-depolarizing component (arrow). For both recordings, the membrane potential was adjusted to approx. -70mV.

5.3.4 Relation between action potential firing and $[Ca^{2+}]_i$ transients

To investigate the relationship between membrane depolarization, AP firing, and Ca transients we performed simultaneous electrical and GCaMP6f recordings.

We first analyzed all recordings together without separating cells according to their electrophysiological classification into AH and S type enteric neurons. Data were collected from 41 neurons, all of which displayed a $[Ca^{2+}]_i$ transient elicited by a long

(500 ms) single current pulse (**Figure 5.4B,B'**). In response to a single short (10 ms) depolarizing current pulse, 33 of these 41 neurons also exhibited both an AP and a detectable $[Ca^{2+}]_i$ transient (**Figure 5.4A**); while in 8 neurons, only an AP was elicited, without a detectable $[Ca^{2+}]_i$ transient (**Figure 5.4A'**). The average amplitude of $[Ca^{2+}]_i$ transients evoked by longer (500 ms) depolarization were significantly larger than for shorter (10 ms) stimuli ($p < 0.001$, **Figure 5.4C**). During 500 ms depolarization, 14/41 cells fired multiple APs (**Figure 5.4B'**), while 27/41 cells only fired a single AP (**Figure 5.4B**). $[Ca^{2+}]_i$ transients responding with multiple APs were higher in amplitude compared to those with a single AP ($p < 0.001$, **Figure 5.4D**). We attempted to examine the relationship between the number of APs and the amplitude of the $[Ca^{2+}]_i$ transient, however there was no obvious correlation (**Figure 5.4E**).

After investigation of AP characteristics, we subdivided neurons into their respective AH and S classification. We found that the amplitude of $[Ca^{2+}]_i$ transients evoked by a 10 ms depolarization pulse was significantly larger in AH neurons (16/33) compared to S (17/33) ($p < 0.05$, **Figure 5.4F**). For the 8 neurons without a detectable $[Ca^{2+}]_i$ transient (**Figure 5.4A'**), one of these was identified to be an AH neuron, and 7 were S neurons. With a longer-duration (500 ms) depolarization, there was no difference in the $[Ca^{2+}]_i$ transient amplitude between AH and S neurons ($p > 0.05$, **Figure 5.4G**). Furthermore, the AP amplitude itself did not differ between the two populations when elicited by a 500 ms pulse ($p > 0.05$, **Figure 5.4G**).

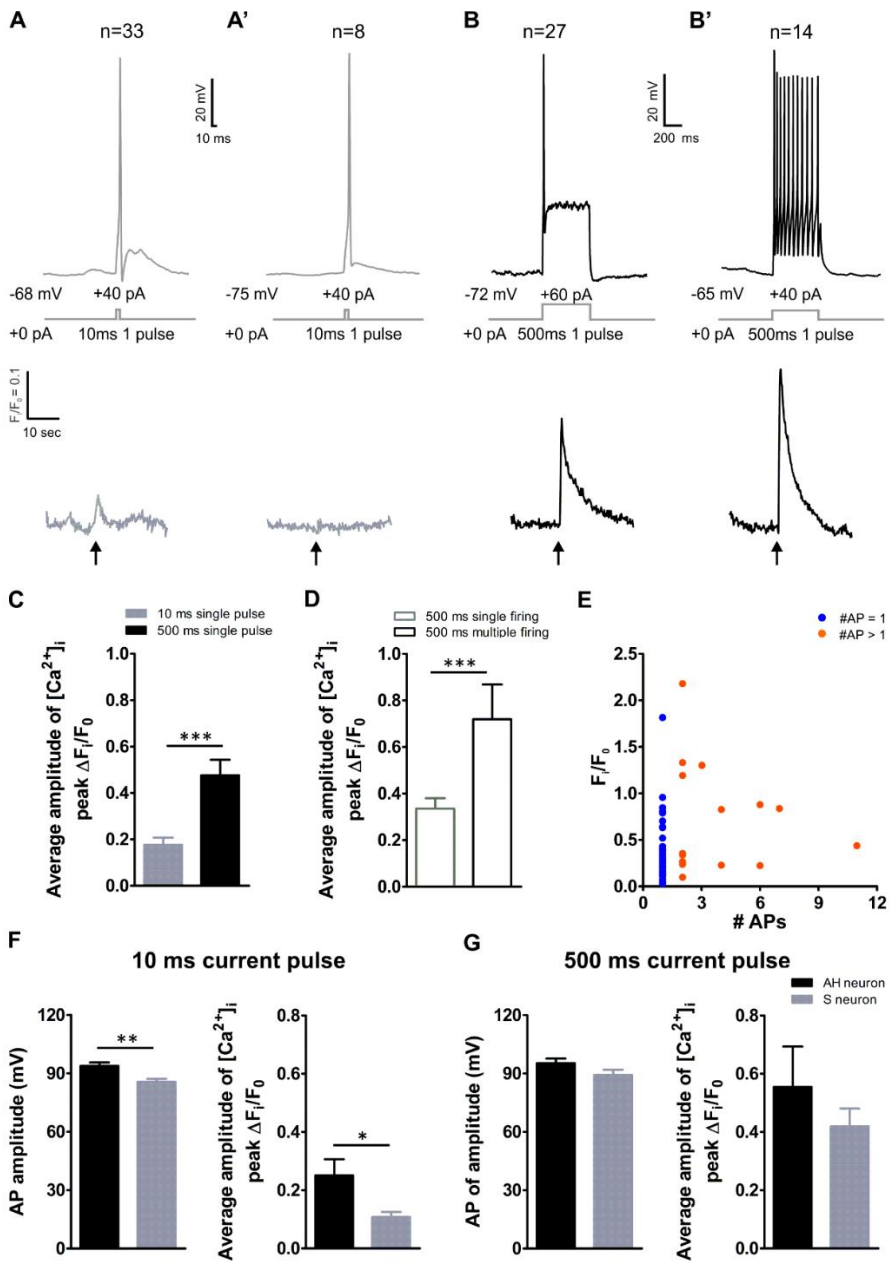


Figure 5.4 | Relation between action potential firing and $[Ca^{2+}]_i$ transients.

Representative traces of APs (top) and corresponding $[Ca^{2+}]_i$ transient (bottom) during 10 ms (A,A') and 500 ms (B,B') current pulses. During a 10 ms depolarization, the majority neurons exhibited both an AP and a detectable $[Ca^{2+}]_i$ transient (A), while for some neurons, only an AP was elicited without a detectable $[Ca^{2+}]_i$ transient

(A'). During a 500ms depolarization, both single firing (B) and multiple firing (B') neurons elicited $[Ca^{2+}]_i$ transients. Please note, different time scales are used for AP and $[Ca^{2+}]_i$ traces. **C**, Comparison of AP evoked $[Ca^{2+}]_i$ transient between 10 ms (n = 33) and 500 ms (n = 41) current pulses (***) $p < 0.001$. **D**, Comparison of AP evoked $[Ca^{2+}]_i$ transient between single firing (n = 27) and multiple firing (n = 14) neurons (***) $p < 0.001$. **E**, Relationship between the number of APs and the amplitude of the $[Ca^{2+}]_i$ transients. **F - G**, Differences in AP and $[Ca^{2+}]_i$ transient amplitudes between AH and S neurons during 10 ms and 500 ms depolarization current pulses.

To further examine the role of the APs in eliciting a $[Ca^{2+}]_i$ transient, we used tetrodotoxin (TTX) to block the majority of voltage-dependent Na^+ channels (VDSCs). Both short (10 ms, n = 7) and long (500 ms, n = 10) depolarization current pulses were applied three times to each individual neuron. First in normal extracellular solution, then after the cells had been incubated in a solution containing TTX (1 μ M) for 5 min, and lastly back in normal solution after washout of TTX. All APs were reduced or abolished by TTX for both 10 ms and 500 ms depolarizing current pulses (**Figure 5.5A,B,C**). $[Ca^{2+}]_i$ responses to the 10 ms depolarizing current pulse were also completely abolished (from 0.16 ± 0.04 to 0, n = 7, **Figure 5.5A'D**), whereas in response to 500 ms depolarization, a small but detectable $[Ca^{2+}]_i$ transient remained in the presence of TTX (from 0.69 ± 0.19 to 0.23 ± 0.11 , $p < 0.05$, n = 10, **Figure 5.5B'C'E**). Hence, it appears that although $[Ca^{2+}]_i$ transients are elicited by APs, the presence of an AP is not necessary for depolarization-induced $[Ca^{2+}]_i$ transients, particularly in the case of longer duration depolarizations.

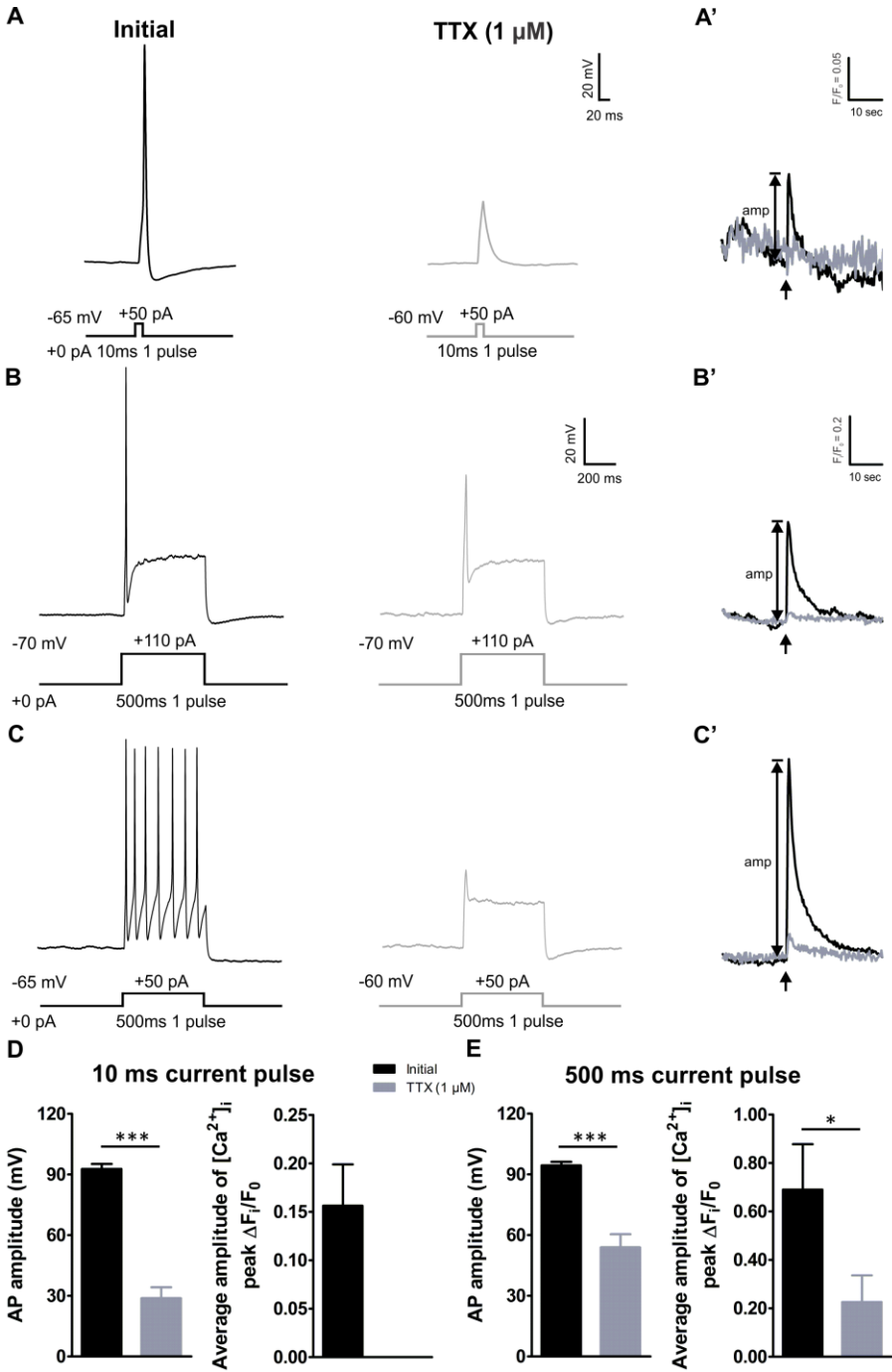


Figure 5.5 | Effect of blocking voltage-dependent Na^+ channels on AP-evoked $[Ca^{2+}]_i$ transients.

A, Representative traces of 10 ms current pulse induced AP (A) and $[Ca^{2+}]_i$ responses (A') in control conditions (black traces) and in the presence of TTX (1 μ M, 5 min, grey traces). **B - C**, Representative traces of single firing (B-B') and multiple firing (C-C') AP and $[Ca^{2+}]_i$ responses during 500 ms depolarization in control conditions (black traces) and in the presence of TTX (grey traces). **D - E**, Differences in AP and $[Ca^{2+}]_i$ transient amplitudes between control and TTX incubation during 10 ms (***) and 500 ms (***) depolarization current pulses.

To determine the temporal relation between the electrical and $[Ca^{2+}]_i$ responses, and to further assess whether $[Ca^{2+}]_i$ responses are phase-locked to AP firing events, fast imaging (1 kHz) was conducted in response to both 10 and 500 ms single depolarizing current pulses (**Figure 5.6**). The rise in $[Ca^{2+}]_i$ was found to start simultaneously with the onset of an AP (**Figure 5.6A**). When multiple APs were elicited, as during a 500 ms depolarizing current pulse, individual AP spikes gave rise to step-wise fluorescence changes, which was resolvable if APs were separated by an interval larger than the rise time of the indicator. Of the 7 neurons that we have recorded from so far, the shortest inter-AP interval that have generated individual step-wise increases in $[Ca^{2+}]_i$ was found to be 170 ms (**Figure 5.6B**). In other neurons, where the inter-APs interval was too small, the individual $[Ca^{2+}]_i$ steps could not be resolved and submerged in a continuously increasing trend (**Figure 5.6C**).

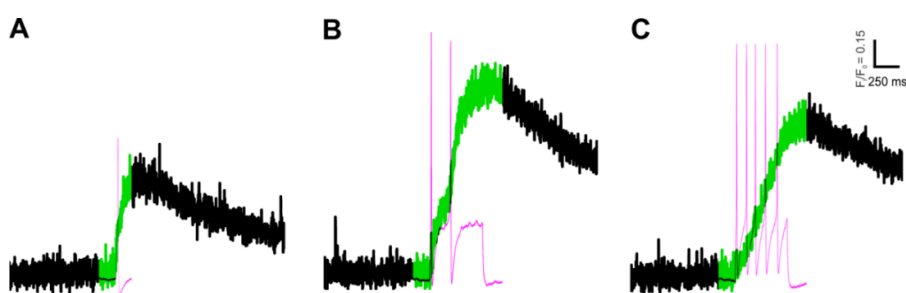


Figure 5.6 | Combined fast Ca imaging and electrophysiology.

A - C, Representative traces of simultaneous whole cell patch clamp recording (pink) and fast Ca imaging (black, 1kHz) during 10ms (A) and 500ms (B - C) depolarization current pulses. The $[Ca^{2+}]_i$ trace is shown in green for the duration of the (pink)

electrical recording. Step-wise GCaMP6f increases could be identified from two individual spikes with an interval of 170ms (B), while no visible steps were detectable once APs were too frequent (C).

5.3.5 [Ca²⁺]_i transients properties evoked by repetitive short or long depolarizing current steps

Apart from single current pulse injections, we also performed pulse train stimulations. Data were collected from 20 neurons, all of which displayed APs elicited by a series of repetitive stimuli of increasing current amplitude (500 ms, 10 pA increments). The average maximum amplitude of the [Ca²⁺]_i transient was 2.44 ± 0.21 .

Next, we grouped the neurons into AH and S type neurons according to their AP repolarization characteristics. We found that the number of [Ca²⁺]_i peaks was significantly less in AH than in S neurons during 500 ms depolarization ($p < 0.05$, **Figure 5.7C**). This is most likely because larger current depolarizations appeared to be required in order to trigger the first [Ca²⁺]_i transient in AH neurons compared to S neurons, although this did not reach statistical significance (100 ± 13 vs. 67 ± 10 pA, $p = 0.062$, **Figure 5.7C**).

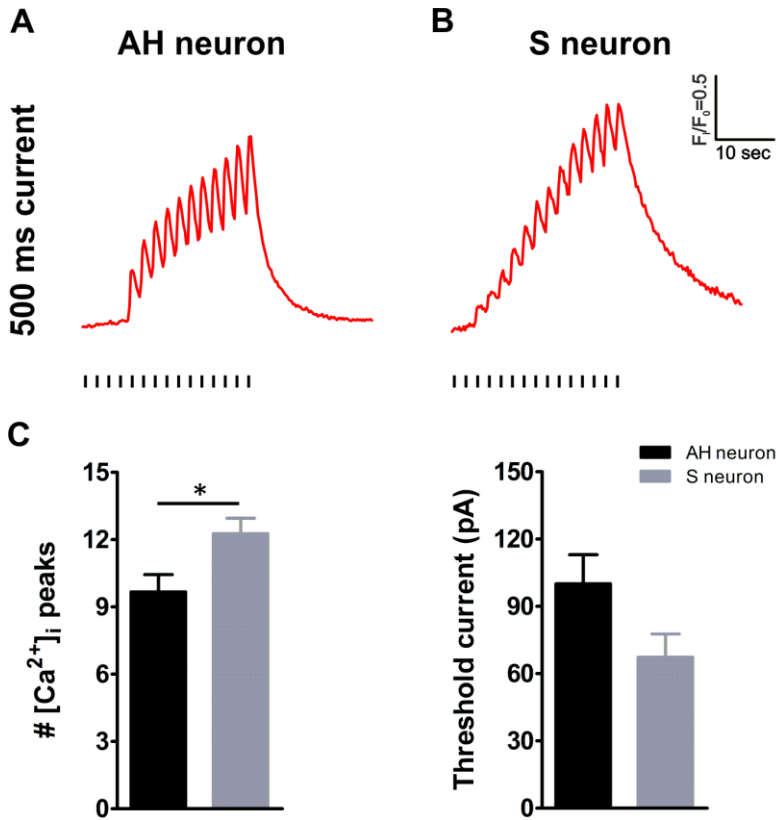


Figure 5.7] Properties of $[Ca^{2+}]_i$ transient evoked by repetitive long depolarizing current steps in AH and S neurons.

A - B, $[Ca^{2+}]_i$ transients (top) during a series of repetitive stimuli with 10 pA increments (black trace, bottom) in an AH (A) and S (B) neuron. **C**, Comparison of the number of $[Ca^{2+}]_i$ peaks (left) and the threshold current to trigger the first $[Ca^{2+}]_i$ peak (right) during 500 ms depolarization current pulses in AH vs. S neurons. (* $p < 0.05$).

5.3.6 Potassium induced depolarization and Ca transients

We also used high K^+ (75 mM) to chemically depolarize neurons and examine the consequence on both $[Ca^{2+}]_i$ transients and membrane voltage ($n = 17$). Twelve out of 17 cells responded with APs (**Figure 5.8A**), whereas 5 cells showed sub-threshold membrane depolarizations (**Figure 5.8B**). Interestingly, there was no significant difference in the average $[Ca^{2+}]_i$ amplitude between these two types of responses (2.66 ± 0.55 vs. 1.87 ± 0.73 , $p > 0.05$).

In addition, we also examined the effect of TTX on high K^+ evoked $[Ca^{2+}]_i$ transients and found that TTX blocked the APs (**Figure 5.8C**) and $[Ca^{2+}]_i$ transients were reduced (from 1.52 to 1.07 F/F_0 , $n = 1$, **Figure 5.8D**).

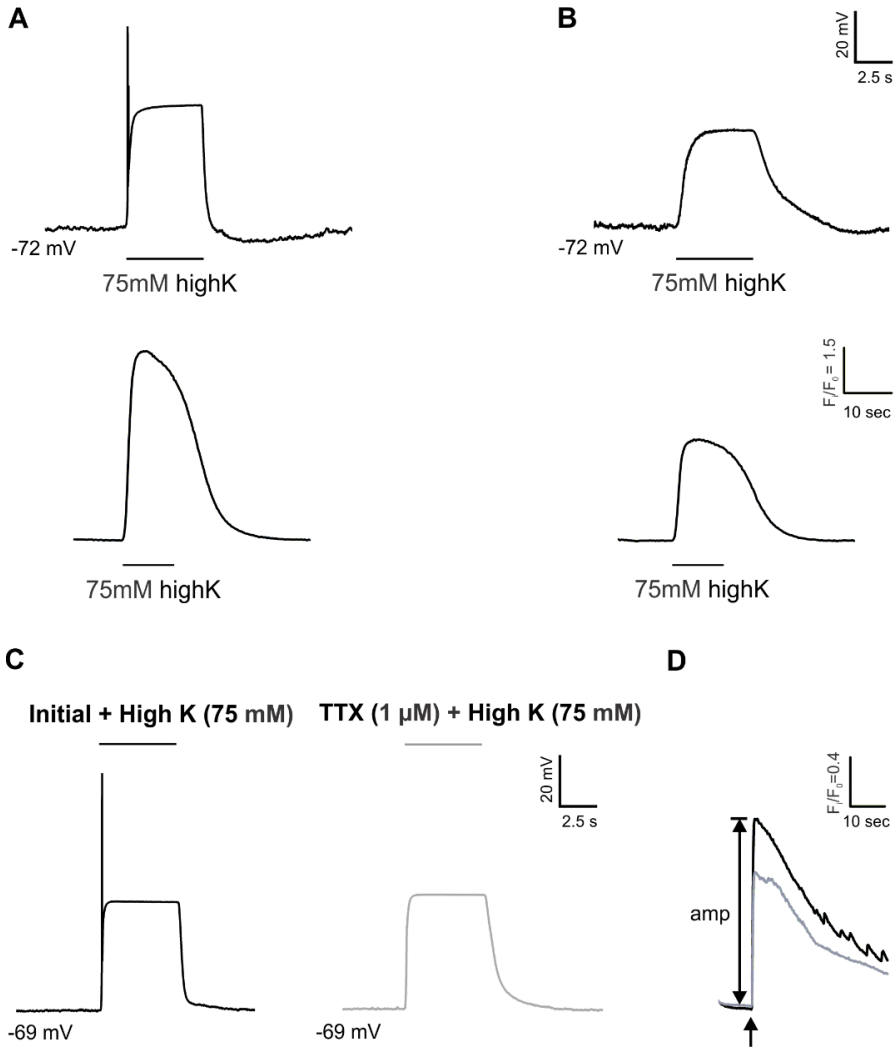


Figure 5.8 | High K^+ induced depolarization and Ca transients.

A - B, Examples of two types of responses to high potassium (high K^+ , 75 mM): (A) high K^+ -evoked AP (top) and accompanying $[Ca^{2+}]_i$ transient (bottom) (B) high K^+ -evoked sub-threshold membrane potential increase (top) with $[Ca^{2+}]_i$ transient (bottom). High K^+ application indicated by dash. **C**, High K^+ -evoked membrane potential changes in control conditions (black trace) and after application of TTX (1

μM , 5 min grey trace). **D**, The accompanying $[\text{Ca}^{2+}]_i$ changes before (black trace) and after TTX incubation (grey trace).

5.3.7 Nicotinic receptor agonist stimulation

Cholinergic neurotransmission is a crucial component of the enteric circuitry in the distinct regions of gut (see also **Chapter 4**). In order to use Ca^{2+} imaging to investigate how individual neurons communicate with each other to build a functional network, it is important to examine the relationship between agonist-induced AP firing and $[\text{Ca}^{2+}]_i$ transients during cholinergic stimulation. Local perfusion of DMPP (10 μM , 10 sec), an agonist of nicotinic cholinergic receptors (nAChR), was applied to mimic fast cholinergic transmission. Data from 28 neurons were collected, which were divided into three groups according to the changes in membrane potential and $[\text{Ca}^{2+}]_i$ evoked by DMPP: type I, in which DMPP triggered APs and $[\text{Ca}^{2+}]_i$ transients ($n = 9$, **Figure 5.9A**); type II, in which DMPP evoked $[\text{Ca}^{2+}]_i$ transients but only sub-threshold membrane voltage responses ($n = 7$, **Figure 5.9B**); and type III, in which DMPP did not elicit either a membrane potential change or $[\text{Ca}^{2+}]_i$ transient ($n = 12$, **Figure 5.9C**). The average $[\text{Ca}^{2+}]_i$ amplitude was significantly larger in type I compared to type II ($p < 0.01$, **Figure 5.9D**) responsive cells. Previous studies have shown that intrinsic sensory neurons, which are AH-type neurons with large diameters, have reduced responses to nicotinic receptor activation⁸⁶. In our study, we found that 10 out of 12 type III neurons were classified as AH neurons based on the inflection on AP repolarization (**Figure 5.9F**), and 2 of these cells showed a prominent sAHP (**Figure 5.9G**). Only one out of 9 type I neurons and one out of 7 type II neurons were also classified as AH neurons. Interestingly, in line with the elevated capacitance, we found the neuronal size of type III neurons to be significantly larger than type I and type II (I: 197.9 ± 15.4 , $p < 0.01$; II: 168.4 ± 12.3 and III: 327.9 ± 31.8 in μm^2 , $p < 0.001$, one-way ANOVA, **Figure 5.9E**). Therefore, it appears that the cells least responsive to DMPP identified in our study are larger sized, AH type neurons, and are therefore, likely to be intrinsic sensory neurons.

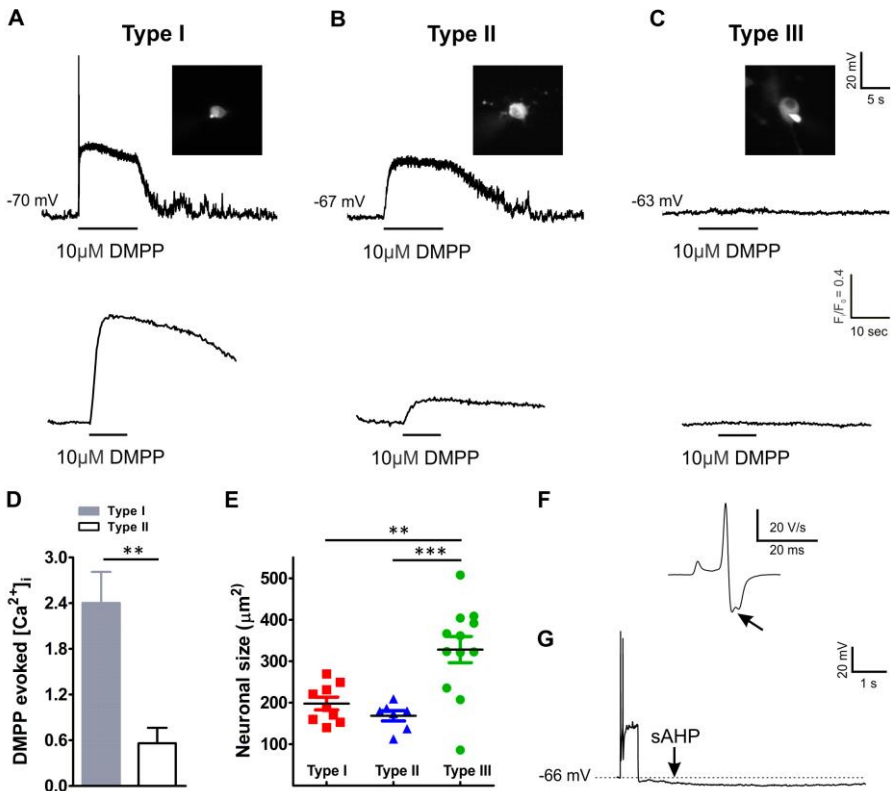


Figure 5.9] Properties of membrane potentials and $[Ca^{2+}]_i$ transient evoked by nicotinic receptor agonist DMPP.

A - C, changes in membrane potential evoked by DMPP ($10\ \mu\text{M}$, $10\ \text{s}$) and snapshots of different types of neurons: (A) Type I – AP-firing, (B) Type II – sub-threshold membrane depolarizations and (C) Type III – unresponsive. Dash indicates DMPP perfusion. Corresponding $[Ca^{2+}]_i$ transients evoked by DMPP are shown below. **D**, Comparison of DMPP evoked $[Ca^{2+}]_i$ transients between Type I ($n = 9$) and Type II (** $p < 0.01$, $n = 7$, one-way ANOVA). **E**, Comparison of neuronal size (μm^2) for each of the three response types (** $p < 0.01$; *** $p < 0.001$, one-way ANOVA). **F - G**, Electrophysiological properties of type III AH neurons, (F) the first time derivative (dV/dt) showing an inflection (arrow) on the repolarization phase of AP, (G) typical sAHP following the action potential of an AH neuron.

We also used TTX in these experiments to block the AP and investigate its effect on the DMPP induced $[Ca^{2+}]_i$ transients. When type I cells were incubated in the presence of TTX ($1\ \mu\text{M}$, $n = 3$), APs were blocked (**Figure 5.10A**), however, the amplitude of the $[Ca^{2+}]_i$ transient appeared to be reduced, but was not statistically

different (from 3.5 ± 0.6 to 1.5 ± 0.9 , $p > 0.05$, **Figure 5.10B**), effectively turning them into type II cells. Post-immunohistochemistry was performed on one of the patched neurons, which was identified to be calretinin+ (**Figure 5.10C**) and NOS-negative (not shown).

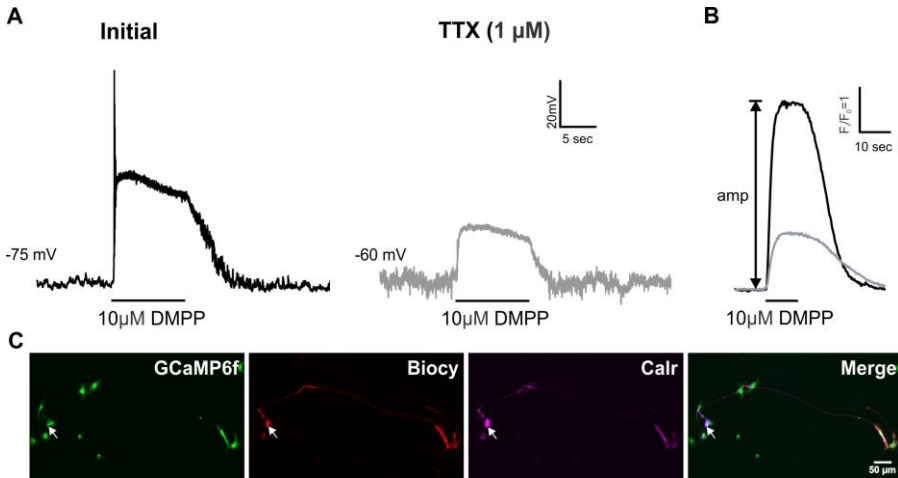


Figure 5.10 | Effect of blocking voltage-gated Na^+ channels on membrane potential and $[\text{Ca}^{2+}]_i$ transients evoked by nicotinic receptor agonist DMPP.

A, A representative response to DMPP ($10 \mu\text{M}$, 10 s , black trace) with AP that were blocked by TTX ($1 \mu\text{M}$, 5 min , grey trace). **B**, Calcium changes before (black trace) and after TTX incubation (grey trace). **C**, Post immunostaining showing that the GCaMP6f (green) and biocytin labeled (red) neuron (arrow) is calretinin+ (magenta).

5.4 Discussion

This study has been the first to extensively characterize the correlation between membrane potential and intracellular calcium changes in mouse myenteric neurons. Using simultaneous whole cell patch clamp recording and Ca imaging with GCaMP6f, we explored the relationship between membrane potential depolarizations and $[\text{Ca}^{2+}]_i$ transients. We found that although AP firing leads to $[\text{Ca}^{2+}]_i$ transients, there is no strict correlation between $[\text{Ca}^{2+}]_i$ amplitude and the number of APs. The amplitude of $[\text{Ca}^{2+}]_i$ transients varied according to the duration of stimulation. Prolonged elevations in membrane potential, induced by either direct current

injection or agonist depolarization, led to larger $[Ca^{2+}]_i$ transients, sometimes even in the absence of APs. We also investigated the $[Ca^{2+}]_i$ properties between the two distinct electrophysiological classes of neurons in the gut, and found that in contrast to previous findings in the guinea pig, both AH and S-type myenteric neurons were capable of eliciting $[Ca^{2+}]_i$ transients with single APs. Lastly, we show that GCaMP6f can be used to detect individual action potential firing at high frequency imaging (1 kHz).

5.4.1 Cell culture

For historical reasons, previous electrophysiological studies characterizing the ENS have been mostly performed in guinea pig small intestine. However, the use of transgenic mice to investigate the role of specific genes and as animal models of disease has substantial advantages for future studies and has pushed the focus towards mouse research. The distribution of enteric neuron subtypes in whole-mount tissues of the mouse has already been investigated⁹². However, there is no proof that this distribution can be extrapolated to primary cell cultures of the ENS. In the current study, we optimized primary myenteric mouse culture protocols based on previous studies^{286,287} to obtain access to individual neurons, which is necessary for patch-clamping. Our immunohistochemical results show that the proportions of sensory (calbindin+), excitatory (calretinin+) and inhibitory (nNOS+) neurons in primary myenteric cell cultures remain consistent to the proportions observed in freshly dissected tissue.

5.4.2 Electrical properties of cultured mouse enteric neurons

There are two main electrophysiological classes of enteric neurons, which have distinct calcium handling properties. Previous studies have shown that AH neurons have a prominent calcium component to their action potential, which is shown by a “hump” or “inflection” on the repolarizing phase^{26,34}. Using the presence of this characteristic inflection, approx. 40% (17/41) of neurons that we recorded from were identified as AH neurons. In accordance with previous studies, our AH neurons had

larger capacitance, presumably due to their larger size, and larger AP amplitude compared to S neurons^{26,34,288}. AH neurons in the guinea pig are usually identified by a prolonged sAHP, however, this has been more difficult to detect in mouse neurons using whole-cell patch-clamp, particularly in culture^{12,283}. Only 2 of our AH neurons exhibited a clear sAHP.

5.4.3 Relationship between AP-firing and calcium transients in mouse enteric neurons

The majority of AH (94%, 16/17) and S neurons (71%, 17/24) evoked resolvable $[Ca^{2+}]_i$ transients to a short (10 ms) depolarizing current pulses. This is in contrast to previous studies in guinea pig tissue, which have reported that a single AP is capable of inducing a detectable $[Ca^{2+}]_i$ transient only in AH neurons, whereas multiple APs are required to elicit a $[Ca^{2+}]_i$ transient in S neurons^{41,89,284}. This could be due to differences in calcium-handling properties between the two species. We observed that the amplitude of $[Ca^{2+}]_i$ transients were larger in AH neurons than S neurons, which could result from higher recruitment of voltage-dependent calcium channels in AH neurons. Indeed, the inflection during action potential repolarization used to identify AH neurons has been shown to be driven by a voltage-dependent calcium current^{24,36,37}. The inflection is lacking in S neurons, which lack a prominent calcium current^{24,36,37}. Therefore, it appears that in mouse S neurons, there is sufficient Ca influx to elicit a detectable $[Ca^{2+}]_i$ transient, but this calcium component is too small to be detected as part of the action potential.

The mode of depolarization is also important for eliciting $[Ca^{2+}]_i$ transients. All AP-firing neurons responded to a long (500 ms) depolarizing current pulse, compared to only 80% for a short (10 ms) current pulse. Interestingly, there were no longer any differences in $[Ca^{2+}]_i$ transient amplitude between AH and S neurons during 500 ms depolarization. It is unclear why this is the case, but the effect likely arises from intracellular calcium handling. Increased Ca^{2+} influx due to longer depolarization is more likely to trigger release of internal Ca^{2+} stores (for example, from the ER), which would lead to further increases in $[Ca^{2+}]_i$ ¹⁹³. $[Ca^{2+}]_i$ transients evoked by these

tonically-firing cells had significantly larger amplitudes compared to single AP-firing cells. Interestingly, the increase in $[Ca^{2+}]_i$ was not graded with the number of APs, which is in contrast to previous studies describing that the $[Ca^{2+}]_i$ increase depends on the number of AP⁸⁹. In addition, we found that inhibiting action potentials using TTX did not completely eliminate $[Ca^{2+}]_i$ transient in response to 500 ms depolarization, indicating that the prolonged depolarization alone might be sufficient to directly activate VDCCs.

We also used high K^+ , to artificially mimic a long lasting depolarization and the high K^+ induced $[Ca^{2+}]_i$ transients, resulting from the opening of all VDCCs²⁸⁹. Such stimulus can be used to physiologically distinguish between neurons and other cell types such as glia cells, since the latter do not seem to express VDCCs²⁸⁹. Here we show that high K^+ depolarization always produces a $[Ca^{2+}]_i$ transient, however, it does not always elicit an action potential. It was also not possible to differentiate between AH and S neurons subtypes based on their $[Ca^{2+}]_i$ response shape to high K^+ . Our preliminary data show that in the presence of TTX (and therefore the absence of APs), high K^+ depolarization is sufficient to initiate a robust $[Ca^{2+}]_i$ response. Therefore, it appears that although $[Ca^{2+}]_i$ transients can be driven by APs, the presence of a $[Ca^{2+}]_i$ transient can also be driven by sub-threshold membrane depolarizations even in the absence of APs. The overall shape of $[Ca^{2+}]_i$ transients did not appear to differ between AP-dependent and non-AP dependent events. To further examine to what extent the $[Ca^{2+}]_i$ response reflects the fast components of neuronal activity, we used fast (kHz) imaging in combination with whole-cell patch-clamp. GCaMP6f has been demonstrated to be the fastest GECI for cytoplasmic free calcium in neurons, with a sensitivity comparable to synthetic calcium indicators, such as Oregon Green Bapta - 1 - AM (OGB1-AM)²⁰². Individual APs can be detected by GCaMP6f with an interval on the order of the rise time of 50-75 ms²⁰². In our study, the smallest interval between APs that could be detected by increases in $[Ca^{2+}]_i$ using fast calcium imaging has been 170 ms. More recordings are needed to investigate progressively smaller inter-AP intervals. In addition, in the future, we aim to apply this method to examine the profile of non-AP dependent $[Ca^{2+}]_i$ transients.

5.4.4 Cholinergic transmission

To further understand how neurotransmitters induce a $[Ca^{2+}]_i$ rise in myenteric neurons, we mimicked the $[Ca^{2+}]_i$ changes observed by electrically-induced synaptic transmission via application of an exogenous agent. We used DMPP, a potent agonist of nAChRs that is commonly used in ENS studies ^{77,86}.

ACh acting on nAChR is the predominant fast excitatory pathway involved in the regulation of many aspects of gut function. nAChRs are non-specific cation channels permeable to Na^+ , K^+ and Ca^{2+} ^{290,291}. To date, it has been determined that there are eight α -subunits ($\alpha 2-9$) and three β -subunits ($\beta 2-4$) to assemble the homopentameric or heteropentameric structures of nAChRs in mammals ²⁹². Using optical imaging, radioimmunoassay combined with immunohistochemistry has shown that $\alpha 3\beta 2$, $\alpha 3\beta 4$, and/or $\alpha 7$ nAChRs are involved in excitatory and inhibitory pathways in the guinea pig myenteric plexus ⁷³. Recently, the different contributions of $\alpha 3\beta 2$, $\alpha 4\beta 2$ and $\alpha 2\beta 4$ to synaptic transmission during different stages of development have been revealed ⁷⁷.

Here, we examined the relationship between DMPP evoked voltage changes and corresponding intracellular $[Ca^{2+}]_i$ changes. Upon application of DMPP, individual cells displayed three distinct types of responses: APs accompanied by large $[Ca^{2+}]_i$ transient (type I); sub-threshold membrane potential increase with smaller amplitude $[Ca^{2+}]_i$ transient (type II); and no detectable membrane potential change or $[Ca^{2+}]_i$ transient (type III). Our data suggest that Type I and type II DMPP responsive cells are S-neurons and that type III cells are AH intrinsic primary afferent neurons. The fact that DMPP triggered AP in some but not other neurons, could result from higher expression of either $\alpha 3\beta 2$, $\alpha 4\beta 2$ and $\alpha 2\beta 4$ or combinations of these subunits on the myenteric neurons, which have been identified to be expressed in enteric neurons and have higher cation conductance ⁷³. Our immunostaining data also confirmed that one example of a type I DMPP-responsive neuron is calretinin+, with small size ($220 \mu m^2$) and S type electrophysiology. This is consistent with the study describing that neurons expressing the higher conductance $\alpha 3\beta 2$, $\alpha 4\beta 2$ and $\alpha 2\beta 4$

nicotinic subunits are likely to be S neurons in guinea pig intestine^{70,79}. It has also been shown that nAChR-mediated currents from calbindin-immunoreactive neurons were significantly smaller than those recorded from calbindin-negative neurons⁸⁶. As calbindin is a widely used marker for intrinsic sensory neurons (AH neurons) in both guinea pig and mouse^{86,92,117}, these data imply that there is lower density of nAChRs on AH neurons in comparison to cells where DMPP triggered APs⁸⁶. Our results support this as we found that the majority of type III DMPP-responsive neurons had AH type electrophysiology. Therefore, it appears to be possible to distinguish between AH and S type enteric neurons based on their responses to DMPP.

5.4.5 Activation of enteric neurons using channelrhodopsin

In addition, to explore the possibility of optical manipulation further simultaneously manipulate and record the activity of multiple neurons with cellular resolution, here we first examined whether light illumination could excite the enteric neurons expressed with optogenetic actuator, ChR2, which can passage cations (such as Na⁺, Ca²⁺) across the cell membrane thus to depolarize neurons upon blue light illumination^{188,189}. We observed blue light successfully evoke action potential firing in ChR2+ enteric neurons, which is consistent with previous studies^{109,293}. Both AH neurons that we have recorded from thus far showed a prominent after-depolarising potential following light stimulation. Further studies are required to examine whether this is unique to AH neurons, or whether it is dependent on channelrhodopsin-evoked depolarization.

5.5 Conclusion

In this study, we extensively investigated the relationship between the membrane potential and [Ca²⁺]_i transients in mouse primary cultured neurons. We show that in contrast to previous studies, single action potentials in both AH and S type enteric neurons were capable of eliciting [Ca²⁺]_i transients, In addition, [Ca²⁺]_i transients were stimulated not only by action potentials, but also by prolonged, sub-threshold

membrane depolarization. The properties of non-AP associated $[Ca^{2+}]_i$ transients remain to be investigated further. Future studies will be needed to combine optogenetic advantages with $[Ca^{2+}]_i$ signaling to further explore the specific subpopulation in enteric circuitry establishment.

5.6 Author Contributions

Z.L.L. collected the data, performed the main analysis and drafted the manuscript. Y.K. performed the fast imaging and train stimulation analysis. W.B., M.M.H., and P.V.B. determined the experimental design and revised the manuscript.

5.7 Acknowledgements

The study was supported by the FWO (G.0921.15) and Hercules foundation (AKUL/11/37 and AKUL/13/37). Z.L.L. is supported by the China Scholarship Council (CSC) (201408370078). M.M.H. (2013-2016) and W.B. (2010-2016) received support as postdoctoral fellows of the Fund for Scientific Research Flanders (FWO) and the NHMRC, Australia (M.M.H. 2014-2018). We also would like to thank Micky Moons for the excellent technical assistance during experiments.

5.8 Conflicts of Interest

The authors declare no conflicts of interest.

CHAPTER 6

General discussion and Future perspectives

6.1 General Discussion

Correct control of gut motility is crucial for the health and function of all animals. Coordinated gut motility relies on the function of the enteric nervous system (ENS). Understanding how functional subpopulations in the ENS connect to each other and exchange the signals necessary to orchestrate the different gut functions is therefore a basic but important subject. Over the years, many elegant studies with different perspectives, such as neurochemical or electrophysiological, have generated a lot of information about the enteric circuitry, primarily in the guinea pig, and especially with respect to the minimal neuronal circuit that controls “the peristalsis reflex”²⁵⁵. In this thesis, we extended the concept of this paradigm to examine differences in nerve circuits that underlie different motility patterns, using the mouse proximal and distal colon as our model. Using viral vector transduction technology and optogenetic recording techniques, we uncovered nerve circuits that reflect the complexity of motility patterns in these two different regions. In addition, we extensively explored the relationship between membrane potential and calcium characteristics in myenteric neurons in mouse primary cell cultures. The principal findings of this thesis are:

- 1) By controlling the concentration of AAVs, we reached the sparse labeling of individual enteric neurons (**Chapter 3**), which is an essential tool to enable the study of individual neurons in a network.
- 2) Using Ca^{2+} imaging, we determined the specific location and response fingerprint of large populations of enteric neurons upon focal network stimulation (**Chapter 4**).
- 3) Using neuronal tracing and volumetric reconstructions of synaptic contacts, we showed that the multifunctional proximal colon requires specific additional circuit components as compared to the distal colon, where peristalsis is the predominant motility pattern (**Chapter 4**).

- 4) Current pulse injection elicited AP-dependent Ca transients with different characteristics for AH and S neurons (**Chapter 5**).
- 5) $[Ca^{2+}]_i$ transients were stimulated not only by action potentials, but also by prolonged, sub-threshold membrane depolarization (**Chapter 5**).
- 6) GCaMP6f could be used in kHz imaging to detect individual action potential firing up to 5 Hz (**Chapter 5**).

6.1.1 Application of virus tracing tools in ENS investigation

Gene delivery through viral vectors has been used ubiquitously in CNS research, allowing the use of the most novel optogenetic genes to examine neural activity and neural circuits. However, there have been a limited number of studies using viral transduction in the ENS. One explanation for this shortage of use of viral technology may be because the ENS is not easily accessible as it resides in a special environment embedded between two muscle layers and protected by a tight epithelial defense barrier against millions of microbes. Its location, as well as its architecture, a single cell layer network, has restricted the ability of the ENS field to adopt and use the plethora of expression constructs that are being newly developed at an extraordinary pace^{184,185}. In the past few decades, recombinant adeno-associated viruses (rAAVs) have received a lot of attention as gene delivery vectors both in research as well as in clinical trials, owing to their low immunogenicity and non-pathogenic characteristics compared with other viruses, such as lenti- or adenoviruses¹⁵⁹⁻¹⁶¹. At the beginning of my PhD in 2014, there were limited reports of successful transfection and transduction of enteric neurons *in situ*. Since then, *in vivo* transduction of the ENS has been achieved through the use of AAVs^{164,166,171}. In my PhD project, we optimized an approach to express functional imaging constructs in selected and identified neurons in the ENS (described in **Chapter 3**). Given the published reports that rAAVs have been reported to transduce enteric neurons, we tested various different rAAVs for their efficacy to transducing enteric neurons in adult mice when injected via the tail vein. Our findings validated the published

approaches as rAAV2/8 and rAAV2/9 were found to be capable of introducing expression of the reporter, eGFP, in enteric neurons with limited transduction of other gastrointestinal cells. By adjusting the concentration of rAAVs, we were able to control density of reporter gene expression, resulting in sparse labeling of enteric neurons that allows the tracing of individual axons (**Chapter 3**). We were able to apply this sparse labelling technique to compare the differences in neuronal projection orientation in two different regions of the gut: the proximal vs. distal colon, identifying that there was a higher proportion of descending interneurons in the distal compared to the proximal colon (**Chapter 4**). Now that we have demonstrated successful transduction of enteric neurons, in future, we aim to drive expression of optogenetic constructs to further investigate neuronal communication on a cell-by-cell level (discussed further in 6.2).

6.1.2 Application of optogenetic tools in ENS investigation

Although for a long time electrophysiological recordings have been the main approach to investigate neuronal circuitry, live imaging microscopy and genetically encoded fluorescent probes to monitor cellular activity have become increasingly important. These optical imaging tools have revolutionized neuroscience as they enable visualization of multiple different forms of neuronal activity at the circuit level in integrated systems¹⁸⁴⁻¹⁸⁶.

The peristaltic reflex is one of the best characterized motility patterns in the gut, resulting in the movement of intestinal contents aborally along the gut. The minimal neuronal circuit necessary to direct peristalsis is well-characterized, but there are also other motility patterns for which the underlying circuits are poorly understood. In addition, ENS defects not only affect digestive disorders but also manifest in neurological disorders. The ENS shares plenty of neurotransmitters and signaling systems with the CNS, and can be affected during aging and neurodegeneration. Therefore, the study of the ENS and ENS dysfunction is also interesting from a neurodegenerative point of view. The ENS has even been reported to be at the origin

of some CNS diseases, to that end the gut-brain axis could serve as a conduit in the development of these diseases²⁹⁴⁻²⁹⁷.

To examine different circuits in the ENS, we investigated the mouse proximal and distal colon, two regions with distinct motility patterns. This was first confirmed by our video imaging data, which show that the proximal colon exhibits richer motility patterns and the distal colon only shows more simple motility (**Chapter 4**). We also used live calcium imaging experiments in order to explore whether those motility patterns are driven by distinct circuits. The specialty of this configuration is that we simply chose to image the gut using a 5x lens instead of the more commonly used 20x magnification. This approach had the advantage of recording large-scale circuit activity while still keeping a single-cell resolution. We found that more neurons respond to a single site stimulus in the proximal colon compared with the distal colon. Although part of this can be explained by the presence of a higher number of neurons and neuronal fibers in the proximal colon, this anatomical difference was not sufficient to completely explain the differences in functional output. This indicated to us that the differences in underlying circuits cannot simply be related to visible morphological differences between these two regions.

Then, we applied the antagonist (hexamethonium) of the main neurotransmitter (ACh) in the ENS to evaluate the role of each individual neuron and its synaptic inputs in the enteric circuit. We found that 1) there are differences in responses to electrical stimulation in hexamethonium in the proximal vs. distal colon; 2) the distribution of response fingerprints is different in the proximal vs. distal colon, suggesting that underlying circuits in which nicotinic cholinergic neurotransmission is involved differ between these two regions and the neuronal wiring in the distal colon depends more importantly on cholinergic excitatory synaptic potentials.

Subsequently, we verified our assumption via immunostaining against the cholinergic neuronal marker, ChAT and the synaptic vesicle marker, vAChT. Although no difference in the proportion of cholinergic neurons was detected, we did find that the area of overlap between neuronal soma and vAChT positive terminals was

notably larger in the distal colon compared to the proximal colon, a finding that confirms our functional Ca^{2+} recordings. In addition, neuronal projection tracing using rAAV9 transduction showed that there was a higher proportion of descending interneurons in the myenteric plexus of the distal than that in the proximal colon.

Taken together, we found regional differences in the connections of neurons in the myenteric plexus in different parts of the colon and advanced the understanding of how segmental enteric neural circuitry confers regional-specific intestinal function. However, whether or not the distinct types of neural activity or projection patterns match any of the known neurochemical subtypes still needs further investigation. Similarly, more experimental work will be required to determine how the newly discovered circuits underlie differences in motility between the two regions.

6.1.3 Application of simultaneous electrophysiological recording with optical imaging in ENS investigation

Much of our understanding of the ENS was established based on studies of the guinea pig intestine. It has historically been the preferred animal model since its intestinal layers can be easily separated and its enteric neurons are readily accessible. To date, a lot of information on the electrophysiological characterization of enteric neurons remains based on conventional intracellular recording techniques, including the identification of the two electrophysiological classes of enteric neurons: AH and S neurons^{26,34}. The key feature that discriminates between AH and S neurons is that for AH neurons Ca^{2+} ions play an important role in the generation of the APs and a prolonged after-hyperpolarization. AH neurons are widely accepted as primary afferent neurons, which are responsible for sensing luminal signals or intestinal distension, and provide this input to other neurons in the ENS. S neurons on the other hand act as interneurons and motor neurons to accept these signals and regulate the final effectors. With the increasing availability of transgenic mouse models of gastrointestinal diseases as well as general reporter mouse lines, there is an increasing interest to more extensively characterize the mouse ENS. However, at present there is only indirect information from guinea pig studies about the

relationship between electrophysiological and calcium characteristics of mouse enteric neurons.

Although the patch-clamp approach is superior to measuring currents underlying membrane potential changes and synaptic behavior, it has been difficult to apply to enteric neurons *in situ* as each ENS ganglion is wrapped with a collagen coating. Therefore, it is difficult to access enteric neurons with a wide patch electrode and only two labs have been successful in patching enteric neurons *in situ*. As an alternative to electrode recordings, optical recordings have attracted more attention to be used to derive information about electrical activity either using fluorescent molecules that sense voltage directly or report the concentration of the second messenger Ca^{2+} . However, it remains a big challenge to distinguish subpopulations based on live calcium imaging.

Our simultaneous patch-clamp and live calcium imaging experiments show that there are some differences in calcium handling characteristics between mouse and guinea pig enteric neurons. Firstly, our experiments show that in primary mouse culture, both AH and S neurons are capable of eliciting detectable $[\text{Ca}^{2+}]_i$ transients in response to single action potentials. This may indicate a greater calcium component to S neuron action potentials, however, this was not reflected in the shape of the action potential itself, as S neurons did not exhibit the hump during AP repolarization. We also observed that although APs are capable of eliciting $[\text{Ca}^{2+}]_i$ transients, sub-threshold membrane depolarizations were also capable of eliciting $[\text{Ca}^{2+}]_i$ transients in the absence of APs, presumably by directly activating voltage-dependent Ca^{2+} channels. What parameters are capable of directly opening VDCCs and what is the role of internal calcium stores remain to be investigated further. In addition, we have shown that in agreement with previous studies, AH type neurons are not commonly excited by the nicotinic receptor agonist, DMPP⁸⁶.

These findings provide new insight into the enteric circuitry building in different regions of the gut and lay the foundation for further identification of neuron subtypes in an all-optical way.

6.2 Future Perspectives

Although we found different circuitry in the proximal and distal colon that may underlie the function of a specific region, it is not clear how these neurons connect and how their neurites extend to their target cells. In future experiments, we aim to extend this study and track the postsynaptic partners of individual neurons using sparse neuronal labeling via viral transduction and wide-field calcium imaging. To do so, we aim to use the rAAV9 sparse labeling approach developed in **Chapter 3** in combination with promoter specific Cre-lox mice, to establish several mouse lines that express functional constructs, such as a genetically encoded actuator (ChR2) and indicator (GCaMP6f), in specific subsets of neurons.

In preliminary experiments, we have transduced enteric neurons from *Wnt1::Cre;R26R-RCL-GCaMP6f* mouse using AAV2/9-CAG-Flex-tdTomato. The tdTomato fluorescent reporter is exclusively expressed in the GCaMP6f+ enteric neurons, and by virtue of its brightness, it can be traced over long distances. By controlling the concentration of AAV2/9-CAG-Flex-tdTomato, our experiments showed sparse labeling of individual myenteric neurons (**Figure 6.1**).

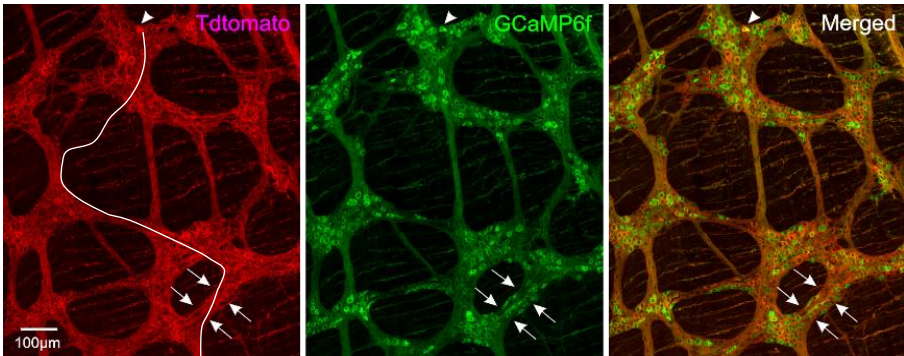


Figure 6.1| Representative confocal images of colonic myenteric plexuses preparation.

AAV2/9-CAG-Flex-tdTomato transduction of a *Wnt1-Cre::R26R-GCaMP6f* mouse, showing tdTomato expression (red) in a neuron (arrowhead) with a long process that could be traced over different ganglion rows. GCaMP6f (Green) is expressed in all myenteric neurons. The white line is a tracing of the axon of a single neuron.

The next step will be to stimulate tdTomato+ neurons and record the Ca²⁺ changes (using GCaMP6f+) from neurons that are in contact with tdTomato+ projections. Single-pulse electrical stimulation of the individual neuronal body will be used to evoke fast and intermediate EPSPs in post-synaptic cells. *Post-hoc* immunohistochemistry will be performed after Ca²⁺ imaging to identify responsive neurons and map the connections between them.

Although ChR2 has become a mature modality for imaging neural activity in CNS, it remains challenging in ENS. Stamp et al (2017)²⁹³ employed ChR2 to demonstrate the functional innervation of the mouse colon by neurons derived from transplanted neural cells. Another remarkable work also applied ChR2 expressed in enteric neurons to modify gut motility¹⁰⁹. In our preliminary experiments, we have been able to excite enteric neurons using blue light in Wnt1-Cre::R26R-ChR2YFP mouse culture (**Chapter 5**). In the future, we will also transduce ChAT::Cre mice via tail vein injection of rAAV-FLEX-rev-ChR2mCherry to specifically express the marker ChR2 in cholinergic enteric neurons. We aim to stimulate specific enteric neurons optogenetically and record Ca²⁺ responses in their post-synaptic partners, thereby linking individual cell activation and population recordings. This will allow us to further explore the role of cholinergic neurons in the myenteric network. The information that results from **Chapter 5** will help to link the Ca imaging readout, the optical stimulation paradigms and the actual electrical activity of the neurons involved.

CHAPTER 7

Summary

7.1 English summary

The enteric nervous system (ENS) is a crucial part of the autonomic nervous system that runs along the entire length of the gastrointestinal tract and comprises a complex network of neurons and glia organized in two ganglionated plexuses: the myenteric and submucosal plexus. The mature ENS can communicate directly or indirectly with other components in the gut, such as interstitial cells (ICC), muscle cells, epithelial cells, and the vasculature, to control GI functions independent of input from the central nervous system (CNS). Notably, myenteric neurons consist of a heterogeneous population of cells, including intrinsic sensory neurons, ascending and descending interneurons and motor neurons, which coordinate different intestinal motor patterns that function in concert to regulate intestinal transit.

Over a century ago, Bayliss and Starling established the “law of the intestine” which described the classical circuit in the gut that directs peristalsis. The physiological circumstance is that there are multiple motility patterns either in the same or distinct regions, which work together to maintain body homeostasis. However, the circuits underlying different motility patterns and their connections which coordinate the transition between these patterns remain unclear. In this PhD project, we aimed to better understand the enteric circuits driving the various motility patterns that differ between colonic regions. To address this, we used live calcium imaging in combination with viral vector tracing to examine the activity, phenotypic properties, location, and projection orientation of individual enteric neurons in an integrated fashion.

In **Chapter 3**, we tested the transduction of adeno-associated viruses (AAVs) in the ENS and optimized the application of functional constructs for investigating the enteric circuitry. Our data confirmed the existing reports on viral vector-mediated gene delivery in the ENS. Moreover, we extended the application of AAVs in the ENS by controlling the dose of rAAV2/9 to achieve sparse labelling of neurons, which allows the identification of individual neuronal processes and tracking of their axons to target cells. Its applicability is effectively demonstrated in **Chapter 4**.

In **Chapter 4**, we first defined different motility patterns in the proximal vs. distal colon, and then used calcium imaging to show that the proximal colon has a larger number of myenteric neurons responding to electrical stimulation of an interganglionic fiber tract. Second, we showed that there is a higher density of myenteric neurons in the proximal colon as compared to the distal colon, and that these neurons display slightly different response properties. Specifically, neuronal connections within the distal colon are more dependent on cholinergic transmission. In addition, our immunohistochemical studies confirmed that the contribution of cholinergic nerves to circuit composition is much more pronounced in the distal colon. Finally, we used viral transduction to sparsely label neurons within the ENS, and found that there is a higher number of longer range projecting neurons in the distal colon than that in the proximal colon. Together with our calcium response profiling of large populations of enteric neurons, these data reveal hard-wired neural circuits that reflect the portfolio of motility programs unique to the intestinal region they occupy.

In **Chapter 5**, we further investigated how the calcium response signatures in our large-scale recording of myenteric neural circuitry relate to their electrophysiological properties. We characterized the relationship between the membrane potential of myenteric neurons and their intracellular calcium changes. We found that injecting current pulses could activate action-potential dependent $[Ca^{2+}]_i$ transients and prolonged elevations in membrane potential, induced by both direct current injection or agonist depolarization mimicking the synaptic input, led to larger $[Ca^{2+}]_i$ transients. Additionally, we showed that GCaMP6f is sufficiently sensitive to resolve individual action potentials using high frequency imaging (1 kHz).

In conclusion, findings from this PhD project demonstrate that the control of intestinal motility is hard-wired in the enteric neural networks and that the degree of circuit complexity within a specific intestinal region matches its portfolio of motor patterns. This finding is not only important from a basic neurobiological point of view, but can also advance clinical practice. Dysfunctional wiring of the ENS has been

suggested as a possible underlying mechanism for many functional gastrointestinal motility disorders where the etiology is not well understood, such as chronic intestinal pseudo-obstruction and slow-transit constipation. Furthermore, an accumulating body of literature points to ENS dysfunction as a factor in many central nervous system disorders. Thus, we contribute to a better understanding of the enteric circuitry underlying gastrointestinal function, which can provide a new perspective on pathophysiological mechanisms for neuron-related diseases.

7.2 Nederlandse Samenvatting

Het enterisch zenuwstelsel is een noodzakelijk onderdeel van het autonoom zenuwstelsel. Het begint aan de slokdarm tot aan de anus waar een complex netwerk van neuronen en glia cellen zich in de myenterische en submucosale plexus van het gastro-intestinaal stelsel bevinden. Een volgroeid enterisch zenuwstelsel communiceert in een directe of indirecte manier met andere celsystemen in de darm zoals interstitiële cellen, spiercellen, epitheelcellen of het vaatstelsel om gastro-intestinale functies uit te voeren zonder bewuste input van het centraal zenuwstelsel. Myenterische neuronen bestaan uit een heterogene groep van cellen waaronder intrinsieke sensorische neuronen, stijgende en dalende interneuronen en motor neuronen (Furness et al., 1990). Deze coördineren verschillende unieke intestinale motiliteitspatronen die leiden tot een goede werking van de intestinale transit.

Meer dan een eeuw geleden hebben Bayliss en Starling de “wet van de darm” geformuleerd die het klassieke circuit in de darm beschrijft dat motiliteit te coördineert. Verschillende motiliteitspatronen, zowel lokale als deze verspreid over meerdere segmenten van de darm, werken samen om lichaamshomeostase te bewaren. De exacte circuits die de basis vormen voor deze motiliteitspatronen en de manier waarop deze circuits samenwerken om verschillende patronen samen te laten werken voor een gezonde transit zijn echter nog steeds onbekend. In deze PhD thesis gebruiken we calcium imaging in levend weefsel in combinatie met virale vector technologie om de activiteit, de fenotypische eigenschappen, locatie en projectie orientatie van individuele neuronen te bestuderen. Deze resultaten kunnen

verder gebruikt worden om regionale verschillen in het netwerk van het enterisch zenuwstelsel in het colon te begrijpen in functie van het verschil in het motiliteitspatroon in het proximale en distale deel.

Voor het gebruik van virale vectoren in het enterisch zenuwstelsel te optimaliseren hebben we de transductie in het ENS vergeleken met verschillende adeno-geassocieerde virussen, zoals beschreven in hoofdstuk 3. Onze data komen overeen met eerder gepubliceerd werk dat virale transductie met adeno virussen in het enterisch zenuwstelsel mogelijk is. We tonen verder aan dat we, door middel van de dosis van het virus aan te passen, sporadisch gelabelde neuronen kunnen verkrijgen wat het mogelijk maakt om axonale projecties van individuele neuronen te volgen. Het gebruik van deze techniek werd vervolgens toegepast in hoofdstuk 4.

In hoofdstuk 4 beschrijven we eerst de verschillende motiliteitspatronen in het proximale en distale colon. We gebruiken calcium imaging om aan te tonen dat het proximale colon meer myenterische neuronen bevat die reageren op elektrische stimulatie van de neuronale projecties tussen verschillende ganglia. Vervolgens bewijzen we dat het proximale colon een hogere dichtheid aan myenterische neuronen bevat in vergelijking met het distale colon en dat deze neuronen verschillen in hun respons eigenschappen. Neuronale connecties in het distale colon zijn bijvoorbeeld meer afhankelijk van cholinerge transmissie. Door middel van het gebruik van immunohistochemische kleuringen tonen we verder ook aan dat er een prominente rol is voor cholinerge transmissie in het enterisch zenuwstelsel circuit van het distale colon. Tot slot gebruiken we virale transductie om sporadisch neuronen te labelen, wat het mogelijk maakt om neuronale projecties te volgen in intact weefsel. Onze resultaten beschrijven dat het distale colon meer neuronen bevat met lange projecties in vergelijking met het proximale colon. We besluiten dat we aan de hand van calcium imaging van grote populaties neuronen in enterisch zenuwstelsel weefsel, de complexe neuronale circuits en hun gecoördineerde activiteit een weergave zijn van de complexe en regionale verschillen in de darm.

Om verder te bestuderen hoe calcium imaging relateert aan de elektrofysiologische eigenschappen van myenterische neuronen, hebben we in hoofdstuk 5 de relatie tussen membraam potentiaal en intracellulaire calcium metingen gekarakteriseerd. We tonen aan dat veranderingen in calcium niveaus in myenterische neuronen zowel afhankelijk als onafhankelijk van geïnduceerde actiepotentialen voorkomen. Vervolgens beschrijven we door gebruik te maken van hoge snelheids (1 kHz) beeldvorming dat GCaMP6f voldoende gevoelig is om individuele actiepotentialen tot 5 Hz optisch te volgen.

Als conclusie van deze PhD thesis, besluiten we dat motiliteit in de darm overeenstemt met specifieke circuits in de darm en dat de regionale verschillen in circuit complexiteit overeen komen met de motor motiliteits patronen in de verschillende regio's van de darm. Deze bevinding is niet alleen belangrijk voor basis neurobiologisch onderzoek maar is ook van belang in klinisch onderzoek. Verschillende gastro-intestinale aandoeningen, zoals chronische intestinale pseudo-obstructie en trage transit constipatie, worden gelinkt aan foute connecties in het circuit van het enterisch zenuwstelsel. Volgens recent onderzoek zouden ook dysfuncties in het enterisch zenuwstelsel gevolgen kunnen hebben voor aandoeningen in het centraal zenuwstelsel. Met dit onderzoek dragen we bij tot het beter begrijpen van de zenuwcircuits in de darmwand, wat een nieuw perspectief kan bieden in het onderzoek naar de pathofysiologische mechanismen bij neuronale aandoeningen.

References

1. Gulbrandsen, B. D. Enteric Glia. *Colloquium Series on Neuroglia in Biology and Medicine: From Physiology to Disease* **1**, 1–70 (2014).
2. Furness, J. B. *The enteric nervous system* Blackwell Publishing. (Melbourne, 2006).
3. Timmermans, J.-P., Hens, J. & ADRIAENSEN, D. Outer submucous plexus: an intrinsic nerve network involved in both secretory and motility processes in the intestine of large mammals and humans. *Anat. Rec.* **262**, 71–78 (2001).
4. Metzger, M., Caldwell, C., Barlow, A. J., Burns, A. J. & Thapar, N. Enteric Nervous System Stem Cells Derived From Human Gut Mucosa for the Treatment of Aganglionic Gut Disorders. *Gastroenterology* **136**, 2214–2225.e3 (2009).
5. Gershon, M. *The Second Brain*. (Harper Collins, 1999).
6. Hao, M. M. *et al.* Enteric nervous system assembly_ Functional integration within the developing gut. *Dev. Biol.* **417**, 168–181 (2016).
7. Yntema, C. L. & Hammond, W. S. The origin of intrinsic ganglia of trunk viscera from vagal neural crest in the chick embryo. *J. Comp. Neurol.* **101**, 515–541 (1954).
8. Le Douarin, N. M. & Teillet, M. A. The migration of neural crest cells to the wall of the digestive tract in avian embryo. *J Embryol Exp Morphol* **30**, 31–48 (1973).
9. Kapur, R. P., Yost, C. & Palmiter, R. D. A transgenic model for studying development of the enteric nervous system in normal and aganglionic mice. *Development* **116**, 167–175 (1992).
10. Wallace, A. S. & Burns, A. J. Development of the enteric nervous system, smooth muscle and interstitial cells of Cajal in the human gastrointestinal tract. *Cell Tissue Res* **319**, 367–382 (2005).
11. Hao, M. M. & Young, H. M. Development of enteric neuron diversity. *Journal of Cellular and Molecular Medicine* **13**, 1193–1210 (2009).
12. Hao, M. M. *et al.* Early Development of Electrical Excitability in the Mouse Enteric Nervous System. *Journal of Neuroscience* **32**, 10949–10960 (2012).
13. Foong, J. P. P., Nguyen, T. V., Furness, J. B., Bornstein, J. C. & Young, H. M. Myenteric neurons of the mouse small intestine undergo significant electrophysiological and morphological changes during postnatal development. *The Journal of Physiology* **590**, 2375–2390 (2012).
14. Brehmer, A., Schrödl, F., Neuhuber, W., Hens, J. & Timmermans, J.-P. Comparison of enteric neuronal morphology as demonstrated by Dil-tracing under different tissue-handling conditions. *Anatomy and Embryology* **199**, 57–62 (1999).
15. Timmermans, J.-P., ADRIAENSEN, D., Cornelissen, W. & SCHEUERMANN, D. W. Structural organization and neuropeptide distribution in the mammalian enteric nervous system, with special attention to those components involved in mucosal reflexes. *Comp. Biochem. Physiol. A Physiol.* **118**, 331–340 (1997).
16. Timmermans, J.-P. *et al.* Distribution pattern, neurochemical features and projections of nitrergic neurons in the pig small intestine. *Annals of Anatomy - Anatomischer Anzeiger* **176**, 515–525 (1994).

17. Timmermans, J.-P., Scheuermann, D. W., Stach, W., Adriaensen, D. & De Groot-Lasseel, M. H. A. Distinct distribution of CGRP-, enkephalin-, galanin-, neuromedin U-, neuropeptide Y-, somatostatin-, substance P-, VIP- and serotonin-containing neurons in the two submucosal ganglionic neural networks of the porcine small intestine. *Cell Tissue Res* **260**, 367–379 (1990).
18. Timmermans, J.-P. *et al.* Calcitonin Gene-Related Peptide-Like Immunoreactivity in the Human Small Intestine. *Cells Tissues Organs (Print)* **143**, 48–53 (1992).
19. Bornstein, J. C., North, R. A., Costa, M. & Furness, J. B. Excitatory synaptic potentials due to activation of neurons with short projections in the myenteric plexus. *Neuroscience* **11**, 723–731 (1984).
20. Nurgali, K., Stebbing, M. J. & Furness, J. B. Correlation of electrophysiological and morphological characteristics of enteric neurons in the mouse colon. *J. Comp. Neurol.* **468**, 112–124 (2004).
21. Mao, Y. Characterization of Myenteric Sensory Neurons in the Mouse Small Intestine. *J. Neurophysiol.* **96**, 998–1010 (2006).
22. Cornelissen, W. *et al.* Electrophysiological Features of Morphological Dogiel Type II Neurons in the Myenteric Plexus of Pig Small Intestine. *J. Neurophysiol.* **84**, 102–111 (2000).
23. Brookes, S. J., Ewart, W. R. & Wingate, D. L. Intracellular recordings from myenteric neurones in the human colon. *The Journal of Physiology* **390**, 305–318 (1987).
24. Clerc, N., Furness, J. B., Bornstein, J. C. & Kunze, W. A. Correlation of electrophysiological and morphological characteristics of myenteric neurons of the duodenum in the guinea-pig. *Neuroscience* **82**, 899–914 (1998).
25. Nishi, S. & North, R. A. Intracellular recording from the myenteric plexus of the guinea-pig ileum. *The Journal of Physiology* **231**, 471–491 (1973).
26. Hirst, G. D., Holman, M. E. & Spence, I. Two types of neurones in the myenteric plexus of duodenum in the guinea-pig. *The Journal of Physiology* **236**, 303–326 (1974).
27. Schemann, M. & Wood, J. D. Electrical behaviour of myenteric neurones in the gastric corpus of the guinea-pig. *The Journal of Physiology* **417**, 501–518 (1989).
28. Tack, J. F. & Wood, J. D. Electrical behaviour of myenteric neurones in the gastric antrum of the guinea-pig. *The Journal of Physiology* **447**, 49–66 (1992).
29. Neunlist, M., Dobрева, G. & Schemann, M. Characteristics of mucosally projecting myenteric neurones in the guinea-pig proximal colon. *The Journal of Physiology* **517 (Pt 2)**, 533–546 (1999).
30. Tamura, K., Ito, H. & Wade, P. R. Morphology, electrophysiology, and calbindin immunoreactivity of myenteric neurons in the guinea pig distal colon. *J. Comp. Neurol.* **437**, 423–437 (2001).
31. Browning, K. N. & Lees, G. M. Myenteric neurons of the rat descending colon: Electrophysiological and correlated morphological properties. *Neuroscience* **73**, 1029–1047 (1996).
32. Carbone, S. E., Jovanovska, V., Nurgali, K. & Brookes, S. J. H. Human enteric neurons: morphological, electrophysiological, and neurochemical identification. *Neurogastroenterol. Motil.* **26**, 1812–1816 (2014).

33. Carbone, S. E., Jovanovska, V., Brookes, S. J. H. & Nurgali, K. Electrophysiological and morphological changes in colonic myenteric neurons from chemotherapy-treated patients: a pilot study. *Neurogastroenterol. Motil.* **28**, 975–984 (2016).
34. Bornstein, J. C., Furness, J. B. & Kunze, W. A. Electrophysiological characterization of myenteric neurons: how do classification schemes relate? *J. Auton. Nerv. Syst.* **48**, 1–15 (1994).
35. Hirst, G. D., Johnson, S. M. & van Helden, D. F. The calcium current in a myenteric neurone of the guinea-pig ileum. *The Journal of Physiology* **361**, 297–314 (1985).
36. Rugiero, F. *et al.* Analysis of whole-cell currents by patch clamp of guinea-pig myenteric neurones in intact ganglia. *The Journal of Physiology* **538**, 447–463 (2002).
37. Bian, X., Zhou, X. & Galligan, J. J. R-type calcium channels in myenteric neurons of guinea pig small intestine. *AJP: Gastrointestinal and Liver Physiology* **287**, G134–G142 (2004).
38. Osorio, N., Korogod, S. & Delmas, P. Specialized Functions of Nav1.5 and Nav1.9 Channels in Electrogenesis of Myenteric Neurons in Intact Mouse Ganglia. *Journal of Neuroscience* **34**, 5233–5244 (2014).
39. Rugiero, F. *et al.* Selective expression of a persistent tetrodotoxin-resistant Na⁺ current and Nav1.9 subunit in myenteric sensory neurons. *J. Neurosci.* **23**, 2715–2725 (2003).
40. Obaid, A. L., Koyano, T., Lindstrom, J., Sakai, T. & Salzberg, B. M. Spatiotemporal patterns of activity in an intact mammalian network with single-cell resolution: optical studies of nicotinic activity in an enteric plexus. *Journal of Neuroscience* **19**, 3073–3093 (1999).
41. Tatsumi, H., Hirai, K. & Katayama, Y. Measurement of the intracellular calcium concentration in guinea-pig myenteric neurons by using fura-2. *Brain Research* **451**, 371–375 (1988).
42. Hillsley, K., Kenyon, J. L. & Smith, T. K. Ryanodine-sensitive stores regulate the excitability of AH neurons in the myenteric plexus of guinea-pig ileum. *J. Neurophysiol.* **84**, 2777–2785 (2000).
43. Vanden Berghe, P., Kenyon, J. L. & Smith, T. K. Mitochondrial Ca²⁺ uptake regulates the excitability of myenteric neurons. *J. Neurosci.* **22**, 6962–6971 (2002).
44. Vogalis, F., Harvey, J. R. & Furness, J. B. TEA- and apamin-resistant KCa channels in guinea-pig myenteric neurons: slow AHP channels. *The Journal of Physiology* **538**, 421–433 (2002).
45. Vogalis, F., Harvey, J. R., Neylon, C. B. & Furness, J. B. Regulation of K channels underlying the slow afterhyperpolarization in enteric afterhyperpolarization-generating myenteric neurons: Role of calcium and phosphorylation. *Clinical and Experimental Pharmacology and Physiology* **29**, 935–943 (2002).
46. Vogalis, F., Furness, J. B. & Kunze, W. A. Afterhyperpolarization current in myenteric neurons of the guinea pig duodenum. *J. Neurophysiol.* **85**, 1941–1951 (2001).
47. Neylon, C. B. *et al.* Intermediate-conductance calcium-activated potassium channels in enteric neurones of the mouse: pharmacological, molecular and immunochemical evidence for their role in mediating the slow afterhyperpolarization. *J. Neurochem.* **90**, 1414–1422 (2004).

48. Nguyen, T. V. *et al.* Effects of compounds that influence IK (KCNN4) channels on afterhyperpolarizing potentials, and determination of IK channel sequence, in guinea pig enteric neurons. *J. Neurophysiol.* **97**, 2024–2031 (2007).
49. Arnold, S. J. *et al.* Decreased potassium channel IK1 and its regulator neurotrophin-3 (NT-3) in inflamed human bowel. *Neuroreport* **14**, 191–195 (2003).
50. Furness, J. B. *et al.* Intermediate conductance potassium (IK) channels occur in human enteric neurons. *Auton Neurosci* **112**, 93–97 (2004).
51. Kunze, W. A. A., Bornstein, J. C., Furness, J. B., Hendriks, R. & Stephenson, D. S. H. Charybdotoxin and iberiotoxin but not apamin abolish the slow after-hyperpolarization in myenteric plexus neurons. *Pflügers Archiv* **428**, 300–306 (1994).
52. Davies, P. J., Thomas, E. A. & Bornstein, J. C. Different types of potassium channels underlie the long afterhyperpolarization in guinea-pig sympathetic and enteric neurons. *Auton Neurosci* **124**, 26–30 (2006).
53. Furness, J. B. Novel gut afferents: Intrinsic afferent neurons and intestinofugal neurons. *Autonomic Neuroscience* **125**, 81–85 (2006).
54. Wood, J. D. & Mayer, C. J. Adrenergic inhibition of serotonin release from neurons in guinea pig Auerback's plexus. *J. Neurophysiol.* **42**, 594–603 (1979).
55. wang, B. *et al.* Lactobacillus reuteri ingestion and IK Channel blockade have similar effects on rat colon motility and myenteric neurones. *Neurogastroenterol. Motil.* **7**, 688–11 (2009).
56. Chambers, J. D., Bornstein, J. C. & Thomas, E. A. Multiple Neural Oscillators and Muscle Feedback Are Required for the Intestinal Fed State Motor Program. *PLoS ONE* **6**, e19597–(2011).
57. Linden, D. R., Sharkey, K. A. & Mawe, G. M. Enhanced excitability of myenteric AH neurones in the inflamed guinea-pig distal colon. *The Journal of Physiology* **547**, 589–601 (2003).
58. Lomax, A. E., Mawe, G. M. & Sharkey, K. A. Synaptic facilitation and enhanced neuronal excitability in the submucosal plexus during experimental colitis in guinea-pig. *The Journal of Physiology* **564**, 863–875 (2005).
59. Nurgali, K. *et al.* Phenotypic changes of morphologically identified guinea-pig myenteric neurons following intestinal inflammation. *The Journal of Physiology* **583**, 593–609 (2007).
60. Kunze, W. A. *et al.* Lactobacillus reuteri enhances excitability of colonic AH neurons by inhibiting calcium-dependent potassium channel opening. *Journal of Cellular and Molecular Medicine* **13**, 2261–2270 (2009).
61. Mao, Y.-K. *et al.* Bacteroides fragilis polysaccharide A is necessary and sufficient for acute activation of intestinal sensory neurons. *Nat Comms* **4**, 1465–10 (1AD).
62. McVey Neufeld, K. A., Perez-Burgos, A., mao, Y. K., bienenstock, J. & Kunze, W. A. The gut microbiome restores intrinsic and extrinsic nerve function in germ-free mice accompanied by changes in calbindin. *Neurogastroenterol. Motil.* **27**, 627–636 (2015).
63. Galligan, J. J., Tatsumi, H., Shen, K. Z., Surprenant, A. & North, R. A. Cation current activated by hyperpolarization (IH) in guinea pig enteric neurons. *Am. J. Physiol. Gastrointest. Liver Physiol.* **259**, G966–G972 (1990).

64. Momin, A., Cadiou, H., Mason, A. & McNaughton, P. A. Role of the hyperpolarization-activated current I_h in somatosensory neurons. *The Journal of Physiology* **586**, 5911–5929 (2008).
65. DiFrancesco, D. Pacemaker mechanisms in cardiac tissue. *Annu. Rev. Physiol.* **55**, 455–472 (1993).
66. Pape, H. C. Queer Current and Pacemaker: The Hyperpolarization-Activated Cation Current in Neurons. *Annu. Rev. Physiol.* **58**, 299–327 (1996).
67. Nolan, M. F. *et al.* The hyperpolarization-activated HCN1 channel is important for motor learning and neuronal integration by cerebellar Purkinje cells. *Cell* **115**, 551–564 (2003).
68. Xiao, J. *et al.* Molecular and functional analysis of hyperpolarisation-activated nucleotide-gated (HCN) channels in the enteric nervous system. *Neuroscience* **129**, 603–614 (2004).
69. Bornstein, J. C., Furness, J. B. & Costa, M. Sources of excitatory synaptic inputs to neurochemically identified submucous neurons of guinea-pig small intestine. *J. Auton. Nerv. Syst.* **18**, 83–91 (1987).
70. Galligan, J. J. & North, R. A. Pharmacology and function of nicotinic acetylcholine and P2X receptors in the enteric nervous system. *Neurogastroenterol. Motil.* **16 Suppl 1**, 64–70 (2004).
71. Surprenant, A. Slow excitatory synaptic potentials recorded from neurones of guinea-pig submucous plexus. *The Journal of Physiology* **351**, 343–361 (1984).
72. Kirchgessner, A. L. & Liu, M. T. Differential localization of Ca^{2+} channel $\alpha 1$ subunits in the enteric nervous system: Presence of $\alpha 1B$ channel-like immunoreactivity in intrinsic primary afferent neurons. *J. Comp. Neurol.* **409**, 85–104 (1999).
73. Obaid, A. L. Optical studies of nicotinic acetylcholine receptor subtypes in the guinea-pig enteric nervous system. *Journal of Experimental Biology* **208**, 2981–3001 (2005).
74. Hirst, G. D. & McKirdy, H. C. Synaptic potentials recorded from neurones of the submucous plexus of guinea-pig small intestine. *The Journal of Physiology* **249**, 369–385 (1975).
75. Pan, H. & Gershon, M. D. Activation of intrinsic afferent pathways in submucosal ganglia of the guinea pig small intestine. *J. Neurosci.* **20**, 3295–3309 (2000).
76. wong, V., blennerhassett, M. & Vanner, S. Electrophysiological and morphological properties of submucosal neurons in the mouse distal colon. *Neurogastroenterol. Motil.* **20**, 725–734 (2008).
77. Foong, J. P. P. *et al.* Changes in Nicotinic Neurotransmission during Enteric Nervous System Development. *Journal of Neuroscience* **35**, 7106–7115 (2015).
78. LePard, K. J., Messori, E. & Galligan, J. J. Purinergic fast excitatory postsynaptic potentials in myenteric neurons of guinea pig: distribution and pharmacology. *Gastroenterology* **113**, 1522–1534 (1997).
79. Galligan, J. J., LePard, K. J., Schneider, D. A. & Zhou, X. Multiple mechanisms of fast excitatory synaptic transmission in the enteric nervous system. *J. Auton. Nerv. Syst.* **81**, 97–103 (2000).

80. Gwynne, R. M. & Bornstein, J. C. Synaptic transmission at functionally identified synapses in the enteric nervous system: roles for both ionotropic and metabotropic receptors. *Curr Neuropharmacol* **5**, 1–17 (2007).
81. Johnson, P. J., Shum, O. R., Thornton, P. D. J. & Bornstein, J. C. Evidence that inhibitory motor neurons of the guinea-pig small intestine exhibit fast excitatory synaptic potentials mediated via P2X receptors. *Neuroscience Letters* **266**, 169–172 (1999).
82. Johnson, S. M., Katayama, Y. & North, R. A. Slow synaptic potentials in neurones of the myenteric plexus. *The Journal of Physiology* **301**, 505–516 (1980).
83. Surprenant, A. & Crist, J. Electrophysiological characterization of functionally distinct 5-hydroxytryptamine receptors on guinea-pig submucous plexus. *Neuroscience* **24**, 283–295 (1988).
84. Mawe, G. M., Branchek, T. A. & Gershon, M. D. Peripheral neural serotonin receptors: identification and characterization with specific antagonists and agonists. *Proc. Natl. Acad. Sci. U.S.A.* **83**, 9799–9803 (1986).
85. Vanner, S. & Surprenant, A. Effects of 5-HT₃ receptor antagonists on 5-HT and nicotinic depolarizations in guinea-pig submucosal neurones. *Br. J. Pharmacol.* **99**, 840–844 (1990).
86. Zhou, X. & Galligan, J. J. Synaptic activation and properties of 5-hydroxytryptamine(3) receptors in myenteric neurons of guinea pig intestine. *Journal of Pharmacology and Experimental Therapeutics* **290**, 803–810 (1999).
87. Ren, J. *et al.* P2X₂ subunits contribute to fast synaptic excitation in myenteric neurons of the mouse small intestine. *The Journal of Physiology* **552**, 809–821 (2004).
88. Smith, T. K., Burke, E. P. & Shuttleworth, C. W. Topographical and electrophysiological characteristics of highly excitable S neurones in the myenteric plexus of the guinea-pig ileum. *The Journal of Physiology* **517 (Pt 3)**, 817–830 (1999).
89. Shuttleworth, C. W. & Smith, T. K. Action potential-dependent calcium transients in myenteric S neurons of the guinea-pig ileum. *Neuroscience* **92**, 751–762 (1999).
90. Messenger, J. P., Bornstein, J. C. & Furness, J. B. Electrophysiological and morphological classification of myenteric neurons in the proximal colon of the guinea-pig. *Neuroscience* **60**, 227–244 (1994).
91. Buhner, S. *et al.* Submucous rather than myenteric neurons are activated by mucosal biopsy supernatants from irritable bowel syndrome patients. *Neurogastroenterol. Motil.* **24**, 1134–e572 (2012).
92. Qu, Z.-D. *et al.* Immunohistochemical analysis of neuron types in the mouse small intestine. *Cell Tissue Res* **334**, 147–161 (2008).
93. SCHEUERMANN, D. W., STACH, W., De Groot-Lasseel, M. H. A. & Timmermans, J.-P. Calcitonin Gene-Related Peptide in Morphologically Well-Defined Type II Neurons of the Enteric Nervous System in the Porcine Small Intestine. *Cells Tissues Organs (Print)* **129**, 325–328 (1987).
94. Gulbransen, B. D. & Sharkey, K. A. Novel functional roles for enteric glia in the gastrointestinal tract. *Nature Publishing Group* **9**, 625–632 (2012).
95. Jessen, K. R. & Mirsky, R. Astrocyte-like glia in the peripheral nervous system: an immunohistochemical study of enteric glia. *Journal of Neuroscience* **3**, 2206–2218 (1983).

96. Boesmans, W., Lasrado, R., Vanden Berghe, P. & Pachnis, V. Heterogeneity and phenotypic plasticity of glial cells in the mammalian enteric nervous system. *Glia* **63**, 229–241 (2014).
97. Neunlist, M. *et al.* The digestive neuronal–glial–epithelial unit: a new actor in gut health and disease. *Nature Reviews Gastroenterology & Hepatology* **10**, 90–100 (2012).
98. De Schepper, S. *et al.* Self-Maintaining Gut Macrophages Are Essential for Intestinal Homeostasis. *Cell* **175**, 400–415.e13 (2018).
99. Sanders, K. M., Ward, S. M. & Koh, S. D. Interstitial cells: regulators of smooth muscle function. *Physiological Reviews* **94**, 859–907 (2014).
100. De Schepper, S., Stakenborg, N., Matteoli, G., Verheijden, S. & Boeckstaens, G. E. Muscularis macrophages: Key players in intestinal homeostasis and disease. *Cellular immunology* **330**, 142–150 (2018).
101. Said, H. M. *Physiology of the Gastrointestinal Tract*. 1–1752 (2011).
102. Kunze, W. A. A. & Furness, J. B. THE ENTERIC NERVOUS SYSTEM AND REGULATION OF INTESTINAL MOTILITY. *Annu. Rev. Physiol.* **61**, 117–142 (1999).
103. Beckett, E. A., Young, H. M., Bornstein, J. C. & Jadcherla, S. R. in *Pediatric Neurogastroenterology* (eds. Faure, C., Thapar, N. & Di Lorenzo, C.) **20**, 21–37 (Springer International Publishing, 2016).
104. Dinning, P. G., Szczesniak, M. M. & Cook, I. J. Twenty-four hour spatiotemporal mapping of colonic propagating sequences provides pathophysiological insight into constipation. *Neurogastroenterol. Motil.* **20**, 1017–1021 (2008).
105. Heredia, D. J., Dickson, E. J., Bayguinov, P. O., Hennig, G. W. & Smith, T. K. Localized Release of Serotonin (5-Hydroxytryptamine) by a Fecal Pellet Regulates Migrating Motor Complexes in Murine Colon. *Gastroenterology* **136**, 1328–1338 (2009).
106. Huizinga, J. D. & Lammers, W. J. E. P. Gut peristalsis is governed by a multitude of cooperating mechanisms. *AJP: Gastrointestinal and Liver Physiology* **296**, G1–G8 (2009).
107. Sanders, K. M., Hwang, S. J. & Ward, S. M. Neuroeffector apparatus in gastrointestinal smooth muscle organs. *The Journal of Physiology* **588**, 4621–4639 (2010).
108. Sanders, K. M., Kito, Y., Hwang, S. J. & Ward, S. M. Regulation of Gastrointestinal Smooth Muscle Function by Interstitial Cells. *Physiology (Bethesda, Md.)* **31**, 316–326 (2016).
109. Spencer, N. J. *et al.* Identification of a Rhythmic Firing Pattern in the Enteric Nervous System That Generates Rhythmic Electrical Activity in Smooth Muscle. *Journal of Neuroscience* **38**, 5507–5522 (2018).
110. Huizinga, J. D. Two independent networks of interstitial cells of Cajal work cooperatively with the enteric nervous system to create colonic motor patterns. 1–14 (2011). doi:10.3389/fnins.2011.00093/abstract
111. Schneider, S., Wright, C. M. & Heuckeroth, R. O. Unexpected Roles for the Second Brain: Enteric Nervous System as Master Regulator of Bowel Function. *Annu. Rev. Physiol.* **81**, annurev-physiol-021317-121515-25 (2018).
112. Latorre, R., Sternini, C., De Giorgio, R. & Greenwood-Van Meerveld, B. Enteroendocrine cells: a review of their role in brain-gut communication. *Neurogastroenterol. Motil.* **28**, 620–630 (2015).

113. Kunze, W. A. A., Furness, J. B. & Bornstein, J. C. Simultaneous intracellular recordings from enteric neurons reveal that myenteric ah neurons transmit via slow excitatory postsynaptic potentials. *Neuroscience* **55**, 685–694 (1993).
114. Furness, J. B., Trussell, D. C., Pompolo, S., Bornstein, J. C. & Smith, T. K. Calbindin neurons of the guinea-pig small intestine: quantitative analysis of their numbers and projections. *Cell Tissue Res* **260**, 261–272 (1990).
115. Song, Z.-M., Costa, M. & Brookes, S. J. H. Projections of submucous neurons to the myenteric plexus in the guinea pig small intestine. *J. Comp. Neurol.* **399**, 255–268 (1998).
116. Brookes, S. J., Song, Z. M., Ramsay, G. A. & Costa, M. Long aboral projections of Dogiel type II, AH neurons within the myenteric plexus of the guinea pig small intestine. *Journal of Neuroscience* **15**, 4013–4022 (1995).
117. Furness, J. B., Kunze, W. A., Bertrand, P. P., Clerc, N. & Bornstein, J. C. Intrinsic primary afferent neurons of the intestine. *Progress in Neurobiology* **54**, 1–18 (1998).
118. Blackshaw, L. A., Brookes, S. J. H., Grundy, D. & Schemann, M. Sensory transmission in the gastrointestinal tract. *Neurogastroenterol. Motil.* **19**, 1–19 (2007).
119. Kunze, W. A., Clerc, N., Furness, J. B. & Gola, M. The soma and neurites of primary afferent neurons in the guinea-pig intestine respond differentially to deformation. *The Journal of Physiology* **526 Pt 2**, 375–385 (2000).
120. Spencer, N. J. & Smith, T. K. Mechanosensory S-neurons rather than AH-neurons appear to generate a rhythmic motor pattern in guinea-pig distal colon. *The Journal of Physiology* **558**, 577–596 (2004).
121. Mazzuoli, G. & Schemann, M. Multifunctional rapidly adapting mechanosensitive enteric neurons (RAMEN) in the myenteric plexus of the guinea pig ileum. *The Journal of Physiology* **587**, 4681–4694 (2009).
122. Schemann, M. & Mazzuoli, G. Multifunctional mechanosensitive neurons in the enteric nervous system. *Auton Neurosci* **153**, 21–25 (2010).
123. Song, Z. M., Brookes, S. J. H., Steele, P. A. & Costa, M. Projections and pathways of submucous neurons to the mucosa of the guinea-pig small intestine. *Cell Tissue Res* **269**, 87–98 (1992).
124. Bertrand, P. P., Kunze, W. A., Bornstein, J. C., Furness, J. B. & Smith, M. L. Analysis of the responses of myenteric neurons in the small intestine to chemical stimulation of the mucosa. *Am. J. Physiol.* **273**, G422–35 (1997).
125. Bertrand, P. P., Kunze, W. A., Bornstein, J. C. & Furness, J. B. Electrical mapping of the projections of intrinsic primary afferent neurones to the mucosa of the guinea-pig small intestine. *Neurogastroenterol. Motil.* **10**, 533–541 (1998).
126. Kirchgessner, A. L., Tamir, H. & Gershon, M. D. Identification and stimulation by serotonin of intrinsic sensory neurons of the submucosal plexus of the guinea pig gut: activity-induced expression of Fos immunoreactivity. *Journal of Neuroscience* **12**, 235–248 (1992).
127. Evans, R. J., Jiang, M. M. & Surprenant, A. Morphological properties and projections of electrophysiologically characterized neurons in the guinea-pig submucosal plexus. *Neuroscience* **59**, 1093–1110 (1994).
128. Moore, B. A. & Vanner, S. Organization of intrinsic cholinergic neurons projecting within submucosal plexus of guinea pig ileum. *Am. J. Physiol.* **275**, G490–7 (1998).

129. Foong, J. P. P., Tough, I. R., Cox, H. M. & Bornstein, J. C. Properties of cholinergic and non-cholinergic submucosal neurons along the mouse colon. *The Journal of Physiology* **592**, 777–793 (2014).
130. Furness, J. B. Types of neurons in the enteric nervous system. *J. Auton. Nerv. Syst.* **81**, 87–96 (2000).
131. Sang, Q. & Young, H. M. Chemical coding of neurons in the myenteric plexus and external muscle of the small and large intestine of the mouse. *Cell Tissue Res* **284**, 39–53 (1996).
132. Sang, Q. & Young, H. M. The identification and chemical coding of cholinergic neurons in the small and large intestine of the mouse. *Anat. Rec.* **251**, 185–199 (1998).
133. Sang, Q., Williamson, S. & Young, H. M. Projections of chemically identified myenteric neurons of the small and large intestine of the mouse. *J. Anat.* **190 (Pt 2)**, 209–222 (1997).
134. Pompolo, S. & Furness, J. B. Sources of inputs to longitudinal muscle motor neurons and ascending interneurons in the guinea-pig small intestine. *Cell Tissue Res* **280**, 549–560 (1995).
135. Bornstein, J. C., Costa, M. & Grider, J. R. Enteric motor and interneuronal circuits controlling motility. *Neurogastroenterol. Motil.* **16**, 34–38 (2004).
136. Neal, K. B. & Bornstein, J. C. Targets of myenteric interneurons in the guinea-pig small intestine. *Neurogastroenterol. Motil.* **20**, 566–575 (2008).
137. Li, Z. S. & Furness, J. B. Inputs from intrinsic primary afferent neurons to nitric oxide synthase-immunoreactive neurons in the myenteric plexus of guinea pig ileum. *Cell Tissue Res* **299**, 1–8 (1999).
138. Young, H. M., Furness, J. B. & Povey, J. M. Analysis of connections between nitric oxide synthase neurons in the myenteric plexus of the guinea-pig small intestine. *Journal of Neurocytology* **24**, 257–263 (1995).
139. FURNESS, I. B., Johnson, P. J., Pompolo, S. & Bornstein, J. C. Evidence that enteric motility reflexes can be initiated through entirely intrinsic mechanisms in the guinea-pig small intestine. *Neurogastroenterol. Motil.* **7**, 89–96 (1995).
140. Monro, R. L., Bornstein, J. C. & Bertrand, P. P. Slow excitatory post-synaptic potentials in myenteric AH neurons of the guinea-pig ileum are reduced by the 5-hydroxytryptamine7 receptor antagonist SB 269970. *Neuroscience* **134**, 975–986 (2005).
141. Tonini, M. *et al.* 5-HT7 Receptors Modulate Peristalsis and Accommodation in the Guinea Pig Ileum. *Gastroenterology* **129**, 1557–1566 (2005).
142. Li, Z. S., Young, H. M. & Furness, J. B. Do vasoactive intestinal peptide (VIP)-and nitric oxide synthase-immunoreactive terminals synapse exclusively with VIP cell bodies in the submucous plexus of the guinea-pig ileum? *Cell Tissue Res* **281**, 485–491 (1995).
143. Song, Z. M., Brookes, S. J. H., Ramsay, G. A. & Costa, M. Characterization of myenteric interneurons with somatostatin immunoreactivity in the guinea-pig small intestine. *Neuroscience* **80**, 907–923 (1997).
144. Meedeniya, A. C., Brookes, S. J., Hennig, G. W. & Costa, M. The projections of 5-hydroxytryptamine-accumulating neurones in the myenteric plexus of the small intestine of the guinea-pig. *Cell Tissue Res* **291**, 375–384 (1998).

145. Moore, B. A. & Vanner, S. Properties of synaptic inputs from myenteric neurons innervating submucosal S neurons in guinea pig ileum. *AJP: Gastrointestinal and Liver Physiology* **278**, G273–80 (2000).
146. Song, Z. M., Brookes, S. J. H., Ramsay, G. A. & Costa, M. Characterization of myenteric interneurons with somatostatin immunoreactivity in the guinea-pig small intestine. *Neuroscience* **80**, 907–923 (1997).
147. Monro, R. L., Bornstein, J. C. & Bertrand, P. P. Synaptic transmission from the submucosal plexus to the myenteric plexus in Guinea-pig ileum. *Neurogastroenterol. Motil.* **20**, 1165–1173 (2008).
148. Reed, D. E. & Vanner, S. J. Converging and diverging cholinergic inputs from submucosal neurons amplify activity of secretomotor neurons in guinea-pig ileal submucosa. *Neuroscience* **107**, 685–696 (2001).
149. Furness, J. B., Alex, G., Clark, M. J. & Lal, V. V. Morphologies and projections of defined classes of neurons in the submucosa of the guinea-pig small intestine. *Anat. Rec.* **272A**, 475–483 (2003).
150. Mongardi Fantaguzzi, C., Thacker, M., Chiocchetti, R. & Furness, J. B. Identification of neuron types in the submucosal ganglia of the mouse ileum. *Cell Tissue Res* **336**, 179–189 (2009).
151. Bornstein, J. C., Costa, M. & Furness, J. B. Synaptic inputs to immunohistochemically identified neurones in the submucous plexus of the guinea-pig small intestine. *The Journal of Physiology* **381**, 465–482 (1986).
152. Bornstein, J. C., Costa, M. & Furness, J. B. Intrinsic and extrinsic inhibitory synaptic inputs to submucous neurones of the guinea-pig small intestine. *The Journal of Physiology* **398**, 371–390 (1988).
153. Hu, H.-Z. *et al.* Actions of bradykinin on electrical and synaptic behavior of neurones in the myenteric plexus of guinea-pig small intestine. *Br. J. Pharmacol.* **138**, 1221–1232 (2003).
154. Foong, J. P. P., Parry, L. J., Gwynne, R. M. & Bornstein, J. C. 5-HT_{1A}, SST1, and SST2 receptors mediate inhibitory postsynaptic potentials in the submucous plexus of the guinea pig ileum. *AJP: Gastrointestinal and Liver Physiology* **298**, G384–G394 (2010).
155. Furness, J. B. Types of neurons in the enteric nervous system. *J. Auton. Nerv. Syst.* **81**, 87–96 (2000).
156. Monro, R. L., Bertrand, P. P. & Bornstein, J. C. ATP and 5-HT are the principal neurotransmitters in the descending excitatory reflex pathway of the guinea-pig ileum. *Neurogastroenterol. Motil.* **14**, 255–264 (2002).
157. Blacklow, N. R., Hoggan, M. D. & Rowe, W. P. Isolation of adenovirus-associated viruses from man. *Proc. Natl. Acad. Sci. U.S.A.* **58**, 1410–1415 (1967).
158. Muzyczka, N. in *Viral Expression Vectors* **158**, 97–129 (Springer, Berlin, Heidelberg, 1992).
159. Daya, S. & Berns, K. I. Gene Therapy Using Adeno-Associated Virus Vectors. *Clin. Microbiol. Rev.* **21**, 583–593 (2008).
160. Mueller, C. & Flotte, T. R. Clinical gene therapy using recombinant adeno-associated virus vectors. *Gene Therapy* **15**, 858–863 (2008).

161. Samulski, R. J. & Muzyczka, N. AAV-Mediated Gene Therapy for Research and Therapeutic Purposes. *Annu. Rev. Virol.* **1**, 427–451 (2014).
162. Rahim, A. A. *et al.* Intravenous administration of AAV2/9 to the fetal and neonatal mouse leads to differential targeting of CNS cell types and extensive transduction of the nervous system. *The FASEB Journal* **25**, 3505–3518 (2011).
163. Fu, H., DiRosario, J., Killedar, S., Zaraspe, K. & McCarty, D. M. Correction of Neurological Disease of Mucopolysaccharidosis IIIB in Adult Mice by rAAV9 Trans-Blood–Brain Barrier Gene Delivery. *Mol Ther* **19**, 1025–1033 (2009).
164. Gombash, S. E. *et al.* Intravenous AAV9 efficiently transduces myenteric neurons in neonate and juvenile mice. *Front Mol Neurosci* **7**, 81 (2014).
165. Garcia, J. *et al.* Targeted Gene Delivery to the Enteric Nervous System Using AAV: A Comparison Across Serotypes and Capsid Mutants. *Mol Ther* **23**, 488–500 (2015).
166. Buckinx, R., Van Remoortel, S., Gijbsers, R., Waddington, S. N. & Timmermans, J.-P. Proof-of-concept: neonatal intravenous injection of adeno-associated virus vectors results in successful transduction of myenteric and submucosal neurons in the mouse small and large intestine. *Neurogastroenterol. Motil.* **28**, 299–305 (2016).
167. Chan, K. Y., Jang, M. J., Yoo, B. B. & Greenbaum, A. Engineered AAVs for efficient noninvasive gene delivery to the central and peripheral nervous systems. *Nature* (2017). doi:10.1038/nn.4593
168. Bedbrook, C. N., Deverman, B. E. & Gradinaru, V. Viral Strategies for Targeting the Central and Peripheral Nervous Systems. *Annu. Rev. Neurosci.* **41**, 323–348 (2018).
169. Buckinx, R. & Timmermans, J.-P. Targeting the gastrointestinal tract with viral vectors: state of the art and possible applications in research and therapy. *Histochemistry and Cell Biology* **146**, 709–720 (2016).
170. Natarajan, D. *et al.* Lentiviral labeling of mouse and human enteric nervous system stem cells for regenerative medicine studies. *Neurogastroenterol. Motil.* **26**, 1513–1518 (2014).
171. Benskey, M. J. *et al.* Targeted Gene Delivery to the Enteric Nervous System Using AAV: A Comparison Across Serotypes and Capsid Mutants. *Mol Ther* **23**, 488–500 (2015).
172. Kotterman, M. A. & Schaffer, D. V. Engineering adeno-associated viruses for clinical gene therapy. *Nat Rev Genet* **15**, 445–451 (2014).
173. Sonntag, F., Schmidt, K. & Kleinschmidt, J. A. A viral assembly factor promotes AAV2 capsid formation in the nucleolus. *Proc. Natl. Acad. Sci. U.S.A.* **107**, 10220–10225 (2010).
174. McLaughlin, S. K., Collis, P., Hermonat, P. L. & Muzyczka, N. Adeno-associated virus general transduction vectors: analysis of proviral structures. *Journal of Virology* **62**, 1963–1973 (1988).
175. Senapathy, P., Tratschin, J.-D. & Carter, B. J. Replication of adeno-associated virus DNA: Complementation of naturally occurring rep- mutants by a wild-type genome or an fori-mutant and correction of terminal palindrome deletions. *Journal of Molecular Biology* **179**, 1–20 (1984).
176. Samulski, R. J., Chang, L. S. & Shenk, T. A recombinant plasmid from which an infectious adeno-associated virus genome can be excised in vitro and its use to study viral replication. *Journal of Virology* **61**, 3096–3101 (1987).

177. Kaufmann, B., Simpson, A. A. & Rossmann, M. G. The structure of human parvovirus B19. *Proc. Natl. Acad. Sci. U.S.A.* **101**, 11628–11633 (2004).
178. Girod, A. *et al.* The VP1 capsid protein of adeno-associated virus type 2 is carrying a phospholipase A2 domain required for virus infectivity. *J. Gen. Virol.* **83**, 973–978 (2002).
179. Weitzman, M. D. & Linden, R. M. in *Adeno-Associated Virus* **807**, 1–23 (Humana Press, 2012).
180. Schultz, B. R. & Chamberlain, J. S. Recombinant Adeno-associated Virus Transduction and Integration. *Mol Ther* **16**, 1189–1199 (2008).
181. Rabinowitz, J. E. *et al.* Cross-Packaging of a Single Adeno-Associated Virus (AAV) Type 2 Vector Genome into Multiple AAV Serotypes Enables Transduction with Broad Specificity. *Journal of Virology* **76**, 791–801 (2002).
182. Wu, Z., Miller, E., Agbandje-McKenna, M. & Samulski, R. J. 2,3 and 2,6 N-Linked Sialic Acids Facilitate Efficient Binding and Transduction by Adeno-Associated Virus Types 1 and 6. *Journal of Virology* **80**, 9093–9103 (2006).
183. Nonnenmacher, M. & Weber, T. Intracellular transport of recombinant adeno-associated virus vectors. **19**, 649–658 (2012).
184. Boesmans, W., Hao, M. M. & Berghe, P. V. Optical Tools to Investigate Cellular Activity in the Intestinal Wall. *J Neurogastroenterol Motil* **21**, 337–351 (2015).
185. Boesmans, W., Hao, M. M. & Berghe, P. V. Optogenetic and chemogenetic techniques for neurogastroenterology. *Nature Reviews Gastroenterology & Hepatology* **14**, 21–38 (2017).
186. Ji, N., Freeman, J. & Smith, S. L. Technologies for imaging neural activity in large volumes. *Nat Neurosci* **19**, 1154–1164 (2016).
187. Miesenböck, G. The optogenetic catechism. *Science* **326**, 395–399 (2009).
188. Nagel, G. *et al.* Channelrhodopsin-2, a directly light-gated cation-selective membrane channel. *Proc. Natl. Acad. Sci. U.S.A.* **100**, 13940–13945 (2003).
189. Boyden, E. S., Zhang, F., Bamberg, E., Nagel, G. & Deisseroth, K. Millisecond-timescale, genetically targeted optical control of neural activity. *Nat Neurosci* **8**, 1263–1268 (2005).
190. Asrican, B. *et al.* Next-generation transgenic mice for optogenetic analysis of neural circuits. *Frontiers in Neural Circuits* **7**, (2013).
191. Packer, A. M., Russell, L. E., Dagleish, H. W. P. & Häusser, M. Simultaneous all-optical manipulation and recording of neural circuit activity with cellular resolution in vivo. *Nat Meth* **12**, 140–146 (2014).
192. Gradinaru, V., Thompson, K. R. & Deisseroth, K. eNpHR: a *Natronomonas* halorhodopsin enhanced for optogenetic applications. *Brain Cell Bio* **36**, 129–139 (2008).
193. Grienberger, C. & Konnerth, A. Imaging Calcium in Neurons. *Neuron* **73**, 862–885 (2012).
194. Abdelfattah, A. S. *et al.* Bright and photostable chemigenetic indicators for extended in vivo voltage imaging. *bioRxiv* 1–105 (2018). doi:10.1101/436840
195. Lin, M. Z. & Schnitzer, M. J. Genetically encoded indicators of neuronal activity. *Nat Neurosci* **19**, 1142–1153 (2016).

196. Miyawaki, A., Griesbeck, O., Heim, R. & Tsien, R. Y. Dynamic and quantitative Ca²⁺ measurements using improved cameleons. *Proc. Natl. Acad. Sci. U.S.A.* **96**, 2135–2140 (1999).
197. Huber, D. *et al.* Multiple dynamic representations in the motor cortex during sensorimotor learning. *Nature* **484**, 473–478 (2012).
198. Dombeck, D. A., Harvey, C. D., Tian, L., Looger, L. L. & Tank, D. W. Functional imaging of hippocampal place cells at cellular resolution during virtual navigation. *Nat Neurosci* **13**, 1433–1440 (2010).
199. Hennig, G. W. *et al.* Use of Genetically Encoded Calcium Indicators (GECIs) Combined with Advanced Motion Tracking Techniques to Examine the Behavior of Neurons and Glia in the Enteric Nervous System of the Intact Murine Colon. *Front. Cell. Neurosci.* **9**, 13819–12 (2015).
200. Badura, A., Sun, X. R., Giovannucci, A., Lynch, L. A. & Wang, S. S. H. Fast calcium sensor proteins for monitoring neural activity. *Neurophoton* **1**, 025008–13 (2014).
201. Podor, B. *et al.* Comparison of genetically encoded calcium indicators for monitoring action potentials in mammalian brain by two-photon excitation fluorescence microscopy. *Neurophoton* **2**, 021014–8 (2015).
202. Chen, T. W., Wardill, T. J., Sun, Y., Pulver, S. R. & Renninger, S. L. Ultrasensitive fluorescent proteins for imaging neuronal activity. *Nature* **499**, 295–300 (2013).
203. Bayliss, W. M. & Starling, E. H. The movements and innervation of the small intestine. *The Journal of Physiology* **24**, 99–143 (1899).
204. Gwynne, R. M. & Bornstein, J. C. Mechanisms underlying nutrient-induced segmentation in isolated guinea pig small intestine. *AJP: Gastrointestinal and Liver Physiology* **292**, G1162–G1172 (2007).
205. Smith, T. K. & Koh, S. D. A model of the enteric neural circuitry underlying the generation of rhythmic motor patterns in the colon: the role of serotonin. *AJP: Gastrointestinal and Liver Physiology* **312**, G1–G14 (2017).
206. Lake, J. I. & Heuckeroth, R. O. Enteric nervous system development: migration, differentiation, and disease. *AJP: Gastrointestinal and Liver Physiology* **305**, G1–G24 (2013).
207. Haricharan, R. N. & Georgeson, K. E. Hirschsprung disease. *Seminars in Pediatric Surgery* **17**, 266–275 (2008).
208. Sasselli, V. *et al.* Planar cell polarity genes control the connectivity of enteric neurons. *J. Clin. Invest.* **123**, 1763–1772 (2013).
209. Chitkara, D. K. & Lorenzo, C. From the bench to the ‘crib’-side: implications of scientific advances to paediatric neurogastroenterology and motility. *Neurogastroenterol. Motil.* **18**, 251–262 (2006).
210. Wood, J. D. Taming the irritable bowel. *Curr. Pharm. Des.* **19**, 142–156 (2013).
211. Tang, D. M. & Friedenberg, F. K. Gastroparesis: Approach, Diagnostic Evaluation, and Management. *YMDA* **57**, 74–101 (2011).
212. Klingelhoefer, L. & Reichmann, H. Pathogenesis of Parkinson disease—the gut–brain axis and environmental factors. *Nature Publishing Group* **11**, 625–636 (2015).

213. Rao, M. & Gershon, M. D. The bowel and beyond: the enteric nervous system in neurological disorders. *Nature Reviews Gastroenterology & Hepatology* **13**, 517–528 (2016).
214. ANDERSON, G. *et al.* Loss of enteric dopaminergic neurons and associated changes in colon motility in an MPTP mouse model of Parkinson's disease. *Experimental Neurology* **207**, 4–12 (2007).
215. Buie, T. *et al.* Evaluation, diagnosis, and treatment of gastrointestinal disorders in individuals with ASDs: a consensus report. in **125 Suppl 1**, S1–18 (American Academy of Pediatrics, 2010).
216. Wakabayashi, K., Mori, F., Tanji, K., Orimo, S. & Takahashi, H. Involvement of the peripheral nervous system in synucleinopathies, tauopathies and other neurodegenerative proteinopathies of the brain. *Acta Neuropathol* **120**, 1–12 (2010).
217. Natale, G., Pasquali, L., Paparelli, A. & Fornai, F. Parallel manifestations of neuropathologies in the enteric and central nervous systems. *Neurogastroenterol. Motil.* **23**, 1056–1065 (2011).
218. Desmet, A.-S., Cirillo, C., Tack, J., Vandenberghe, W. & Vanden Berghe, P. Live calcium and mitochondrial imaging in the enteric nervous system of Parkinson patients and controls. *Elife* **6**, 197 (2017).
219. Foust, K. D. *et al.* Intravascular AAV9 preferentially targets neonatal neurons and adult astrocytes. *Nat Biotechnol* **27**, 59–65 (2008).
220. Haurigot, V. *et al.* Whole body correction of mucopolysaccharidosis IIIA by intracerebrospinal fluid gene therapy. *J. Clin. Invest.* **123**, 3254–3271 (2013).
221. Van der Perren, A. *et al.* Efficient and stable transduction of dopaminergic neurons in rat substantia nigra by rAAV 2/1, 2/2, 2/5, 2/6.2, 2/7, 2/8 and 2/9. **18**, 517–527 (2011).
222. Boesmans, W., Rocha, N. P., Reis, H. J., Holt, M. & Berghe, P. V. The astrocyte marker Aldh1L1 does not reliably label enteric glial cells. *Neuroscience Letters* **566**, 102–105 (2014).
223. Shen, S., Bryant, K. D., Brown, S. M., Randell, S. H. & Asokan, A. Terminal N-Linked Galactose Is the Primary Receptor for Adeno-associated Virus 9. *J. Biol. Chem.* **286**, 13532–13540 (2011).
224. Duque, S. *et al.* Intravenous Administration of Self-complementary AAV9 Enables Transgene Delivery to Adult Motor Neurons. *Mol Ther* **17**, 1187–1196 (2009).
225. Bell, C. L. *et al.* The AAV9 receptor and its modification to improve in vivo lung gene transfer in mice. *J. Clin. Invest.* **121**, 2427–2435 (2011).
226. Wu, A. M. *et al.* Differential affinities of Erythrina cristagalli lectin (ECL) toward monosaccharides and polyvalent mammalian structural units. *Glycoconj J* **24**, 591–604 (2007).
227. Taymans, J.-M. *et al.* Comparative Analysis of Adeno-Associated Viral Vector Serotypes 1, 2, 5, 7, And 8 in Mouse Brain. *Human Gene Therapy* **18**, 195–206 (2007).
228. Mattar, C. N. *et al.* Systemic delivery of scAAV9 in fetal macaques facilitates neuronal transduction of the central and peripheral nervous systems. 1–15 (2012). doi:10.1038/gt.2011.216

229. Xie, Q., Lerch, T. F., Meyer, N. L. & Chapman, M. S. Structure–function analysis of receptor-binding in adeno-associated virus serotype 6 (AAV-6). *Virology* **420**, 10–19 (2011).
230. Nam, H. J. *et al.* Structure of Adeno-Associated Virus Serotype 8, a Gene Therapy Vector. *Journal of Virology* **81**, 12260–12271 (2007).
231. Akache, B. *et al.* The 37/67-Kilodalton Laminin Receptor Is a Receptor for Adeno-Associated Virus Serotypes 8, 2, 3, and 9. *Journal of Virology* **80**, 9831–9836 (2006).
232. Ng, R. *et al.* Structural Characterization of the Dual Glycan Binding Adeno-Associated Virus Serotype 6. *Journal of Virology* **84**, 12945–12957 (2010).
233. Gombash, S. E. Adeno-Associated Viral Vector Delivery to the Enteric Nervous System: A Review. 1–14 (2016).
234. Syme, M. R., Paxton, J. W. & Keelan, J. A. Drug Transfer and Metabolism by the Human Placenta. *Clin Pharmacokinet* **43**, 487–514 (2004).
235. Ewing, G., Tatarchuk, Y., Appleby, D., Schwartz, N. & Kim, D. Placental Transfer of Antidepressant Medications: Implications for Postnatal Adaptation Syndrome. *Clin Pharmacokinet* **54**, 359–370 (2015).
236. Bevan, A. K. *et al.* Systemic gene delivery in large species for targeting spinal cord, brain, and peripheral tissues for pediatric disorders. *Mol Ther* **19**, 1971–1980 (2011).
237. Samaranch, L. *et al.* Adeno-Associated Virus Serotype 9 Transduction in the Central Nervous System of Nonhuman Primates. *Human Gene Therapy* **23**, 382–389 (2012).
238. Said, H. M. *Physiology of the Gastrointestinal Tract, Two Volume Set*. (Academic Press, 2012).
239. Furness, J. B. The enteric nervous system and neurogastroenterology. *Nature Publishing Group* **9**, 286–294 (2012).
240. Lasrado, R. *et al.* Lineage-dependent spatial and functional organization of the mammalian enteric nervous system. *Science* **356**, 722–726 (2017).
241. James, C. in *Electrical and synaptic behavior of enteric neurons* 939–973 (American Cancer Society, 2011). doi:10.1002/cphy.cp060124
242. Tonini, M., Costa, M., Brookes, S. J. H. & Humphreys, C. M. S. Dissociation of the ascending excitatory reflex from peristalsis in the guinea-pig small intestine. *Neuroscience* **73**, 287–297 (1996).
243. Costa, M. *et al.* Neuromechanical factors involved in the formation and propulsion of fecal pellets in the guinea-pig colon. *Neurogastroenterol. Motil.* **27**, 1466–1477 (2015).
244. Hennig, G. W., Costa, M., Chen, B. N. & Brookes, S. J. Quantitative analysis of peristalsis in the guinea-pig small intestine using spatio-temporal maps. *The Journal of Physiology* **517 (Pt 2)**, 575–590 (1999).
245. Spencer, N. J., Smith, C. B. & Smith, T. K. Role of muscle tone in peristalsis in guinea-pig small intestine. *The Journal of Physiology* **530**, 295–306 (2001).
246. Smith, T. K., Park, K. J. & Hennig, G. W. Colonic Migrating Motor Complexes, High Amplitude Propagating Contractions, Neural Reflexes and the Importance of Neuronal and Mucosal Serotonin. *J Neurogastroenterol Motil* **20**, 423–446 (2014).

247. Boesmans, W. *et al.* Imaging neuron-glia interactions in the enteric nervous system. *Front. Cell. Neurosci.* **7**, 183 (2013).
248. Zariwala, H. A. *et al.* A Cre-dependent GCaMP3 reporter mouse for neuronal imaging in vivo. *J. Neurosci.* **32**, 3131–3141 (2012).
249. Danielian, P. S., Muccino, D., Rowitch, D. H., Michael, S. K. & McMahon, A. P. Modification of gene activity in mouse embryos in utero by a tamoxifen-inducible form of Cre recombinase. *Curr. Biol.* **8**, 1323–1326 (1998).
250. Swaminathan, M. *et al.* Video Imaging and Spatiotemporal Maps to Analyze Gastrointestinal Motility in Mice. *J Vis Exp* 1–8 (2016). doi:10.3791/53828
251. Van der Perren, A. *et al.* Efficient and stable transduction of dopaminergic neurons in rat substantia nigra by rAAV 2/1, 2/2, 2/5, 2/6.2, 2/7, 2/8 and 2/9. *Gene Therapy* **18**, 517–527 (2011).
252. Barnes, K. J., Beckett, E. A., Brookes, S. J., Sia, T. C. & Spencer, N. J. Control of intrinsic pacemaker frequency and velocity of colonic migrating motor complexes in mouse. *Front Neurosci* **8**, 96 (2014).
253. Fung, C. *et al.* VPAC Receptor Subtypes Tune Purinergic Neuron-to-Glia Communication in the Murine Submucosal Plexus. *Front. Cell. Neurosci.* **11**, 354–16 (2017).
254. Spencer, N. J., Hennig, G. W., Dickson, E. & Smith, T. K. Synchronization of enteric neuronal firing during the murine colonic MMC. *The Journal of Physiology* **564**, 829–847 (2005).
255. Trendelenburg, P. Physiological and pharmacological investigations of small intestinal peristalsis. Translation of the article 'Physiologische und pharmakologische Versuche über die Dünndarmperistaltik', Arch. Exp. Pathol. Pharmacol. 81, 55-129, 1917. *Naunyn Schmiedebergs Arch. Pharmacol.* **373**, 101–133 (2006).
256. Dickson, E. J. *et al.* An Enteric Occult Reflex Underlies Accommodation and Slow Transit in the Distal Large Bowel. *Gastroenterology* **132**, 1912–1924 (2007).
257. Thornton, P. D. J. & Bornstein, J. C. Slow excitatory synaptic potentials evoked by distension in myenteric descending interneurons of guinea-pig ileum. *The Journal of Physiology* **539**, 589–602 (2002).
258. Thornton, P. D. J., Gwynne, R. M., McMillan, D. J. & Bornstein, J. C. Transmission to Interneurons Is via Slow Excitatory Synaptic Potentials Mediated by P2Y1 Receptors during Descending Inhibition in Guinea-Pig Ileum. *PLoS ONE* **8**, e40840–10 (2013).
259. Yuan, S. Y., Bornstein, J. C. & Furness, J. B. Investigation of the role of 5-HT3 and 5-HT4 receptors in ascending and descending reflexes to the circular muscle of guinea-pig small intestine. *Br. J. Pharmacol.* **112**, 1095–1100 (1994).
260. Johnson, P. J., Bornstein, J. C. & Burcher, E. Roles of neuronal NK1 and NK3 receptors in synaptic transmission during motility reflexes in the guinea-pig ileum. *Br. J. Pharmacol.* **124**, 1375–1384 (1998).
261. Brookes, S. J. Classes of enteric nerve cells in the guinea-pig small intestine. *Anat. Rec.* **262**, 58–70 (2001).
262. Schemann, M. Control of gastrointestinal motility by the 'gut brain' - The enteric nervous system. *Journal of Pediatric Gastroenterology and Nutrition* **41**, S4–S6 (2005).

263. Furness, J. B., Callaghan, B. P., Rivera, L. R. & Cho, H.-J. The enteric nervous system and gastrointestinal innervation: integrated local and central control. *Adv. Exp. Med. Biol.* **817**, 39–71 (2014).
264. Hao, M. M. *et al.* Early Emergence of Neural Activity in the Developing Mouse Enteric Nervous System. *Journal of Neuroscience* **31**, 15352–15361 (2011).
265. Hao, M. M. *et al.* The emergence of neural activity and its role in the development of the enteric nervous system. *Dev. Biol.* **382**, 365–374 (2013).
266. Erickson, C. S. *et al.* Appearance of cholinergic myenteric neurons during enteric nervous system development: comparison of different ChAT fluorescent mouse reporter lines. *Neurogastroenterol. Motil.* **26**, 874–884 (2014).
267. Vogalis, F., Harvey, J. R., Lohman, R.-J. & Furness, J. B. Action potential afterdepolarization mediated by a Ca²⁺-activated cation conductance in myenteric AH neurons. *Neuroscience* **115**, 375–393 (2002).
268. Johnson, P. J. & Bornstein, J. C. Neurokinin-1 and -3 receptor blockade inhibits slow excitatory synaptic transmission in myenteric neurons and reveals slow inhibitory input. *Neuroscience* **126**, 137–147 (2004).
269. Koussoulas, K., Swaminathan, M., Fung, C., Bornstein, J. C. & Foong, J. P. P. Neurally Released GABA Acts via GABAC Receptors to Modulate Ca²⁺ Transients Evoked by Trains of Synaptic Inputs, but Not Responses Evoked by Single Stimuli, in Myenteric Neurons of Mouse Ileum. *Front. Physiol.* **9**, 227–12 (2018).
270. Martens, M. A., Boesmans, W. & Vanden Berghe, P. Calcium imaging at kHz frame rates resolves millisecond timing in neuronal circuits and varicosities. *Biomed. Opt. Express* **5**, 2648–14 (2014).
271. Thomas, E. A., Sjövall, H. & Bornstein, J. C. Computational model of the migrating motor complex of the small intestine. *AJP: Gastrointestinal and Liver Physiology* **286**, G564–G572 (2004).
272. Costa, M. *et al.* Neurochemical classification of myenteric neurons in the guinea-pig ileum. *Neuroscience* **75**, 949–967 (1996).
273. Bornstein, J. C. Intrinsic sensory neurons of mouse gut - Toward a detailed knowledge of enteric neural circuitry across species. Focus on 'characterization of myenteric sensory neurons in the mouse small intestine'. *J. Neurophysiol.* **96**, 973–974 (2006).
274. Avetisyan, M., Schill, E. M. & Heuckeroth, R. O. Building a second brain in the bowel. *J. Clin. Invest.* **125**, 899–907 (2015).
275. Gershon, M. D. Developmental determinants of the independence and complexity of the enteric nervous system. *Trends in Neurosciences* **33**, 1–11 (2010).
276. Bollmann, J. H., Helmchen, F., Borst, J. G. & Sakmann, B. Postsynaptic Ca²⁺ influx mediated by three different pathways during synaptic transmission at a calyx-type synapse. *Journal of Neuroscience* **18**, 10409–10419 (1998).
277. Avemary, J. & Diener, M. Bradykinin-induced depolarisation and Ca²⁺ influx through voltage-gated Ca²⁺ channels in rat submucosal neurons. *European Journal of Pharmacology* **635**, 87–95 (2010).
278. Neher, E. & Sakaba, T. Multiple Roles of Calcium Ions in the Regulation of Neurotransmitter Release. *Neuron* **59**, 861–872 (2008).

279. Zucker, R. S. Calcium- and activity-dependent synaptic plasticity. *Current Opinion in Neurobiology* **9**, 305–313 (1999).
280. Mattson, M. P. Calcium and neurodegeneration. *Aging Cell* **6**, 337–350 (2007).
281. Pangrsic, T., Singer, J. H. & Koschak, A. Voltage-Gated Calcium Channels: Key Players in Sensory Coding in the Retina and the Inner Ear. *Physiological Reviews* **98**, 2063–2096 (2018).
282. Rosenberg, S. S. & Spitzer, N. C. Calcium Signaling in Neuronal Development. *Cold Spring Harbor Perspectives in Biology* **3**, a004259–a004259 (2011).
283. Mao, Y., Wang, B. & Kunze, W. Characterization of Myenteric Sensory Neurons in the Mouse Small Intestine. *J. Neurophysiol.* **96**, 998–1010 (2006).
284. Vanden Berghe, P., Kenyon, J. L. & Smith, T. K. Mitochondrial Ca²⁺ uptake regulates the excitability of myenteric neurons. *J. Neurosci.* **22**, 6962–6971 (2002).
285. Madisen, L. *et al.* A toolbox of Cre-dependent optogenetic transgenic mice for light-induced activation and silencing. *Nat Neurosci* **15**, 793–802 (2012).
286. Boesmans, W. *et al.* Neurotransmitters involved in fast excitatory neurotransmission directly activate enteric glial cells. *Neurogastroenterol. Motil.* **25**, e151–e160 (2013).
287. Smith, T. H., Ngwainmbi, J., Grider, J. R., Dewey, W. L. & Akbarali, H. I. An *In-vitro* Preparation of Isolated Enteric Neurons and Glia from the Myenteric Plexus of the Adult Mouse. *J Vis Exp* 1–8 (2013). doi:10.3791/50688
288. Iyer, V. *et al.* Electrophysiology of guinea-pig myenteric neurons correlated with immunoreactivity for calcium binding proteins. *J. Auton. Nerv. Syst.* **22**, 141–150 (1988).
289. Vanden Berghe, P., Molhoek, S., Missiaen, L., Tack, J. & Janssens, J. Differential Ca²⁺ signaling characteristics of inhibitory and excitatory myenteric motor neurons in culture. *AJP: Gastrointestinal and Liver Physiology* **279**, G1121–7 (2000).
290. Trouslard, J., Marsh, S. J. & Brown, D. A. Calcium entry through nicotinic receptor channels and calcium channels in cultured rat superior cervical ganglion cells. *The Journal of Physiology* **468**, 53–71 (1993).
291. Galligan, J. J. & Bertrand, P. P. ATP mediates fast synaptic potentials in enteric neurons. *Journal of Neuroscience* **14**, 7563–7571 (1994).
292. Papke, R. L. Merging old and new perspectives on nicotinic acetylcholine receptors. *Biochemical Pharmacology* **89**, 1–11 (2014).
293. Stamp, L. A. *et al.* Optogenetic Demonstration of Functional Innervation of Mouse Colon by Neurons Derived From Transplanted Neural Cells. *Gastroenterology* **152**, 1407–1418 (2017).
294. Rao, M. & Gershon, M. D. The bowel and beyond: the enteric nervous system in neurological disorders. *Nature Reviews Gastroenterology & Hepatology* **13**, 517–528 (2016).
295. Shannon, K. & Vanden Berghe, P. The enteric nervous system in PD: gateway, bystander victim, or source of solutions. *Cell Tissue Res* **373**, 313–326 (2018).
296. Uemura, N. *et al.* Inoculation of α -synuclein preformed fibrils into the mouse gastrointestinal tract induces Lewy body-like aggregates in the brainstem via the vagus nerve. 1–11 (2018). doi:10.1186/s13024-018-0257-5

297. Holmqvist, S. *et al.* Direct evidence of Parkinson pathology spread from the gastrointestinal tract to the brain in rats. *Acta Neuropathol* **128**, 805–820 (2014).

Personal Contribution and Conflicts of Interests

Chapter 1 was written by Zhiling Li and Candice Fung and corrected by the supervisors. Figures were generated by Zhiling Li and Candice Fung.

Chapter 2 was written by Zhiling Li and corrected by the supervisors.

Chapter 3 was written by Zhiling Li and corrected by the supervisors. All figures were generated by Zhiling Li. Marlene M Hao, Werend Boesmans and Pieter Vanden Berghe determined the experimental design, contributed to the conception of the project. Zhiling Li collected the data, performed the analysis. Micky Moons assisted in all experiments. We thank Joris Van Asselberghs (Laboratory for Neurobiology and Gene Therapy) for the help with the tail vein injections.

Chapter 4 was written by Zhiling Li and corrected by the supervisors. Figure 1 was generated by Zhiling Li and Werend Boesmans, figure 2-4, 6 and 7 were generated by Zhiling Li, figure 5, 8 and supplementary figure were generated by Pieter Vanden Berghe. Together with the supervisors, Zhiling Li determined the experimental design, contributed to the conception of the project. Zhiling Li collected the data, performed the main analysis. Pieter Vanden Berghe wrote the analysis routines in Igor pro. Chris Van den Haute from Laboratory for Neurobiology and Gene Therapy (KU Leuven) and Veerle Baekelandt from Leuven Viral Vector Core (KU Leuven) provided materials (viral vectors) and helped with the preliminary viral vector tracing experiments. Micky Moons assisted in all experiments.

Chapter 5 was written by Zhiling Li and corrected by the supervisors. All figures were generated by Zhiling Li. Together with the supervisors, Zhiling Li determined the experimental design, contributed to the conception of the project. Zhiling Li collected the data, performed the main analysis. Pieter Vanden Berghe wrote the analysis routines in Igor pro. Youcef Kazwiny analyzed the train stimulation data. Micky Moons assisted in all experiments.

Chapter 6 and 7 were written by Zhiling Li and corrected by Pieter Vanden Berghe.

There are no conflicts of interest.

Acknowledgements

“Life is like a box of chocolate, you never know what you’re going to get.” — Winston Groom

I still remember how I was excited when I was informed to award the scholarship from the Chinese government to go abroad for a PhD degree. After a couple of days, when I calmed down, I started to think about what I will go through, especially the Chinese food (always miss it). If you don’t live it, you are never gonna know what will happen. Right now when I am writing this section, every frame of the past years just passed by in my mind, good ones or bad ones. In the end, everything will be the cherished memory in my life.

It is time to thank all the people involved in my life here. First, I would like to thank my promotor Pieter Vanden Berghe for all the time, trust, encouragement, and support that he has given me over the years of PhD. I really appreciate what he has done about the extra analysis for my first paper, god knows we have been through a lot for the submission, especially my situation. I also want to thank you for solving the problems immediately, even at the weekend.

Werend and Marlene, I am so lucky to have you both to be my co - promotors. Thank you for giving me all invaluable scientific, career-related suggestions. Marlene, without you, I suppose my beginning life in Leuven would have been much more difficult. You are an amazing woman and a fantastic mother. Werend, I really appreciate you gave me the soothing guidance when I was in a low stage (too many upset moments in the last year). You turned to be soft when you became a father, but you are still a critical scientist. You two are always models in my career. I wish your scientific career brilliant.

I would also like to thank all of my jury members for the time they spent in reading and reviewing my thesis. For my internal jury members, Prof. Dietmar Schmucker and Prof. Joris Dewit, thanks for the follow-up during my whole PhD project. And for my external jury members, Prof. Alan E G Lomax, and Prof. Jean-Pierre Timmermans, I am honored that you accepted my invitation to be the members of my thesis committee, and spent the time to attend my PhD defense.

I further want to thank all my colleagues of LENS, past, and present, for creating a positive working environment: Candice, Carla, Valerie, An-Sofie, Youcef, Micky, Silvia,

Tom, Tobie, Bert, and Robin. You guys know I am not a good talker. But what we have spent in the past years and what we will do in the coming months mean a lot to me.

Candice, thanks for spending the time to correct my manuscript. And I really enjoyed the times at the conferences attended together with you. And also Joe Hisaishi's concert, it was an amazing night. Now I feel it is pretty easy to say a Japanese name. I learn it from the best.

Valérie, you are so smart, funny.... Can't remember what else words I can use to describe you. Anyway, thanks for always solving the dutch problems in my Belgium life. Big welcome you to China to see the animals you are always obsessed in and try the authentic "Hot Pot" you experienced in Vietnam (no, no, no, that was a fake hot pot).

An-Sofie, thanks for taking care of me when I just arrived at Leuven. We spent a wonderful time together in the lab.

Youcef, thanks to you for all the questions I asked about the software stuff and thanks for the project discussion and the patch data analysis. The Chinese always welcome you back home.

Tom, thank you and Anaïs for taking care of Petty, I think I found a nice destination for her. I would like to wish you a lot of success with your PhD.

Silvia, what should I say about you? There is only one word in my mind: "Top". And I bring you these emoji faces 🍷 🌈 🙌 🤔 🥳 🍷, so vividly, right? Thanks for making so much fun in the lab. I will miss you much.

Thank Valérie, Silvia, Candice, Tom and Youcef to organize a fantastic Portugal trip, although there were some "unexpected accidents". I am so appreciated you are part of my life.

Micky, thanks for helping me with experiments during my PhD. And also thanks for caring for my personal life like a "grandma", who is always curious with my weekend activities. I will keep updating myself.

Tobie, thanks for bring so much fun during patch experiments, though I didn't have more time to teach you. I am so sorry about that. Good luck!

I would also like to thank my Chinese friends in Leuven, in particular to Min. Our friendship started from the first Chinese New year gala in Leuven, from then on, we spent a lot of time to travel, to have weekly dinners and drinks, to talk about everything.....Thanks for always listening and caring for me.

Of course, I'd like to thank my family for their love, encouragement, and understanding to support me through the years. Without you, I couldn't have done this.

Thanks for all your support!

The stories are to be continued.....

Best wishes,

Zhiling

Curriculum Vitae

Zhiling Li was born in Shanxi (China) on January 6th, 1986. After her bachelor in Shanxi Medical University in 2010, she started her master thesis in the laboratory pathophysiology of Luo Xu, Qingdao University, from 2011. Three years later, she graduated and received the prize for Best Master Thesis. In the meantime, she was awarded a scholarship under the State Scholarship Fund to pursue her study in Belgium as a PhD. During the next 4.5 years, she devoted herself to her PhD in Biomedical Science at the Lab for Enteric Neuroscience (LENS), Department of Chronic Diseases, Metabolism and Ageing, under the supervision of Prof. Vanden Berghe. Her scientific work has contributed to several abstracts and peer-reviewed publications.

List of Publications

Li ZL, Hao MM, Van den Haute C, Baekelandt V, Boesmans W, Vanden Berghe P. Complexity in enteric neuron wiring reflects diversity of motility patterns in the mouse large intestine. *Elife*. 2019 Feb 12. Doi: 10.7554/eLife.42914.

Boesmans W, Hao MM, Fung C, **Li ZL**, Van den Haute C, Tack J, Pachnis V, Vanden Berghe P. Structurally defined signaling in neuro-glia units in the enteric nervous system. *Glia*. 2019 Feb 7. doi: 10.1002/glia.23596.

Hao MM, Foong JPP, Bornstein JC, **Li ZL**, Vanden Berghe P, Boesmans W. Enteric nervous system assembly: functional integration within the developing gut. *Dev Biol*. 2016; 417(2):168-81.

Li ZL, Fung C, Vanden Bergh P. Electric activity and neuronal components in the gut wall. A chapter of *Encyclopedia of Gastroenterology 2nd Edition*. (under review).

Guo FF, Xu L, Gao SL, Sun XR, **Li ZL**, Gong YL. The effects of nesfatin-1 in the paraventricular nucleus on gastric motility and its potential regulation by the lateral hypothalamic area in rats. *J Neurochem*. 2015; 132(3): 266-75.

Li ZL, Xu L, Sun XR, Guo FF, Gong YL, Gao SL. Central nesfatin-1 influences the excitability of ghrelin-responsive gastric distension neurons in the arcuate nucleus and reduces gastric motility in rats. *Eur J Neurosci*. 2013; 38(11): 3636-43.

Xu L, **Li Z**, Guo F. Curcumin improves expression of ghrelin through attenuating oxidative stress in gastric tissues of streptozotocin-induced diabetic gastroparesis rats. *Eur J Pharmacol*. 2013; 718(1-3): 219-25.

Papers in Preparation

Li ZL, Boesmans W, Kazwiny Y, Hao MM, Vanden Berghe P. Correlation between voltage changes and $[Ca^{2+}]_i$ transients using simultaneous whole-cell patch-clamp electrophysiology and live calcium imaging. (to be submitted 2019).

Participation at International Conferences

2015

Development of the Enteric Nervous System: Cells, Signals, Genes, and Therapy. Rotterdam, Netherlands. 19-21 April, 2015.

Poster presentation: Application of recombinant adeno-associated viral vectors in the study of enteric nerve circuits.

2016

2nd Meeting of the Federation of Neurogastroenterology and Motility. San Francisco, California, USA. 26-28 August, 2016.

Oral presentation: Neuronal circuitry analysis using live calcium imaging in the mouse colon.

2017

12th Biennial Conference of Chinese Neuroscience Society. Tianjin, China. 12-15 October, 2017

Poster presentation: Analysis of enteric neuronal circuitry in the mouse colon using live calcium imaging.

2018

Edition XXVII of Belgium Week of Gastrienterology BGWE, Antwerp. Belgium. 21-23 February, 2018

Oral presentation: Live calcium imaging reveals neuronal circuitry differences in the mouse colon.

Development of the Enteric Nervous System: Cells, Signals, Genes, and Therapy. Boston, MA USA 8-11 April, 2018.

Poster presentation: Live calcium imaging reveals differences in enteric neuron wiring in the mouse colon.

3rd Meeting of the Federation of Neurogastroenterology and Motility. Amsterdam. The Netherlands. August 29th to September 1st, 2018.

Poster presentation: Differences in enteric neuron wiring revealed by live calcium imaging in the mouse colon.